FINAL
CONTRACT REPORT
VTRC 09-CR4

EXPERIMENTAL AND ANALYTICAL INVESTIGATION OF FULL-DEPTH PRECAST DECK PANELS ON PRESTRESSED I-GIRDERS

SEAN SULLIVAN, Ph.D.
Graduate Research Engineer

C. L. ROBERTS-WOLLMANN, Ph.D., P.E.
Associate Professor

Via Department of Civil and Environmental Engineering
Virginia Polytechnic Institute & State University

http://www.virginiadot.org/vtrc/main/online_reports/pdf/09-cr4.pdf

Standard Title Page - Report on Federally Funded Project

1. Report No. FHWA/VTRC 09-CR4	2. Government Accession No.	3. Recipient's Catalog No.
4. Title and Subtitle Experimental and Analytical Investigation of Full-Depth Precast Deck Panels on Prestressed I-Girders		5. Report Date December 2008
		6. Performing Organization Code
7. Author(s) Sean Sullivan, Ph.D., and Carin L. Roberts-Wollmann, Ph.D., P.E.		8. Performing Organization Report No. VTRC 09-CR4
9. Performing Organization and Address Virginia Transportation Research Council 530 Edgemont Road Charlottesville, VA 22903		10. Work Unit No. (TRAIS) 11. Contract or Grant No. 82670
12. Sponsoring Agencies' Name and Address Virginia Department of Transportation 1401 E. Broad Street Richmond, VA 23219 Federal Highway Administration 400 North 8th Street, Room 750 Richmond, VA 23219-4825		13. Type of Report and Period Covered Final Contract 14. Sponsoring Agency Code
15. Supplementary Notes		

16. Abstract

A bridge with precast bridge deck panels was built at the Virginia Tech Structures Laboratory to examine constructability issues, creep and shrinkage behavior, and strength and fatigue performance of transverse joints, different types of shear connectors, and different shear pocket spacings. The bridge consisted of two AASHTO type II girders, 40 ft long and simply supported, and five precast bridge deck panels. Two of the transverse joints were epoxied male-female joints and the other two transverse joints were grouted female-female joints. Two different pocket spacings were studied: 4 ft pocket spacing and 2 ft pocket spacing. Two different shear connector types were studied: hooked reinforcing bars and a new shear stud detail that can be used with concrete girders.

The construction process was well documented. The changes in strain in the girders and deck were examined and compared to a finite element model to examine the effects of differential creep and shrinkage. After the finite element model verification study, the model was used to predict the long term stresses in the deck and determine if the initial level of post-tensioning was adequate to keep the transverse joints in compression throughout the estimated service life of the bridge. Cyclic loading tests and flexural strength tests were performed to examine performance of the different pocket spacings, shear connector types and transverse joint configurations. A finite element study examined the performance of the AASHTO LRFD shear friction equation for the design of the horizontal shear connectors.

The initial level of post-tensioning in the bridge was adequate to keep the transverse joints in compression throughout the service life of the bridge. Both types of pocket spacings and shear connectors performed exceptionally well. The AASHTO LRFD shear friction equation was shown to be applicable to deck panel systems and was conservative for determining the number of shear connectors required in each pocket. A recommended design and detailing procedure was developed for the shear connectors and shear pockets.

17 Key Words	18. Distribution Statement
Full-depth precast bridge deck panels, deck panel girder connection, horizontal shear strength, prestress losses, panel to panel connection	No restrictions. This document is available to the public through NTIS, Springfield, VA 22161.

19. Security Classif. (of this report)	20. Security Classif. (of this page)	21. No. of Pages	22. Price
Unclassified	Unclassified	84	

Form DOT F 1700.7 (8-72) Reproduction of completed page authorized

FINAL CONTRACT REPORT

EXPERIMENTAL AND ANALYTICAL INVESTIGATION OF FULL-DEPTH PRECAST DECK PANELS ON PRESTRESSED I-GIRDERS

Sean Sullivan, Ph.D.
Graduate Research Engineer

C.L. Roberts-Wollmann, Ph.D., P.E.
Associate Professor

Via Department of Civil & Environmental Engineering
Virginia Polytechnic Institute & State University

Project Manager
Michael C. Brown, Ph.D., P.E., Virginia Transportation Research Council

Contract Research Sponsored by
the Virginia Transportation Research Council

In Cooperation with the U.S. Department of Transportation
Federal Highway Administration

Virginia Transportation Research Council
(A partnership of the Virginia Department of Transportation
and the University of Virginia since 1948)

Charlottesville, Virginia

December 2008
VTRC 09-CR4

DISCLAIMER

The project that is the subject of this report was done under contract for the Virginia Department of Transportation, Virginia Transportation Research Council. The contents of this report reflect the views of the authors, who are responsible for the facts and the accuracy of the data presented herein. The contents do not necessarily reflect the official views or policies of the Virginia Department of Transportation, the Commonwealth Transportation Board, or the Federal Highway Administration. This report does not constitute a standard, specification, or regulation. Any inclusion of manufacturer names, trade names, or trademarks is for identification purposes only and is not to be considered an endorsement.

Each contract report is peer reviewed and accepted for publication by Research Council staff with expertise in related technical areas. Final editing and proofreading of the report are performed by the contractor.

ABSTRACT

A bridge with precast bridge deck panels was built at the Virginia Tech Structures Laboratory to examine constructability issues, creep and shrinkage behavior, and strength and fatigue performance of transverse joints, different types of shear connectors, and different shear pocket spacings. The bridge consisted of two AASHTO type II girders, 40 ft long and simply supported, and five precast bridge deck panels. Two of the transverse joints were epoxied male-female joints and the other two transverse joints were grouted female-female joints. Two different pocket spacings were studied: 4 ft pocket spacing and 2 ft pocket spacing. Two different shear connector types were studied: hooked reinforcing bars and a new shear stud detail that can be used with concrete girders.

The construction process was well documented. The changes in strain in the girders and deck were examined and compared to a finite element model to examine the effects of differential creep and shrinkage. After the finite element model verification study, the model was used to predict the long term stresses in the deck and determine if the initial level of post-tensioning was adequate to keep the transverse joints in compression throughout the estimated service life of the bridge. Cyclic loading tests and flexural strength tests were performed to examine performance of the different pocket spacings, shear connector types and transverse joint configurations. A finite element study examined the performance of the AASHTO LRFD shear friction equation for the design of the horizontal shear connectors.

The initial level of post-tensioning in the bridge was adequate to keep the transverse joints in compression throughout the service life of the bridge. Both types of pocket spacings and shear connectors performed exceptionally well. The AASHTO LRFD shear friction equation was shown to be applicable to deck panel systems and was conservative for determining the number of shear connectors required in each pocket. A recommended design and detailing procedure was developed for the shear connectors and shear pockets.

FINAL CONTRACT REPORT

EXPERIMENTAL AND ANALYTICAL INVESTIGATION OF FULL-DEPTH PRECAST DECK PANELS ON PRESTRESSED I-GIRDERS

Sean Sullivan, Ph.D.
Graduate Research Engineer

C.L. Roberts-Wollmann, Ph.D., P.E.
Associate Professor

Via Department of Civil & Environmental Engineering
Virginia Polytechnic Institute & State University

INTRODUCTION

Introduction to Precast Bridge Deck Panel Systems

Full-depth precast bridge deck panels can be used in place of a cast-in-place concrete deck in order to reduce construction time for bridge deck replacements or new bridge construction. Figure 1 shows a representation of a bridge with full-depth precast deck panels and prestressed concrete girders.

The construction process consists of first placing the panels on top of the girders. The self weight of the panels is transferred to the girders through leveling bolts. Leveling bolts are threaded through the depth of the panels and protrude through the bottom of the panels. The protrusion can be adjusted depending on the desired haunch height or desired top-of-deck elevation. The transverse joints are grouted next. If the deck is to be post-tensioned, this operation can then be performed. After the post-tensioning operation is complete, the post-tensioning ducts are typically grouted. Composite action between the deck and girders is provided by shear connectors that extend out of the girder and into the shear pockets of the panels. The haunch and pockets are poured after the post-tensioning operation. Once the grout in the haunch has cured, the leveling bolts can be removed and the panels and girders act as a composite system. Barrier rails can be cast and a wearing surface placed.

The most common type of joint between adjacent panels is a grouted female-female joint. Epoxied male-female shear keys have been used in precast pavements. The panels are typically post-tensioned together to add strength to the joint, act as distribution reinforcement, reduce the chance for water leakage at the joint, and improve the durability of the deck. However, if post-tensioning is not applied, mild reinforcing steel is often placed across the joint in order to reinforce the joint. The mild reinforcing steel must be properly developed on each side of the joint.

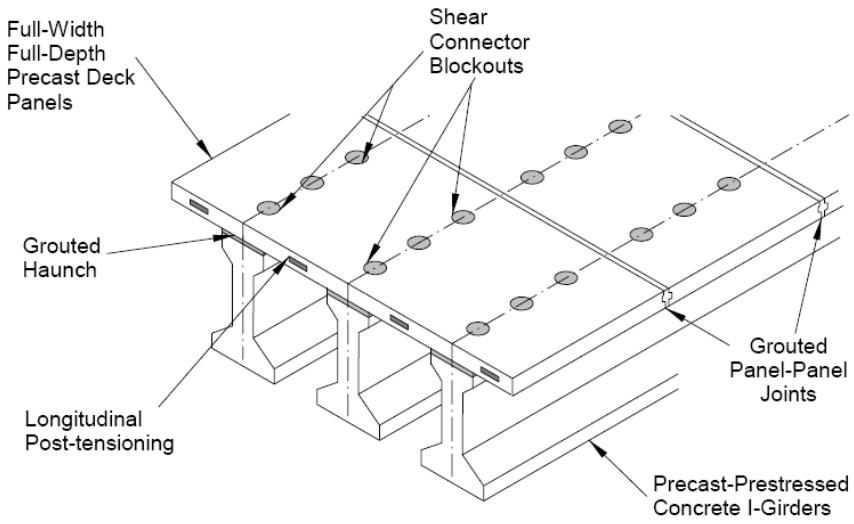

Figure 1. Representation of Bridge Deck Panel System.

Summary of Challenges Associated with Precast Bridge Deck Panel Systems

Horizontal Shear Connectors

Composite action between the panels and girders is provided by the haunch and shear connectors, which are clustered together at the shear pockets instead of having a more uniform shear connector spacing found with cast-in-place concrete decks. The discrete locations of the shear connectors raise questions about the proper way to design for horizontal shear transfer. The pocket spacing is typically 2 ft. Larger pocket spacing is desirable because it results in less grout that has to be poured during the bridge closure, and fewer blockout forms that have to be placed during fabrication. Larger pocket spacing may result in cracking along the interface between the shear pockets where there is no reinforcement present. Current design provisions do not address the design of shear connectors for precast bridge deck panel systems.

There are a variety of shear connectors that can be used with precast bridge deck panel systems. Hooked reinforcing bars can be used for panels installed on prestressed concrete girders. Shear studs are typically used for panels installed on steel girders.

This research program investigated the performance of shear studs and hooked reinforcing bars with precast, prestressed girders. A portion of the hooked reinforcing bar, which was cast into the girder, protruded from the top flange into the shear pocket. The shear connector detail with shear studs was fabricated by casting a steel plate in the top flange of a prestressed girder. Shear studs were located on the bottom of the steel plate, as shown in Figure 2. Additional shear studs were then shot directly onto the top of the steel plate after the girder was erected and the panels were placed. No prior use or testing of this detail was found in the literature review.

Figure 2. New Detail For Horizontal Shear Reinforcement.

Prestress Losses in Post-Tensioned Deck Panels

Long term prestress losses may be significant enough to decrease the pre-compressive stress across a transverse joint to a point where the bottom surface of a transverse joint goes into tension under service load. Current AASHTO[1] equations for prestress loss address losses in a prestressed girder made composite with a cast-in-place deck. The equations are not applicable to precast deck panels. In precast decks, the post-tensioning is applied to the deck alone, after which the deck is connected to the supporting beams when the grout in the haunch and pockets is placed. From this point forward in time, the deck creep and shrinkage is partially restrained by the beam. This causes force and moment redistributions in the system, which are not taken into account in the AASHTO equations.

Many states have reported problems with leaking at the transverse joints.[2,3] This can often be attributed to a lack of post-tensioning or poor construction practices. There has been much speculation as to which type of transverse joint is the best to use in terms of strength, durability, ease of construction, and cost. The transverse joints are often thought of as one of the "weak links" of the system and special consideration needs to be given to these joints. Recommended levels of post-tensioning have been given to keep the joint in compression under live loads.[4,5]

PURPOSE AND SCOPE

The purpose of this research program was to investigate the performance of shear studs and hooked reinforcing bars with precast, prestressed girders. By doing so, current design provisions and practices can be improved and modifications to code provisions can be proposed, if necessary.

The first objective was to examine the constructability of the system. A bridge consisting of precast deck panels and precast, prestressed concrete girders was built in the Virginia Tech Structures and Materials Laboratory. This bridge is referred to as the lab mockup. The

construction process was well documented. Particular attention was given to the transverse joint details and the types of shear connectors.

The second objective was to study the composite action of the system. The hooked reinforcing bars and the new detail with shear studs were both considered in the testing program. Both cyclic and overload tests were performed. The cracking patterns at the interface between the haunch and girder, the strains in the shear connectors and the vertical deflections of the system were used as the primary indicators for the level of composite action. The shear pocket spacing was also examined to see if 4 ft pocket spacing performed adequately compared to 2 ft pocket spacing. Finite element studies were also conducted to aid in making more general conclusions about the composite action of the system by modeling push-off specimens and the lab mockup.

The third objective was to investigate to what extent creep and shrinkage affects the long term prestress losses and deck stresses in the lab mockup. Forces in the post-tensioning strands in the lab mockup were monitored along with the longitudinal strains in the deck and girders. The experimental results were used to verify the results of the finite element models. The results were used to recommend an initial level of post-tensioning.

The fourth objective was to study the structural behavior of the transverse joints and evaluate constructability issues associated with the transverse joints used in the lab mockup. Epoxied male-female joints and grouted female-female joints were used. Both cyclic and overload tests were performed and relative displacements and crack patterns were compared to see if one joint performed better than the other. Water was also ponded at selected intervals during the testing program to determine if the joints leaked.

The recommendations in this report are based on a test bridge with full-depth panels on prestressed I-beams. The bridge was simple span. Although steel girder bridges, and multi-span continuous bridges can be constructed with full-depth precast panels, they are not specifically addressed in this research.

METHODS

Introduction

An experimental research program and analytical research program were developed in order to accomplish the objectives outlined in the previous section. The experimental research program consisted of static and cyclic tests on a simply supported, full scale bridge built at the Virginia Tech Structures Laboratory. The analytical program consisted of finite element analyses using the commercial software DIANA.[6]

Experimental Program

Design of Lab Mockup

The design was based upon a 40 ft long, simply supported bridge with five girder lines, spaced at 8 ft center to center. The lab mockup consisted of two AASHTO Type II girders, 40 ft

long, spaced at 8 ft center-to-center. The AASHTO Type II girder was the most efficient girder to use for the 40 ft simple span. The deck was 8 in thick, with a 2 ft overhang on each side. The haunch between the panels and girders was 2 in.

Design Summary

The design of the lab mockup was done per AASHTO LRFD[1] specifications. The design calculations, design drawings and fabrication drawings can be found in Sullivan.[7]

For the flexural design, the strand pattern for the girders was selected to satisfy service load levels. The girders had 12 1/2 in diameter Grade 270 strands in a straight pattern. The eccentricity of the strand group below the girder centroid was 7.83 in. The strand pattern selected for the girders also provided a flexural strength that exceeded the required flexural strength. Mild reinforcing bars were also provided in addition to the prestressing strands in the girder. Four No. 5 bars were provided in both the top flange and bottom flange of the girders. The mild steel bars were provided to increase the flexural capacity of the lab mockup. The flexural strength of the lab mockup was calculated to be 24,800 k-in, which was 60 percent greater than the AASHTO LRFD required flexural strength of 15,500 k-in. The additional flexural capacity was provided to prevent the system from failing prematurely in flexure before gaining insight into the behavior of the horizontal shear connectors.

The AASHTO LRFD required vertical shear strength was 152 k at the critical section. The critical section was 3 ft 8 in from the center of the bearing. In order to satisfy this requirement, No. 4 stirrups spaced at 20 in are required. However, No. 5 stirrups spaced at 20 in were provided to prevent the system from failing prematurely in vertical shear before gaining insight in to the behavior of the horizontal shear connectors. The vertical shear capacity with the No. 5 stirrups was 230 k.

For the transverse deck design, each panel was provided with 16½ in diameter Grade 270 strands. Eight strands were provided 2½ in from the top of the deck (clear spacing) and 8 strands were provided 2½ in from the bottom of the deck (clear spacing). Each panel had a different strand pattern because of the shear pocket layout, the transverse joint configurations, and the post-tensioning blockouts. The panels were approximately 8 ft x 12 ft x 8 in; slight variations existed between the panel types.

Twelve ½ in diameter strands were provided in the longitudinal post-tensioning ducts to provide a compressive stress across the transverse joints. The calculated initial level of post-tensioning after all initial losses was -298 psi. The calculated effective level of post-tensioning after all long term losses was -200 psi. The sign convention is negative (-) for compression and positive (+) for tension.

For the horizontal shear connectors, No. 5 stirrups extending from the top flange were used for girder 1, and 7 in long, ¾ in diameter shear studs were used for girder 2. The following equation, from AASHTO LRFD, was used to select the required number of connectors per pocket and calculate the capacity provided at a shear pocket:

$$V_n = cA_{cv} + \mu(A_{vf}\, f_y + P_c) \le \min(0.2\, f_c{}' A_{cv}, 5.5 A_{cv}) \qquad [1]$$

Where: c = cohesion factor
= 75 psi for not intentionally roughened surface between two concrete surfaces cast at different times
= 25 psi for concrete cast on steel
A_{cv} = area of concrete engaged in shear transfer (in^2)
μ = friction factor
= 0.6 for not intentionally roughened surface between two concrete surfaces cast at different times
= 0.7 for a surface formed by steel and concrete
A_{vf} = area of shear reinforcement crossing the interface (in^2)
f_y = yield strength of the shear reinforcement (ksi)
P_c = permanent net compressive force normal to the interface (kips)
f_c' = 28 day compressive strength of the weakest concrete at the interface(s) (ksi)

A_{cv} usually is the product of the width of the top flange and the spacing between the shear reinforcement. However, the shear connectors in precast deck panels are grouped together at the shear pockets. AASHTO LRFD does not address how to handle this situation. For calculations performed in this research program, the capacity of each shear pocket, using the tributary length between the pockets to calculate A_{cv}, is compared to the shear force developed at the pocket, using the tributary length between the pockets.

The following equation was used with the tributary pocket spacing to calculate the design shear force for the pockets in k/in.

$$V_h = \frac{V_u}{d_e} \qquad [2]$$

where d_e = distance between the centroid of the steel on the tension side of the girder to the resultant center of the compressive force in the deck.

For the shear stud connectors, Equations 3 through 8 were also satisfied.

$$6d \le p \le \frac{nZ_r I}{V_{sr} Q} \le 24 \text{ in} \qquad [3]$$

Where: d = diameter of the shear stud (in^2)
n = number of shear connectors in a cross section
I = moment of inertia of the short-term composite section (in^4)
Q = first moment of the transformed area of the slab about the neutral axis of the short term composite section (in^3)
V_{sr} = shear force range under LL+I determined for the fatigue limit state (kips)
Z_r = shear fatigue resistance of an individual shear connector (kips)

The fatigue resistance of an individual shear connector is:

$$Z_r = \alpha d^2 \geq \frac{5.5d^2}{2} \quad [4]$$

Where: $\alpha = 34.5 - 4.28\log(N)$ [5]

N = number of cycles

$= 365(y)n(ADTT)_{SL}$ [6]

y = design life (years)

n = number of stress range cycles per truck passage
(see AASHTO LRFD Table 6.6.1.2.5-2)

$(ADTT)_{SL}$ = single lane ADTT

$= p(ADTT)$

p = see AASHTO LRFD Table 3.6.1.4.2-1

ADTT = %trucks(ADT) (See AASHTO LRFD C3.6.1.4.2)

%trucks = see AASHTO LRFD Table C3.6.1.4.2-1

ADT = 20,000 vehicles per lane per day

The strength of the shear connectors is found by:

$$Q_r = \varphi_{sc} 0.5 A_{sc} \sqrt{f_c' E_c} \leq \varphi_{sc} A_{sc} F_u \quad [7]$$

Where: $\varphi_{sc} = 0.85$

A_{sc} = cross sectional area of a shear stud (in^2)

f_c' = 28 day compressive strength of the concrete in the deck (ksi)

E_c = modulus of elasticity of the concrete at 28 days (ksi)

F_u = minimum tensile strength of the shear stud (ksi)

An equation is also given in AASHTO LRFD to calculate the total number of shear studs required between sections of maximum positive moment and each adjacent point of zero moment. This equation is also used to determine the number of shear studs required between points of zero moment and the centerline of an interior support

$$n = \frac{\min(0.85 f_c' b t_s, F_{yw} D t_w + F_{yt} b_t t_t + F_{yc} b_c t_c)}{Q_r} \quad [8]$$

Where: b = effective width of the slab (in)

t_s = slab thickness (in)

F_{yw} = yield strength of the web for steel girders (ksi)

F_{yt} = yield strength of the tension flange for steel girders (ksi)

F_{yc} = yield strength of the compression flange for steel girders (ksi)

D = web depth for steel girders (in)

b_t = width of the tension flange for steel girders (in)

b_c = width of the compression flange for steel girders (in)

t_w = thickness of the web for steel girders (in)

t_t = thickness of the tension flange for steel girders (in)

t_c = thickness of the compressions flange for steel girders (in)

Equation 8 assumes the entire compressive stress block falls in the deck.

Because the shear connectors were clustered together in shear pockets instead being dispersed in a more uniform manner along the length of the bridge, the number of required connectors for each pocket was selected instead of a required connector spacing at a given location. The following design procedure was followed for each pocket:

1. The vertical shear force at the location under consideration was calculated.
2. Equation 2 was used to determine the shear force per inch.
3. The tributary pocket spacing was calculated. The tributary pocket spacing was half the pocket spacing on each side of the pocket under consideration.
4. The horizontal design shear force was calculated by multiplying the shear force per inch by the tributary pocket length.
5. Equation 1 was used to select the number of required shear connectors. The top flange width and the tributary pocket spacing were used to calculate the area of concrete engaged in resisting the shear force.

In order to provide a more uniform shear connector design, the same number of shear connectors was provided in several pockets. This caused many of the pockets in regions with small shear forces to be over designed. Table 1 shows the number of connectors required in each pocket using Equation 1 and the number of connectors provided in each pocket for both girder 1 and girder 2. The pocket numbers are shown in Figure 4.

Lab Mockup Details

Figures 3, 4, and 5 show schematics of the lab mockup. Three post-tensioning ducts were used to accommodate the 12 strands. The live end in Figures 3 and 4 was the stressing end for the post-tensioning operation.

Figure 4 shows the layout of the shear pockets. The pocket spacing was 4 ft at the dead end, 2 ft at the live end, and 2.5 ft for the “transition panel” (Panel Type 3). Grouted female-female joints were used at the dead end and epoxied male-female joints were used at the live end. Figure 3 and Figure 4 label what will be referred to as the inside joints and outside joints. This terminology is used in the description of the instrumentation and test setup.

Figure 4 shows the pocket locations. The width of each pocket in the transverse direction of the bridge was 11 in at the bottom of the pocket, tapering to 1 ft at the top of the pocket. The length of the pockets in panel 1 and panel 2 was 1 ft 5 in at the bottom of the pocket and tapered to 1 ft 6 in at the top of the pocket. The length of the pockets in panel 3, panel 4, and panel 5 was 11 in at the bottom of the pocket and tapered to 1 ft at the top of the pocket. The length of each pocket was sized to allow for at least a 1½ in gap between the edge of the pocket and the edge of the first shear connector in the pocket.

Five ¼ in thick plates were placed in the top flange of girder 2 immediately after the concrete was placed in the formwork, as shown in Figure 2. Five smaller plates were used as opposed to one large plate in order to make placing the plates easier.

Table 1. Comparison of Number of Shear Connectors Required and Number of Shear Connectors Provided

(a) Girder 1

pocket #	# bars required	# bars provided	V_{n_prov}/V_{n_req}
1	8	8	1.03
2	8	8	1.11
3	7	8	1.20
4	6	8	1.31
5	5	8	1.44
6	5	8	1.61
7	4	8	1.81
8	4	8	1.90
9	3	8	2.14
10	2	8	2.76
11	3	8	1.87
12	6	10	1.42
13	10	10	1.06
14	12	16	1.25
15	15	16	1.06

(b) Girder 2

pocket #	# studs required	# studs provided	V_{n_prov}/V_{n_req}
1	7	6	0.93
2	6	6	1.00
3	6	6	1.09
4	5	6	1.19
5	5	6	1.31
6	4	6	1.46
7	4	6	1.65
8	4	6	1.70
9	3	6	1.89
10	3	6	2.44
11	4	6	1.60
12	7	8	1.29
13	9	8	0.96
14	11	12	1.14
15	13	12	0.97

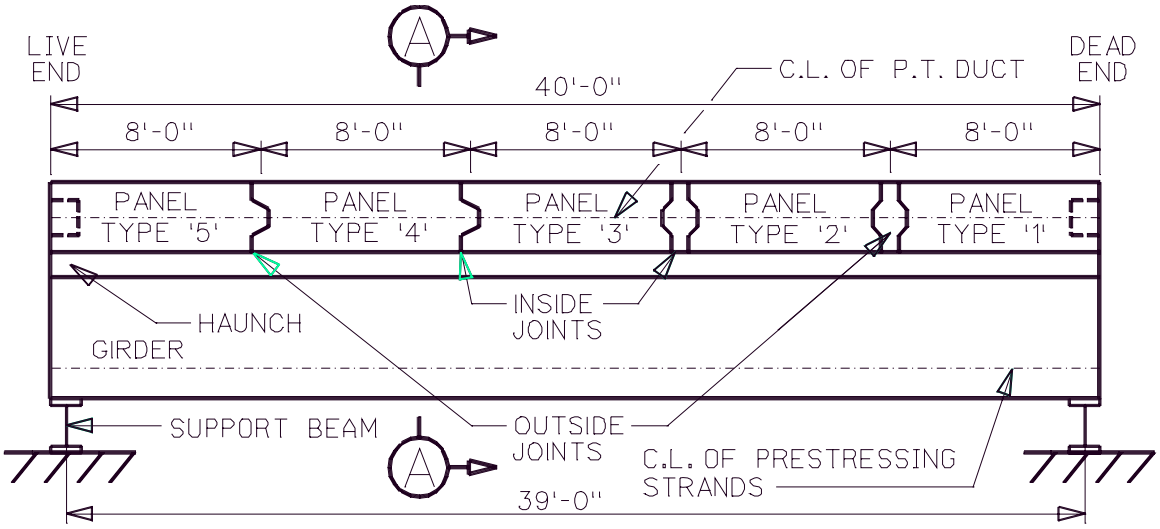

Figure 3. Elevation View of Lab Mockup.

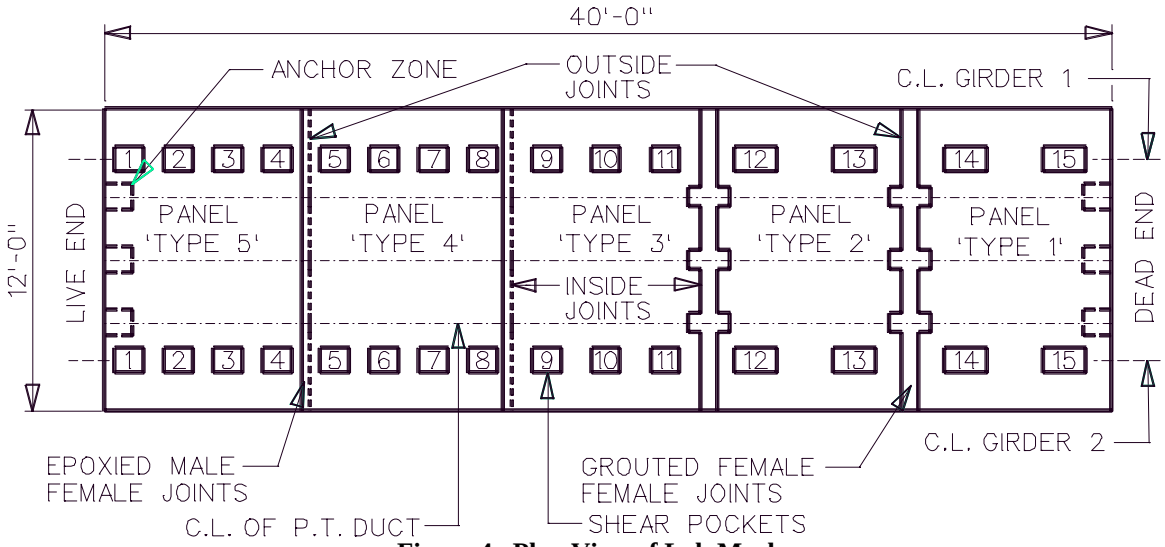

Figure 4. Plan View of Lab Mockup.

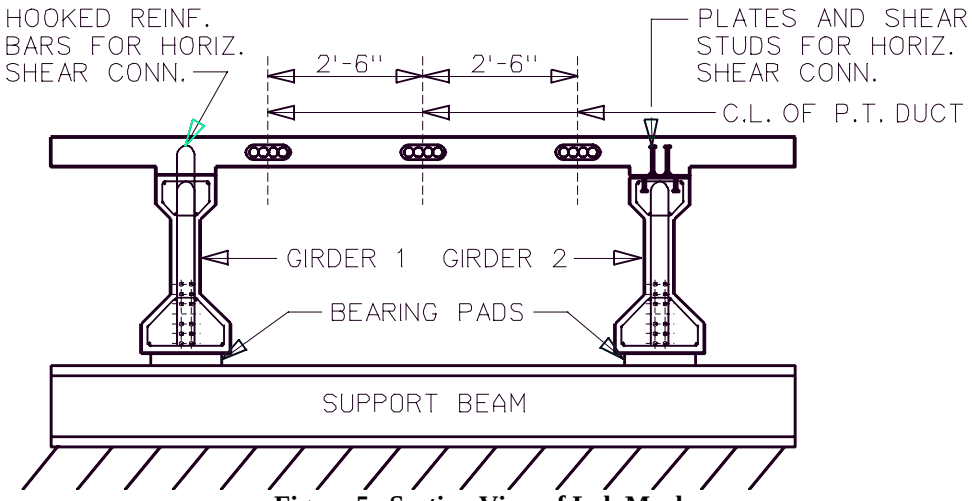

Figure 5. Section View of Lab Mockup.

Leveling bolts were used to allow for the panel elevations to be adjusted. The leveling bolt system consisted of Dayton Richmond F-53 Thin Slab Coil Inserts and B-14 Coil Bolts.

Instrumentation of Panels and Girders

During the casting operation at Bayshore Concrete Products in Chesapeake, Virginia, the panels and girders were instrumented with thermocouples and VWGs (vibrating wire gages). The thermocouples and VWGs were placed such that they would be located at the 1/3 points of the span of the bridge. Figure 6 shows the location of the VWGs and thermocouples through the depth of the cross section. The support beams are not shown for clarity.

The thermocouples and VWGs were used to monitor the change in temperature and strain through the casting process as well as during the investigation of the time-dependent behavior in the lab. The VWGs also aided in calculating the curvature of the girder and composite system during the data analysis. The sensitivity of the VWGs was 1 με.

The panels and girders were instrumented with ER (electrical resistance) strain gages, wirepots, and LVDTs after arriving at the Virginia Tech Structures Laboratory. Figure 6 shows the location of the ER strain gages, which were positioned at the 1/3 points of the span of the bridge. The ER strain gages were used during the cyclic tests and static tests. The sensitivity of the ER strain gages was 5 με. The strain gages aided in establishing strain profiles through the depth, calculating the change in curvature of the composite system, and in establishing whether full or partial composite action was present.

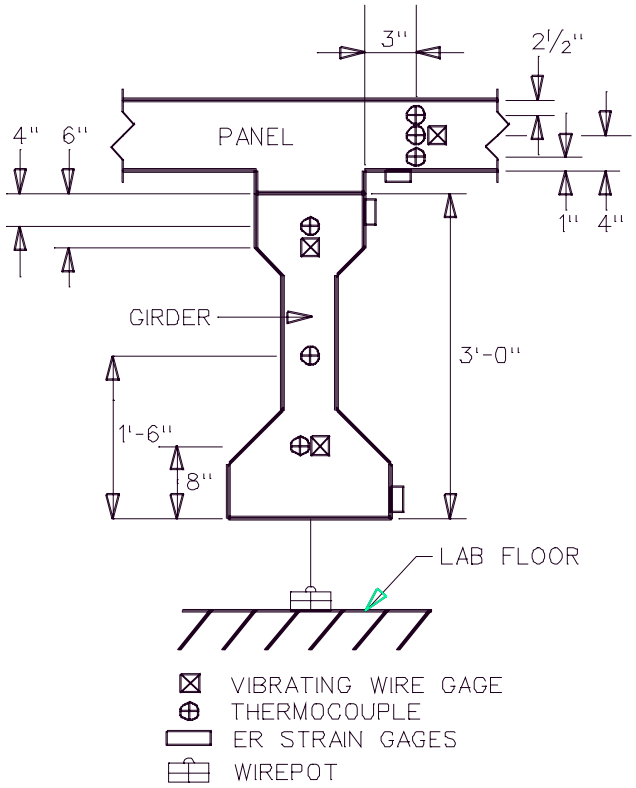

Figure 6. Location of Instrumentation for Panels and Girders.

Wirepots were used to measure the vertical displacement of the bridge. Figure 6 shows the location of the wirepots under the girders. The sensitivity of the wirepots was 0.005 in. The wirepots were located directly under the locations of the applied loads. During loading, the displacement measured by the wirepots located under the applied loads included the displacement of the bearing pads. To measure the displacement of the bearing pads, wirepots were also placed 1 ft away from the centerline of each bearing pad. These bearing pad displacements were used with the displacements measured by the wirepots located under the applied loads to get the true displacement of the system.

Wirepots were also used to measure any relative vertical displacements at the transverse joints between adjacent precast deck panels. Figure 7 shows the setup used with the wirepots to measure the relative vertical displacement between the deck panels.

LVDTs were used to measure any relative horizontal displacement (slip) between the panels and girders. The LVDTs were placed 4 ft from each end of the bridge. This location was half way between the first two pockets at the dead end and half way between the second and third pocket at the live end. The setup to measure the relative displacement with an LVDT is shown in Figure 8. The sensitivity of the LVDTs was 0.005 in.

ER strain gages were placed on selected shear connectors to measure the strain in the horizontal shear connectors during cyclic testing and static testing. Figure 9 shows the locations of the instrumented shear connectors.

Load cells were placed on one strand in each post-tensioning duct. The load cells were located at the dead end of the bridge. During the stressing operation, the load at the live end was measured with a load cell and compared to the load at the dead end. With the initial seating losses, an accurate estimation of the force profile along the length of the strand can be made for the representative strand in each duct. The load cells were also used to measure the loss of force in the strands until the post-tensioning ducts were grouted.

Figure 7. Setup to Measure the Relative Vertical Displacement at the Transverse Joints.

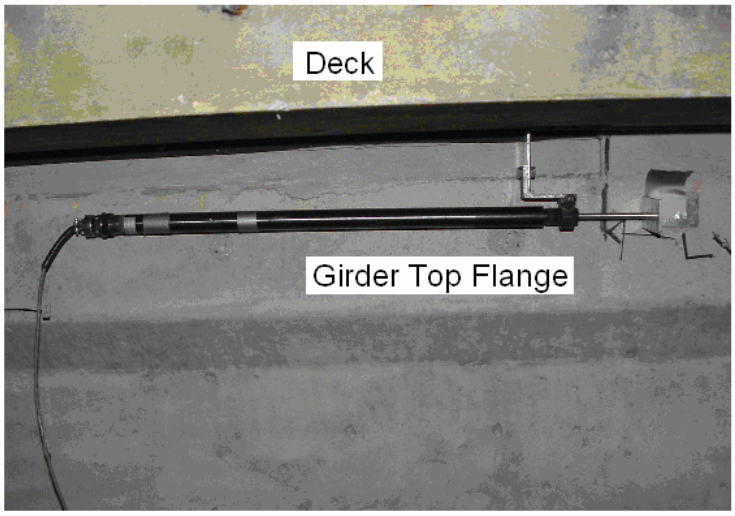

Figure 8. Setup to Measure Relative Horizontal Displacement at Horizontal Interface.

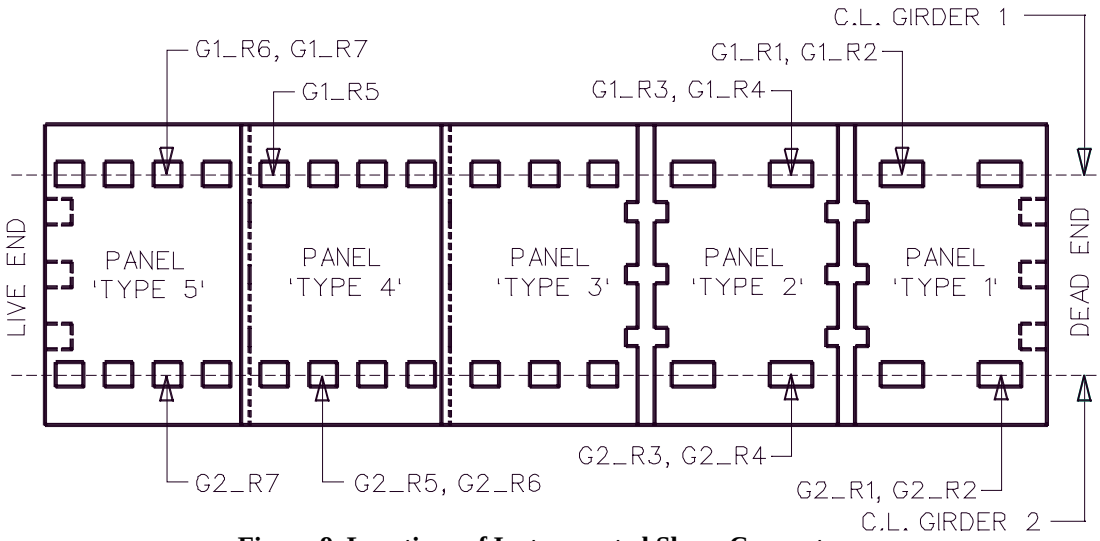

Figure 9. Locations of Instrumented Shear Connectors.

Table 2 presents the names of each instrument, the type of instrument, and a description of where it was located in the lab mockup. The VWG and thermocouple data were gathered with a Campbell CR23X micrologger and two multiplexers. The ER strain gages, wirepots, LVDTs and load cells were connected to a System 5000 scanner produced by Vishay MicroMeasurements Group, Inc.

Table 2. Location of Instrumentation in Lab Mockup

(a) LVDTs

Name	Over Girder Line	Description of Location
H1	Girder 1	Interface between panels and girders.
H2	Girder 2	Interface between panels and girders.

(b) VWGs

Name	Over Girder Line	Description of Location
G1_T_D	Girder 1	In the top flange on the dead end.
G1_B_D	Girder 1	In the bottom flange on the dead end.
G1_T_L	Girder 1	In the top flange on the live end.
G1_B_L	Girder 1	In the bottom flange on the live end.
G2_T_D	Girder 2	In the top flange on the dead end.
G2_B_D	Girder 2	In the bottom flange on the dead end.
G2_T_L	Girder 2	In the top flange on the live end.
G2_B_L	Girder 2	In the bottom flange on the live end.
G1_S2	Girder 1	In panel type 2.
G2_S2	Girder 2	In panel type 2.
G1_S4	Girder 1	In panel type 4.
G2_S4	Girder 2	In panel type 4.

(c) Thermocouples

Name	Over Girder Line	Description of Location
TG1_T_D	Girder 1	In top flange of girder on dead end.
TG1_M_D	Girder 1	In web of girder on dead end.
TG1_B_D	Girder 1	In bottom flange of girder on dead end.
TG1_T_L	Girder 1	In top flange of girder on live end.
TG1_M_L	Girder 1	In web of girder on live end.
TG1_B_L	Girder 1	In bottom flange of girder on dead end.
TG2_T_D	Girder 2	In top flange of girder on dead end.
TG2_M_D	Girder 2	In web of girder on dead end.
TG2_B_D	Girder 2	In bottom flange of girder on dead end.
TG2_T_L	Girder 2	In top flange of girder on live end.
TG2_B_L	Girder 2	In bottom flange of girder on dead end.
TG1_S2_T	Girder 1	In panel type 2 in the top portion of the slab.
TG1_S2_M	Girder 1	In panel type 2 in the middle portion of the slab.
TG1_S2_B	Girder 1	In panel type 2 in the bottom portion of the slab.
TG2_S2_T	Girder 2	In panel type 2 in the top portion of the slab.
TG2_S2_M	Girder 2	In panel type 2 in the middle portion of the slab.
TG2_S2_B	Girder 2	In panel type 2 in the bottom portion of the slab.
TG1_S4_T	Girder 1	In panel type 4 in the top portion of the slab.
TG1_S4_M	Girder 1	In panel type 4 in the middle portion of the slab.
TG1_S4_B	Girder 1	In panel type 4 in the bottom portion of the slab.
TG2_S4_T	Girder 2	In panel type 4 in the top portion of the slab.
TG2_S4_B	Girder 2	In panel type 4 in the bottom portion of the slab.

(d) Load Cells

Name	Over Girder Line	Description of Location
LC A	Duct Closest to Girder 2.	Dead end.

LC B	Middle Duct.	Dead end.
LC C	Duct Closest to Girder 1.	Dead end.

(e) ER Strain Gages

Name	Over Girder Line	Description of Location
G1_R1	Girder 1	See Figure 9
G1_R2	Girder 1	See Figure 9
G1_R3	Girder 1	See Figure 9
G1_R4	Girder 1	See Figure 9
G1_R5	Girder 1	See Figure 9
G1_R6	Girder 1	See Figure 9
G1_R7	Girder 1	See Figure 9
G2_R1	Girder 2	See Figure 9
G2_R2	Girder 2	See Figure 9
G2_R3	Girder 2	See Figure 9
G2_R4	Girder 2	See Figure 9
G2_R5	Girder 2	See Figure 9
G2_R6	Girder 2	See Figure 9
G2_R7	Girder 2	See Figure 9
PG1_D_L	Girder 1	Lower surface of panel on dead end.
PG1_L_L	Girder 1	Lower surface of panel on live end.
PG2_D_L	Girder 2	Lower surface of panel on dead end.
PG2_L_L	Girder 2	Lower surface of panel on live end.
G1_D_L	Girder 1	Lower surface of girder on dead end.
G1_L_L	Girder 1	Lower surface of girder on live end.
G2_D_L	Girder 2	Lower surface of girder on dead end.
G2_L_L	Girder 2	Lower surface of girder on live end.
G1_D_U	Girder 1	Upper surface of girder on dead end.
G1_L_U	Girder 1	Upper surface of girder on live end.
G2_D_U	Girder 2	Upper surface of girder on dead end.
G2_L_U	Girder 2	Upper surface of girder on live end.

(f) Wirepots

Name	Over Girder Line	Description of Location
A1	Girder 1	1 ft. from end of girder on live end.
B1	Girder 1	Under load applied near inside joint (dead end test setup) or near outside joint (live end test setup) to measure vertical displacement of system.
C1	Girder 1	Under load applied near outside joint (dead end test setup) or near inside joint (live end test setup) to measure vertical displacement of system.
D1	Girder 1	1 ft. from end of girder on dead end.
A2	Girder 2	1 ft. from end of girder on live end.
B2	Girder 2	Under load applied near inside joint (dead end test setup) or near outside joint (live end test setup) to measure vertical displacement of system.
C2	Girder 2	Under load applied near outside joint (dead end test setup) or near inside joint (live end test setup) to measure vertical displacement of system.

D2	Girder 2	1 ft. from end of girder on dead end.
Jt_O	NA	Located at outside transverse joints.
Jt_I	NA	Located at inside transverse joints.

Constructability Study

The fabrication of the panels and girders and the construction of the lab mockup were well documented. During the fabrication of the girders, the practicality and ease of construction of the new shear stud detail for the horizontal shear connector system was examined. The method for forming the transverse joints, method for creating an efficient strand pattern, and method for creating the shear pockets were examined during the fabrication of the panels.

The different stages of the construction of the lab mockup were as follows:

1. Placement of the panels on the girders.
2. Pouring the grouted female-female transverse joints.
3. Epoxying the male-female transverse joints.
4. The post-tensioning operation.
5. Placing the formwork for the haunch.
6. Pouring the haunch.
7. Grouting the post-tensioning ducts.
8. Removal of the leveling bolts and lifting eyes.

The duration of each task and notes on the construction process were recorded for each stage.

Time-Dependent Testing of Lab Mockup

The strains and temperatures in the VWGs and thermocouples as well as the forces in the load cells at the dead end of the post-tensioning ducts were measured and recorded over approximately two months to investigate the time-dependent behavior of the lab mockup. Since the temperature remained fairly constant in the lab, the strains were not greatly influenced by the temperature.

The VWG data were used to provide insight into the force and moment redistribution produced by creep and shrinkage effects in the composite system. One of the primary goals was to determine whether the initial level of post-tensioning kept the transverse joints in compression. Although long term stresses could not be measured experimentally in the lab mockup, the experimental data were very useful in verifying the finite element results. The finite element models provided results over a much longer time period than two months so the long term deck stresses could be examined.

Material Testing

Compression tests and split cylinder tests of the concrete in the panels and girders were conducted at selected intervals throughout the testing program. Compression tests were also performed on the grout in the haunch.

The 4 in by 8 in cylinders were filled during the casting of the panels and casting of the girders at Bayshore Concrete Products in Chesapeake, Virginia. The next day the molds were removed. The cylinders then cured at room temperature in the Virginia Tech Structures Laboratory until the time a test was performed with one of the cylinders. The compression and split cylinder tests were performed before the release of the prestress force, at 7 days, 28 days, and during key intervals during the construction process, including the time the panels were placed on the girders, the time the post-tensioning was applied, the time the haunch was poured, and immediately before the live load testing began.

Live Load Test Setup for Lab Mockup

The live load testing program consisted of initial static tests, cyclic testing up to 2 million cycles, intermediate static tests, and final static tests. These tests were performed on both the dead end and live end of the lab mockup in the following order:

1. Initial static test at the dead end.
2. Cyclic testing at the dead end.
3. Intermediate static test at the dead end.
4. Initial static test at the live end.
5. Cyclic testing at the live end.
6. Intermediate static test at the live end.
7. Final static test at the dead end.
8. Final static test at the live end.

Each of these tests is discussed in the following sections. Ponding of water at the transverse joints was also performed before each of the load tests.

Figures 10 and 11 show the test setup on the dead end and live end. The shear pockets are left out of the figure for clarity. The loading for each of the two test setups (dead end and live end) consisted of four load patches placed symmetrically about the longitudinal centerline of the bridge. The symmetric loading was done to attempt to create the same loading on each girder. By doing so, the performance of different shear connectors could be compared. The two test setups are symmetric about the transverse centerline (midspan) of the bridge. This allowed the performance of the system with the different pocket spacings to be compared.

A spreader beam spanned between each pair of wheel loads in the transverse direction. The load was half way between the two load patches, as shown in Figure 11. For the static tests, a 400 kip hydraulic ram was used to apply the load to each spreader beam. For the cyclic tests, a closed-loop, servo-hydraulic testing system was used to apply the loadings.

Initial Static Tests for Lab Mockup

For each initial static test (prior to the cyclic testing), a load of 37.3 kips was applied at each wheel load location. This load was determined by using a typical AASHTO design wheel load of 16 kips, multiplying by an impact factor of 1.33 and a load factor of 1.75. This corresponds to a load of 74.7 k/frame (kips per frame) for each of the two frames used on a given

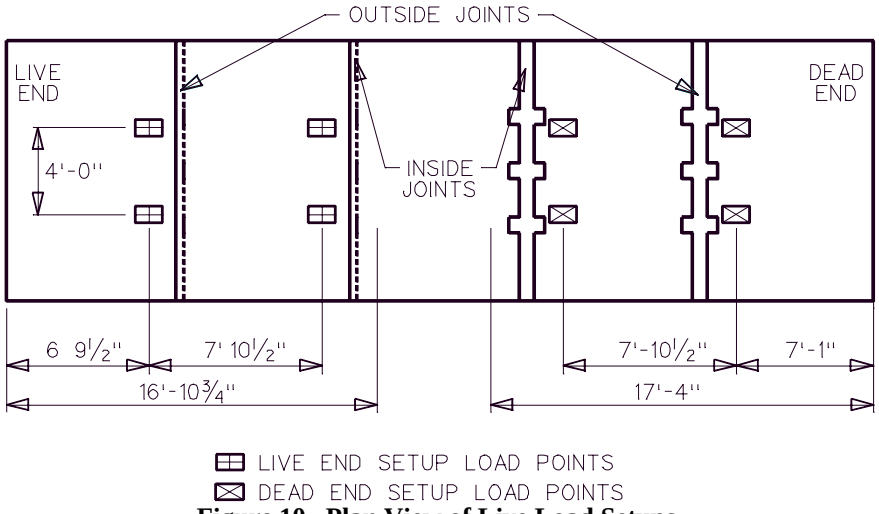

Figure 10. Plan View of Live Load Setups.

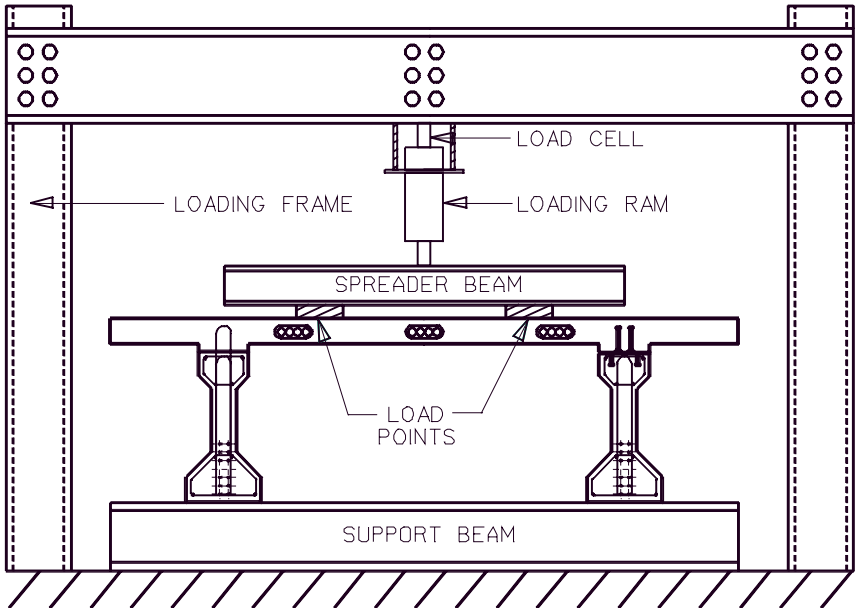

Figure 11. Elevation View of Live Load Test Setup.

test setup. The load was gradually increased up to this limit. At load increments of 20 k/frame, the bridge was inspected for cracking. The data were used to determine if full composite action between the panels and girders over each girder line remained after the load is applied. The performance of the transverse joints and different types of shear connectors was studied.

Cyclic Testing for Lab Mockup

After the initial static test, a total of 2 million cycles of loading was applied to the bridge. The number of cycles used in this study is the same as that found in previous research on precast deck panel systems by Issa[8] for similar loading conditions.

For the first 500,000 cycles, the load ranged from 2 k/frame to 29.4 k/frame. This created the AASHTO LRFD design fatigue moment of 2250 k-in for the girder, which was calculated during the design phase of the study. During the cyclic tests, a compressive force of at least 1 kip was always present to prevent rotational movement of the spreader beam and to prevent damage to the bridge. A wheel load for the next 1,500,000 cycles ranged from 2 k/frame to 44.7 k/frame. The range of the loading, 42.7 k/frame, corresponds to two typical AASHTO design wheel loads of 16 kips, multiplied by an impact factor of 1.33. This was greater than the AASHTO LRFD impact factor of 1.15 for fatigue. The load level of 42.7 k/frame produced a maximum moment in the bridge of 3520 k-in, which was 56 percent greater than the AASHTO LRFD design fatigue moment.

Every 100,000 cycles to 300,000 cycles, the cyclic testing was stopped to conduct a static test on the system. The load was gradually increased up to 44.7 k/frame. These intermediate static tests were done to see if there was any loss in stiffness in the lab mockup due to loss of composite action, cracking, sliding at the joints, etc. throughout the cyclic test program.

Intermediate Static Tests for Lab Mockup

After the cyclic testing was completed for a given test setup, an intermediate static test was performed. The purpose of this test was to attempt to capture some non-linear behavior in the results. These results offer insight into the behavior of the system after cracking, plastic behavior of the reinforcing steel, prestressing strands, and shear connectors, and relative slip at material interfaces occur. The load was gradually increased up to about 130 k/frame, or until sufficient cracking was noticed in the system but the system could still be deemed repairable. A load of 130 k/frame was predicted to cause cracking in the bottom of the girder under the inside load point and cracking at the interface between the haunch and girders.

The load was gradually increased up to this limit. At load increments of 20 k/frame, the bridge was inspected cracking. When the load was above 100 k/frame, the load increments were decreased to every 10 k/frame to 20 k/frame.

Final Static Tests for Lab Mockup

After the testing was completed on the dead end and live ends of the bridge, a final static test was performed on the dead end and then the live end. The purpose of this test was to determine the failure load and failure mode of the system. The load was gradually increased in 20 k/frame increments. The bridge was inspected for cracking at each interval. When the load was above 150 k/frame, the load increments were decreased to every 5 kips to 10 kips. When displacements started increasing in a highly nonlinear manner with respect to the applied load, the loading was switched to displacement control. The displacement increments used at this point were 0.05 in.

Durability Study of Transverse Joints

Water was ponded over the transverse joints at selected intervals. The selected intervals were:

1. Before the initial static test.
2. Before the cyclic testing.
3. Before the intermediate static test.
4. After the intermediate static test.
5. After the final static test.

Water was poured onto the bridge deck over the transverse joints until the depth of the water was approximately ¼ in to ½ in deep. The joints were monitored for a half-hour period. During this period, any leaking at the transverse joints was noted.

Analytical Study

Finite Element Analysis of Time-Dependent Behavior

The finite element software DIANA was used to carry out an analysis of the time-dependent behavior of the lab mockup to provide insight in to the prestress losses in the system as well as the effective long term stresses across the transverse joints. The results were used to examine whether the initial level of post-tensioning provided in the lab mockup was sufficient to keep the transverse joints in compression.

A staged, plane stress analysis was run in DIANA. The following was the staging used for the lab mockup:

1. Girder cured for 1.5 days.
2. The strands in the girder were cut. The girder sat and gained strength over the next 22 days.
3. The panels were cast and cured for 2.5 days. The panels then sat in the casting yard and were transported to the lab. The panels continued to sit in the lab. The same environmental conditions were assumed to exist in the casting yard and lab. The girders continued to sit in the casting yard, then the lab. The time period for this step was 71 days.
4. The panels were placed on the girders. The dead weight of the panels was transferred to the girders through the leveling bolts. The non-composite system sat in the lab for a period of 20 days.
5. The first six strands were tensioned during the post-tensioning operation in the deck. The system then remained idle for two days.
6. The last six strands were tensioned during the post-tensioning operation in the deck. The system remained idle for six days.
7. The haunch was cast. The composite system remained idle for 26 days. (This marks the end of the analysis in the lab.)
8. The composite system remained idle for an additional 25 years to look at the long term effects of the bridge.

The model consisted of one girder with a tributary deck width of 6 ft. Since the results of the finite element model were in good agreement with the results from the lab mockup, a three dimensional model was deemed unnecessary.

Eight node quadrilateral elements were used to model the panels, girder, haunch, and bearing pads. The element size used for this study was approximately 2 in x 2 in. Using 2 in x 2 in elements results in 23 elements through the depth of the composite section. The number of elements used through the depth, along with the higher order polynomial used to model the displacement field, accurately modeled the strain profile through the depth and prevented the model from having an artificially high stiffness.

The prestressing strands in the girder, the post-tensioning strands in the deck, and all the mild reinforcing steel were modeled with embedded reinforcing bars. Embedded reinforcing bars have no degrees of freedom of their own, which makes them computationally cheap. They are embedded in "mother elements," which are the elements that the embedded reinforcement passes through in the geometric layout of the model. The strains in the embedded reinforcement are calculated from the displacement fields of the mother elements. These embedded reinforcing elements contribute to the stiffness of the system.

A prestress load can be assigned to embedded reinforcement, which was required for the precast bridge deck panel system. Initial losses in the post-tensioning system such as anchor loss, wobble friction loss, curvature friction loss, and elastic shortening were calculated by DIANA. These initial losses were based on the CEB-FIP Model Code 1990.[9]

The concrete in the panels and girders, the grout in the haunch, and the steel for the prestressing steel, post-tensioning steel and mild reinforcing steel were all modeled with linear elastic materials since no cracking or yielding of the steel was anticipated during the time-dependent analysis.

In order to carry out the time steps, regular Newton-Raphson iteration was used with explicit time steps. With regular Newton-Raphson, the stiffness is updated every iteration, which typically results in fewer iterations in a given time (or load) step than modified Newton-Raphson iteration, where the stiffness is only updated at the beginning of a time (or load) step. The time steps were broken up to mimic the logarithmic behavior of the time functions for the creep coefficient and shrinkage strains. The smallest time step used was 10 seconds and the largest time step used was 1000 days.

Finite Element Analysis of Push Off Tests

Finite element models were created in DIANA for push-off specimens to propose a methodology for modeling the shear connectors and the interface between the haunch and girders and interface between the haunch and panels. The modeling methodology for the shear connectors and interfaces for the push-off tests was also used in the finite element models for and ultimate load tests of the full system. Load vs. relative displacement curves were developed from the finite element results and compared to experimental results produced by Wallenfelsz.[29]

Figure 12 shows a representation of the push off test specimen. A plane stress analysis was used first to attempt to match the experimental data. Eight node quadrilateral elements were used to model the panel, girder, shear pocket, and haunch, six node triangular elements were used to model the loading pad, three node beam elements were used to model the shear

connectors, and three node interface elements were used to model the interface between the haunch and girder. Beam elements were used instead of truss elements to include the dowel action of the shear connectors. Only the beam elements provide rotational stiffness at the nodes that the beam elements share with the plane stress elements. Interface elements were used to allow slip to occur between the girder and haunch.

It was assumed that a perfect bond existed at the interface of the shear connector(s) and the haunch and the interface between the haunch and panel. The entire length of the interface between the haunch and girder consisted of two dissimilar materials cast at different times. However, the large surface area of grout that passes through the location where the interface between the panel and haunch is located adds strength to the top interface. Therefore, it was assumed that the top interface, between the panel and haunch, was stronger than the bottom interface, between the haunch and girder and cracking would occur at the bottom interface first. This was verified by studying the cracking patterns in the lab mockup.

The paving meshing algorithm was used to vary the size of the elements in the model. The paving algorithm produces a quadrilateral mesh on any type of surface. Figure 13 shows a

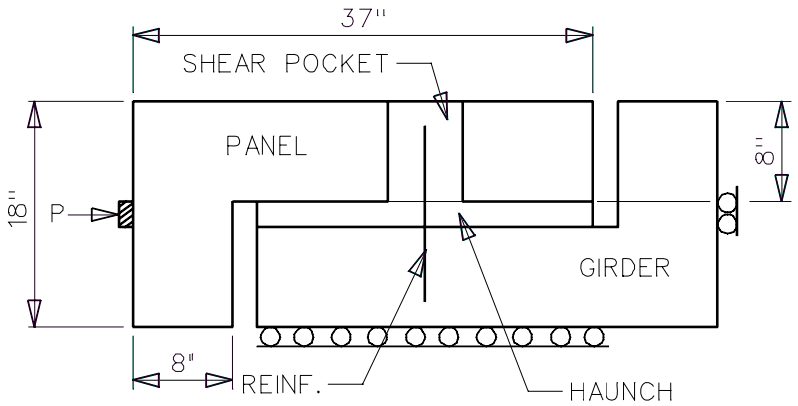

Figure 12. Push-off Specimen Modeled in DIANA.

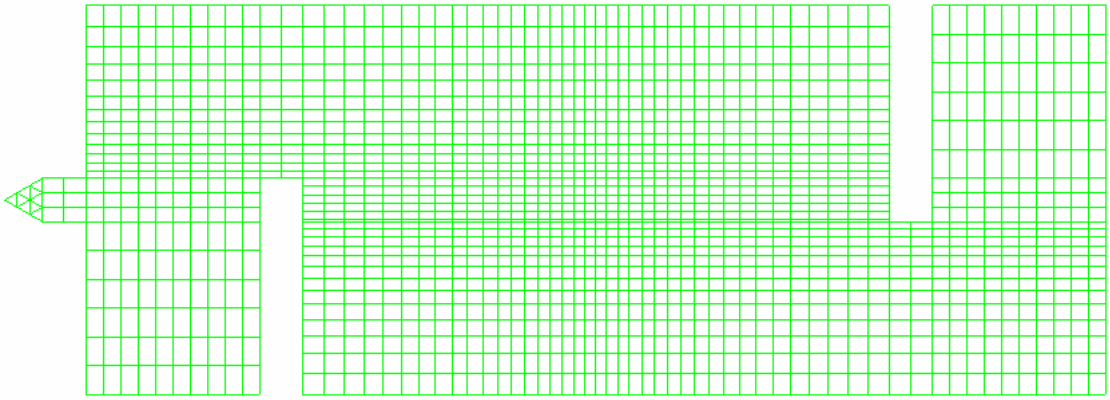

Figure 13. Mesh for Push-Off Models.

push-off test model with the paving mesh algorithm applied to generate the mesh. A mesh quality check was run to check the elements for large aspect ratios, large angle deviation at the corners, midnode offsets, warping, and bulging of the midnodes. The mesh was refined in the vicinity of the interface between the haunch and panel and the shear connectors. Localized cracking and crushing, relative slip, and large stress concentrations in the shear connectors were expected to occur at this location.

Modeling the behavior of the shear connectors in a bridge is a complex problem. When a large shear is transferred from the deck to the girder, the interface cracks causing the two surfaces to separate and slip relative to one another. In turn, a tensile force is developed in the shear connector causing a compressive force and corresponding frictional force to develop at the interface. This frictional force increases the horizontal shear capacity of the system. Accurately modeling this "clamping effect" was difficult to accomplish in DIANA.

DIANA offers several material models that can be used with interface elements. They were examined and considered for the material model for the interface. After consideration of a crack dilatancy model and a Mohr-Coulomb model, a nonlinear, elastic material was selected for the interfaces because of its stable and predictable behavior. The user specifies a normal stress vs. relative opening diagram and a tangential stress vs. slip diagram to define the behavior of the material. The tangential stress vs. slip diagram was defined such that there was still a small amount of shear resistance after the interface "cracks," as shown in Figure 14. The tangential stress vs. slip diagrams used for the push off tests were derived from data from Scholz[11] and Wallenfelsz.[10] The normal stress vs. relative opening diagram was defined such that the stiffness in the normal direction was very large.

Neglecting the clamping effect was conservative and acceptable for this type of analysis and it resulted in larger slip values and higher strains in the shear connectors. Because the strain levels and slip values were larger than expected, the acceptable number of shear connectors from the parametric study was conservative.

Cracking and/or crushing of the concrete occurred in the panels, haunch, and girders in the vicinity of the concrete interfaces and shear connectors. Two approaches were examined to

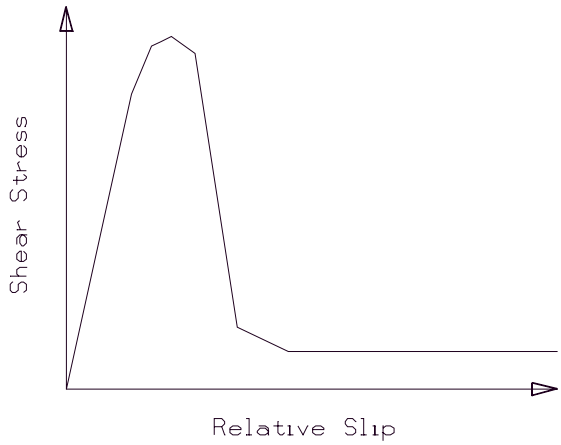

Figure 14. Tangential Stress vs. Slip Diagram for Interface Material Without Shear Connectors.

attempt to capture this local behavior: A smeared cracking approach and a softened elastic modulus approach.

For the smeared cracking approach, the smeared cracking model was activated in DIANA to model any cracks that form. The cracking model was defined by a tension cut-off model, a tension softening model and a shear retention model. A linear tension cut-off relationship was selected for the tension cut-off model, which is shown in Figure 15 with a principle stress orientation. This incorporates the influence of a biaxial stress state on the tensile strength of the concrete. As shown in Figure 15, when a compressive stress exists along one principle stress axis and tension exists along the other principle stress axis, the tensile strength is reduced.

A linear tension softening relationship was selected for the tension softening model, which is shown in Figure 16. The stress σ_{nn} and strain ε_{nn} are normal to the direction of the crack plane. The total strain is divided into an elastic strain and a crack strain. The same is applied for the total stress. In the formulation of the tension softening model, it is assumed that the crack stress is a function of the crack strain for the one crack that was formed and also assumed that coupling effects with other cracks are insignificant. The constant shear retention model was used instead of the full shear retention model. For the full shear retention model, the shear modulus is not reduced after cracking. For this constant shear retention model, the shear modulus is reduced by a user defined amount (β). For the models in this study, it was assumed that 50 percent of the shear stiffness was lost when the crack was formed (β=0.5).

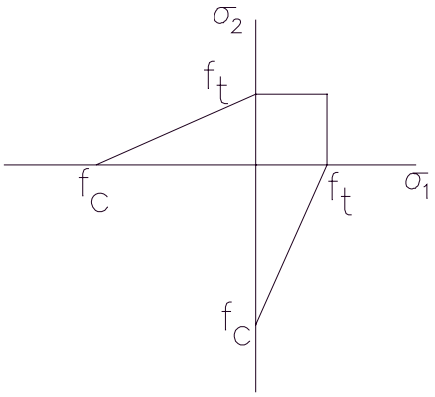

Figure 15. Tension Cut-Off Model.

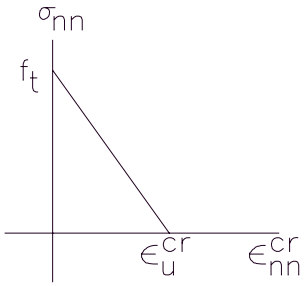

Figure 16. Tension Softening Model.

Crushing was defined by using the Von Mises failure criterion along with a uniaxial, multi-linear stress vs. strain curve to capture the plastic behavior of concrete and grout in compression. For the Von Mises failure criterion, yielding (or crushing) occurs when the distortional strain-energy density at a point becomes greater than or equal to the distortional strain-energy at yield (or crushing) in uniaxial tension or compression. The multi-linear stress vs. strain curve was based upon the modified Hogenstad model presented in MacGregor.[12] The compressive strength of the concrete for the panels and girders was 6 ksi and the compressive strength for the grout in the haunch was 4 ksi.

The second approach to modeling the local cracking and crushing at the interface between the haunch and girder in the vicinity of the shear connectors was the softened elastic modulus approach. In this approach, the region where the localized cracking and crushing occurs was assumed to have very small, constant stiffness through the entire analysis. This "cracked" region is shown in Figure 17. The stiffness was reduced by decreasing the elastic modulus for the grout in the haunch and concrete in the girder. The factor that the elastic modulus was reduced by and the size of the cracked region was determined from the results of the push-off tests run with the smeared cracking approach.

The softened elastic modulus approach produced more stable convergence behavior when attempting to capture the unloading portion of the load vs. displacement curve for the push-off tests. This was because the cracking that occurred was localized and the smeared cracking approach was better suited for capturing cracking on a global scale. The results of the two approaches discussed above were compared and one was selected to run the remaining finite element analyses.

The material for the shear connectors was modeled with the Von Mises failure criterion with a uniaxial stress vs. strain curve, similar to the approach for modeling the crushing of the concrete described above. A nominal stress vs. strain curve for Grade 50 steel was used for the shear studs and a nominal stress vs. strain curve for Grade 60 steel was used for the hooked reinforcing bars.

The preliminary models were run with force control and displacement control and were compared to make sure the results and behavior of the system were the same. Displacement controlled analyses were run for the remaining push off test models. Secant iteration was used with adaptive load steps to carry out the load steps. In general, secant iteration results in more stable convergence behavior than other iteration methods when strong nonlinearities, such as cracking, are involved. This is because the stiffness remains positive even when unloading is present for the load vs. displacement curve.

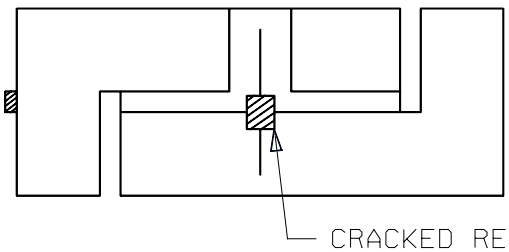

Figure 17. Cracked Region for Softened Elastic Modulus Approach.

Two methods were used to define the load steps. For smaller applied load levels, explicit load steps were used where preliminary analyses indicated the relative slip values were very small, cracking was not extensive, and only the onset of yielding may have occurred in the shear connectors. The size of the load steps was determined from the convergence behavior and decreased in size as the total applied load became larger. For higher applied load levels, an adaptive load stepping scheme was used where cracking started to become more extensive, relative slip values started to become larger, the stresses in the shear connectors were well into the plastic range, and the behavior of the system became harder to predict. DIANA determined the size of the next load step based on the user specified desired number of iterations per load step, the actual number of iterations in a given load step, a maximum step size, and a minimum step size.

Finite Element Analysis of Live Load Tests for the Mockup

A series of plane stress finite element analyses were carried out to examine the flexural and shear capacities of the deck panel system compared to predicted values from the design calculations, any unloading behavior, shear connector behavior, and pocket spacing influence. The failure mode of each model was investigated. Both the live end setup and dead end setup of the lab mockup were used to examine the behavior of the lab mockup. The entire bridge was modeled in DIANA. One girder was modeled at a time with a 6 ft tributary deck width.

A verification study and a parametric study were carried out to examine the behavior of the deck panel system. For the verification study, the lab mockup was duplicated in DIANA. Because only one girder was modeled at a time and two load conditions were examined (live end setup and dead end setup) the following models were examined for the verification study:

1. Girder 1 with dead end setup for static tests (4 ft pockets – hooked bars),
2. Girder 2 with dead end setup for static tests (4 ft pockets – shear studs),
3. Girder 1 with live end setup for static tests (2 ft pockets – hooked bars),
4. Girder 2 with live end setup for static tests (2 ft pockets – shear studs).

The load vs. displacement curves, shear connector strains, strain profiles, cracking patterns in the girder, and cracking patterns in the haunch and interface between the haunch and girder were examined and compared.

Once the results of the finite element models were compared to the experimental results, the parametric study was conducted. The parametric study consisted of varying the amount of shear connectors in each pocket and the distribution of the shear connectors among the pockets. This provided additional information about the influence of the pocket spacing and connector type on the behavior of the deck panel system. The capacities of the models were compared to AASHTO LRFD provisions.

A total of 11 different models were examined for the parametric study. Six of the models were run with No. 5 hooked reinforcing bars as shear connectors and five of the models were run with ¾ in diameter shear studs as shear connectors. Table 3 shows the number of shear connectors per pocket for each model examined with a given shear connector type. Model

Table 3. Number of Shear Connectors per Pocket for Parametric Study

(a) Hooked Reinforcing Bars

Model Name	MOCKUP	1_100	1_75	1_50	8_R	8_L
Pocket #						
1	8	8	6	4	4	6
2	8	7	5	4	4	6
3	8	6	5	3	4	6
4	8	6	4	3	4	6
5	8	5	4	2	4	2
6	8	4	3	2	4	2
7	8	4	3	2	4	2
8	8	3	2	2	4	2
9	8	2	2	1	4	2
10	8	1	1	0	4	2
11	8	3	2	1	6	2
12	10	6	4	3	6	6
13	10	9	7	5	6	6
14	16	12	9	6	6	10
15	16	15	11	8	6	10
Total #	140	91	68	46	70	70

(b) Shear Studs

Model Name	MOCKUP	1_100	1_75	8_R	8_L
Pocket #					
1	6	7	6	3	6
2	6	6	4	3	6
3	6	6	4	3	6
4	6	5	3	3	3
5	6	5	3	3	3
6	6	4	3	3	3
7	6	4	3	3	0
8	6	4	3	3	0
9	6	3	2	3	0
10	6	3	2	3	0
11	6	4	3	4	0
12	8	7	5	4	0
13	8	9	6	4	5
14	12	11	8	4	9
15	12	13	9	4	9
Total #	106	91	64	50	50

MOCKUP had the exact number of shear connectors used for the lab mockup. Model 1_100 had close to the exact number of shear connectors required per pocket using Equation 1. Model 1_75 had approximately 75 percent of shear connectors required per pocket using Equation 1. Model 1_50 had approximately 50 percent of shear connectors required per pocket using Equation 1. Model 8_R had close to the number of shear connectors required using Equation 8. The shear connectors were distributed in an even manner among the pockets. The connectors were also distributed among the shear pockets so the dead end and live end of the bridge had approximately the same amount of shear connectors. Model 8_L had close to the

number of shear connectors required using Equation 8. Unlike model 8_R, the shear connectors were distributed among the pockets such that more shear connectors were placed in locations with high shear stresses. The results of different models were compared using load vs. displacement curves, Von Mises stresses in the shear connectors, and cracking patterns.

Figure 18 shows the mesh for the finite element model. The mesh was refined in the vicinity of the interface between the haunch and girder. Eight node quadrilateral elements were used to model the panels, haunch, girder, and bearing pads. Three node beam elements were used to model the shear connectors. Only the beam elements provide rotational stiffness at the nodes that the beam elements share with the plane stress elements. Three node interface elements were used to model the interface between the haunch and girder. Embedded reinforcing bars were used to model the vertical shear stirrups, the mild longitudinal reinforcing steel, the strands for post-tensioning in the panels, and the strands for prestressing in the girder.

The smeared cracking approach was used instead of the softened elastic modulus approach for two reasons. The first reason was that the cracking in the haunch and the girder in the vicinity of the shear connectors was not as localized as it was for the push-off specimen. The cracking was smeared along the 1 ft 0 in to 1 ft 6 in length of the shear pockets. The second reason was that the load vs. displacement curve for the lab mockup did not have an unloading portion. Therefore, consideration did not need to be given to replacing the cracking model with a softened elastic modulus approach to stabilize the convergence behavior. The models were run under force control since the load vs. displacement curve did not have an unloading portion.

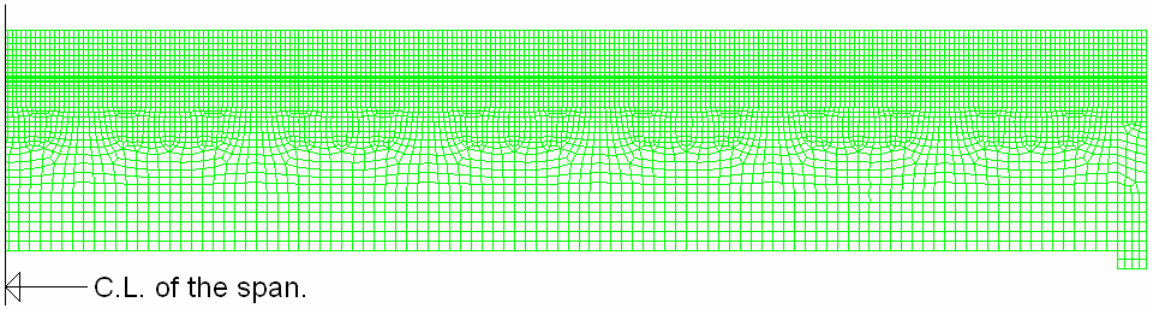

Figure 18. Mesh for Live Load Tests on Lab Mockup.

RESULTS

Experimental Results

Fabrication and Constructability Study

Fabrication of the Girders

The formwork, the reinforcement cage, and the stressing of the prestressing strands for the girders were done on 12/12/05 and 12/13/05. The stressing bed was set up so the two girders were in a single line with the prestressing strands running the length of the entire stressing bed. Refer to Sullivan[7] for more information on the layout of the girders during casting.

Upon arrival at Bayshore on 12/12/05, it was determined that one of the shear connector plates had a conflict with a lifting eye. The lifting eye consists of several strands that are bent to form a hook protruding from the top of the girder. The steel plates were to be installed after the concrete was cast in girder 2. Therefore, it was not possible to cast plate 5 with the top flange because the lifting eye was in the way. In order to solve the problem, a long slot approximately 8 in by 2 in was cut in the steel plate. Caution was exercised not to cut too close to any of the existing studs or near a location where a future stud was to be shot. Figure 19 shows the slot cut in plate 5.

The girders were instrumented with the VWGs and thermocouples on 12/13/05 from approximately 8 a.m. to 12 p.m. The concrete was placed on 12/13/05 at 3 p.m. and the pour lasted approximately 1 hour. The air temperature was approximately 30 °F. Girder 2 was poured first followed by girder 1. Four by 8 in cylinders were filled during the pour for the material testing phase of the study. The QC (quality control) employees at Bayshore reported that the air content in the mix was 7.4 percent, the slump was 8½ in, and the temperature of the concrete mix was 54 °F. The concrete mix design is given in Appendix E of Sullivan. The same mix design was used for the panels. The expected slump in the mix design was between 0 in and 7 in. The expected air content in the mix design was between 3 and 7 percent.

One of the last steps was the placing the steel plates in the top flange of girder 2. The construction crew had difficulty in getting each steel plate into place. The problem was not associated with the length of the plates. The construction workers had no problem lifting the plates to the top of the formwork. The problem encountered was trying to fit the steel plates in between the formwork. The width of the steel plate was 12 in and the top flange width of the girder is 12 in. Slight deviations in the width of the plate or width between the side forms will cause the steel plate not to fit. In order to solve the problem, the construction workers had to remove selected yolks. A yolk is shown in Figure 2. The yolks tie the top of the forms together to keep the dimension correct and prevent side forms from bowing outward from the hydraulic pressure of the fresh concrete. After the yolk was removed, a come-a-long was used to

Figure 19. Slot in Steel Plate for Lifting Eye.

secure the side forms temporarily while the steel plate was hammered into place. Then the come-along was tightened and the yolk was hammered back in to place. It is recommended for future projects that a non-full width steel plate be used.

The beams were steam cured from approximately 10:00 p.m. on 12/13/05 until approximately 9:00 a.m. on 12/14/05. Cylinders were broken the morning of 12/13/05 and compressive strength of the girders was greater than the required compressive strength at release. The prestressing strands were cut on 12/14/05 at 10:30 a.m.

Fabrication of the Panels

The formwork, the reinforcement cage, and the stressing of the prestressing strands for the panels were done on 12/22/05 and 12/23/05. The layout of the prestressing bed is shown in Figure 20 and Figure 21. Each of the five panels had a unique strand layout because of the layout of the horizontal shear connector block-out pockets. When consulting with Bayshore engineers during the production of the shop drawings, an attempt was made to reduce the number of strand patterns. With some effort, the number of strand patterns was reduced to three. It is considerably less expensive to have one strand pattern so all the panels can be cast at once. If each panel was cast separately, the entire bed would be used for each operation wasting several hundred feet of strand each time a panel was cast. Instead, all of the strands required for all five panels were run the entire length of the stressing bed. When a strand passed through a given panel that did not call for that particular strand in the strand pattern, it was debonded. The strands were debonded by wrapping a plastic tube around the strand (see Figure 21).

The blockouts for the shear pockets consisted of foam blocks and can be seen in Figures 20 and 21. The transverse joints were formed by attaching wood blocks conforming to the dimensions of the transverse joint to the side form of the stressing bed.

Figure 20. Layout of Stressing Bed for Precast Panels.

Figure 21. Formwork for Transverse Joint.

On 1/4/06 the panels were instrumented with VWGs and thermocouples from 8 a.m. until 11 a.m. The pour took place from 3:20 p.m. to 4:10 p.m. Cylinders were filled during the pour for the material testing phase of the study. Concrete from the first of two batches was used to fill the cylinders. The QC employees at Bayshore reported that the air content in the mix was 5.4 percent, the slump was 8 in, and the temperature of the concrete mix was 54 °F.

The stressing bed was steam cured from approximately 10:00 p.m. on 1/4/06 until approximately 9:00 a.m. on 1/5/06 when the strands were originally suppose to be cut. Cylinders were broken the morning of 1/5/06 and compressive strength of the panels was slightly less than the required compressive strength at release, so the panels were steam cured for an additional day. On 1/6/06 at 11 a.m. the strands were cut.

Placement of Precast Panels on Girders

When the panels and girders were delivered to the Virginia Tech Structures Laboratory, they were temporarily stored until construction was ready to begin. The girders were set on the reaction floor of the lab and the panels were stacked on top of each other (see Figure 22).

Support beams were bolted to the floor beams, and bearing pads were placed on top of the support beams. The bearing pads were placed so the center-of-bearing to center-of-bearing span was 39 ft and the center-to-center spacing of the two girders was 8 ft. The diagonal distances between the girders were measured to make sure the girders were square with one another.

The panels were placed on the girders on 3/16/06 from 3:00 p.m. until 4:40 p.m. Three members of the Virginia Tech research team completed the operation. Timber 2 x 4s were placed on top of the girders prior to placing the panels. The leveling bolts were installed at a later date. The wood blocks that the panels originally rested on can be seen in Figure 21.

The hooked reinforcing bars greatly hindered the placement of the panels. The shear pockets were only made 2 in longer on each side of the outside hooked reinforcing bars. The hooked reinforcing bars were placed within an acceptable tolerance, but not exactly per the shop

Figure 22. Girders with Wood Blocks in Place for Panel Erection.

drawings. Therefore, there was less than 2 in of play to use when placing the panels. This proved to be especially difficult when placing the panels in which the transverse joints were a male-female configuration. Each panel had to be placed on top of the girders and slid together. In many cases, the length of the male protrusion in the male-female joint of 1 in was very close to the distance from the edge of a shear pocket to the edge of the first hooked reinforcing bar in a shear pocket.

Using the grouted female-female joint allows for the panels to be placed directly on the girders, without having to slide the panels together. The size of the gap between adjacent panels with this joint configuration can be adjusted during construction to account for any small errors that occurred during the fabrication process.

The detail with the steel plate and shear studs cast with the top flange of the girder proved to be easy to deal with when placing the panels. Since there were no studs to interfere with the placing of the panels, the panels could be moved freely on girder 2.

The leveling bolts were installed after all the panels were in place. Typically three leveling bolts are used for each panel. Three leveling bolts are used instead of four leveling bolts to avoid warping the panels. Several of the bolts could not be installed immediately because the coil inserts were not flush with the bottom of the panels. This problem was solved by using a jack hammer to widen the hole above the coil insert. This allowed the leveling bolt to be installed at the same angle as the coil insert. Steel plates approximately 3 in x 3 in x ½ in were placed on top of the girders where the leveling bolts bear on the girders, as shown in Figure 23. Without the steel plates, it was possible that the leveling bolt might crush the concrete in the area it was bearing, creating a small hole in the top flange of the girder. With the leveling bolt in a hole, a significant frictional force would develop between the leveling bolt and girder during the post-tensioning operation. This would introduce problems with a portion of the post-tensioning force being transferred to the girders during the post-tensioning operation.

Figure 23. Leveling Bolt Bearing on Steel Plate.

When the leveling bolts were adjusted so the panels were close to the final elevations, the wood blocks were removed. Surveying equipment was used to adjust the panels to their final elevation.

Next, the post-tensioning strands were fed through the ducts to assure that all four strands could fit through each duct. Long ropes were then tied around each group of strands. The strands were pulled though the dead end until the strands were only present in panel 1, panel 2, and panel 3. This was done to allow panel 4 to be removed for the epoxying of the male-female joints. Once panel 4 was back in place, the rope was used to quickly pull the strands back through panel 4 and 5 so the stands could be post-tensioned shortly after the epoxy was placed.

Grouting the Female-Female Transverse Joints

The grouted female-female joints were formed with ¾ in plyform. Weather stripping was placed around any edges where leaks could possibly occur. The size of the blockout at the PT ducts was 6 in by 9 in on each side of the joint. This allowed enough room to place the duct coupler in the joint and wrap duct tape around the duct segments to prevent grout from leaking in. The lower plywood forms were suspended on thin, threaded metal rods. At the top of the deck, the rods were threaded through holes in short lengths of pipe, which spanned across the joint. This system required one of the Virginia Tech research team members to hold the plyform in place under the bridge while feeding the threaded metal rod through the hole in the plyform to another person on top of the bridge deck. The person would then slide a washer and nut over the top of the rod and tighten it. The steel pipe with the threaded metal rod is shown in Figure 24 in a completed joint.

The grout was poured on 3/28/06. The grout used for the female-female joints was Five Star® Highway Patch. The product data sheet is found in Appendix F of Sullivan.[7] This grout was selected based on a recommendation provided by Wallenfelsz.[10] The grouting operation took place from 1:00 p.m. to 1:45 p.m. Three members of the Virginia Tech research team completed this operation. The hopper used for mixing the grout is capable of mixing 2 - 50 lb bags of grout. The hopper was placed on top of the bridge deck within 5–10 ft of the transverse joints. One person mixed the grout in the hopper, one person poured the grout into the joints, and the other person helped pour bags of grout in to the hopper, vibrate the grout into place, and

Figure 24. Grouted Female-Female Joints with Steel Pipe and Threaded Metal Rod Forming Alternative.

level off the top surface of the grout to be even with the top of the deck. Because the grout sets up quickly, minimal leakage occurred through the bottom formwork.

Epoxying of the Male-Female Transverse Joints

The transverse joints were epoxied on 4/5/06 from 1:20 p.m. to 1:50 p.m. Sikadur 31 Slow Set – SBA was used. This is an epoxy specially formulated for segmental bridges, and was provided at no cost to the research team. Panel 4 was suspended approximately 1 ft above its final elevation. Panel 4 was chosen in order to minimize the number of panels moved during the operation. Expansive foam was placed around the perimeter of the post-tensioning ducts. This was done to prevent epoxy from leaking into the duct.

Epoxy was then placed on each side of panel 4 using chemical resistant gloves. This procedure is shown in Figure 25. Once the panels were in place, the rope was used to pull the strands back through the ducts in panel 4 and panel 5. Three members of the Virginia Tech research team performed the epoxying operation. One person operated the crane to lift panel 4

Figure 25. Epoxy Being Placed on Male-Female Joint.

and placed expansive foam around the edges of the ducts while the other two people placed epoxy on the edges of panel 4. After the procedure was completed, the ends of the transverse joints in the overhangs were not in firm contact. At the time, it was believed these small gaps would close up after the post-tensioning operation was completed.

Post-Tensioning Operation

The first six strands were post-tensioned on 4/5/06 from 2:20 p.m. to 4:00 p.m. The last six strands were post-tensioned on 4/7/06 from 9:30 a.m. to 2:30 p.m. Six strands tensioned to approximately 68 percent of the guaranteed ultimate tensile strength results in a pressure just over 130 psi on the transverse joint. Typically, 50 psi is considered a minimum to adequately seat an epoxied joint. The strands were labeled strand 1 through strand 12. Strand 1 was closest to girder 1 and Strand 12 was closest to girder 2. The strands were stressed in the following order: strand 6, strand 7, strand 2, strand 3, strand 10, strand 11, strand 5, strand 8, strand 9, strand 12, strand 1, strand 4. The strands were tensioned in this order to keep the longitudinal stress distribution in the deck as uniform as possible in the transverse direction.

Three people were used when the first six strands were stressed and one person was used when the last six strands were stressed. Before each strand was released, a mark was spray painted on the dead end of the strand a known distance from the edge of the panel. This mark was measured again after the force was released to determine the dead end seating loss.

Typically, strands in flat four strand ducts are stressed individually with a special mono-strand jack. However, since the mono-strand jack was not used for the lab mockup, a stressing chair had to be used to tension each strand. The stressing chair consisted of three steel tubes welded together as shown in Figure 26.

A hydraulic ram, a small metal tube used as a spacer, a load cell, and a chuck were placed over the strand. Each strand was stressed to approximately 28 kips, measured with the load cell. Twenty eight kips is approximately 68 percent of the guaranteed ultimate tensile strength of a ½ in diameter grade 270 strand. A load cell was also placed at the dead end of one strand in each

Figure 26. Stressing Chair Used for Lab Mockup.

post-tensioning duct. After the full stressing force was achieved, the wedges were inserted into the anchor plate and tapped in with a hammer. The force was then gradually released by the hydraulic ram.

Based on the measurements, a force profile for each strand along the length of the bridge was determined and the force and stress across each transverse joint was calculated. These forces and stresses are shown in Table 4. A table summarizing the calculations can be found in Appendix G of Sullivan.

The deflections of the system were measured with dial gages before and after the deck was post-tensioned. There was no change in the deflection, indicating that none of the post-tensioning force was transmitted to the girder through the leveling bolts. The steel plates the leveling bolts bore on provided a smooth enough surface to allow the panels to slide when the force in the strands was applied.

After all the strands were tensioned, the ends of the transverse joints were still not in complete contact with one another. The panels were in firm contact at the center of the transverse joints. After further observation, it appeared that the ends of panels were bowed, which could have been caused by bowed formwork. To seal the joint, additional epoxy was injected in to the male-female joints on 5/12/06.

Table 4. Force and Stress Across Each Transverse Joint

Transverse Joint	Force (kips)	Stress (psi)
Outside Epoxied	306	266
Inside Epoxied	308	268
Inside Grouted	310	269
Outside Grouted	312	271

Shooting the Shear Studs

After the post-tensioning operation was performed and before the haunch and shear pockets were poured, the shear studs were shot to the steel plates on girder 2. This operation was performed by one member of the Virginia Tech research team. In order to properly weld the shear studs to the plates, the plates must be connected to one another by small, steel bars. This allows the current to flow from one plate to another. Ceramic ferrules and dirt were removed from the top surface of the girders with an air hose before pouring the haunch.

Grouting the Haunch and Shear Pockets

The formwork for the haunch was placed on 4/11/06 from 10:30 a.m. to 12:00 p.m. and from 5:30 p.m. to 8:10 p.m. Plyform sheets were used to form up the sides of the haunch. Weather stripping was placed between the bottom of the panel and top of the plyform to seal the gap at this interface. The plyform was secured to the girder with concrete stud anchors spaced at approximately 14 in. This is shown in Figure 27.

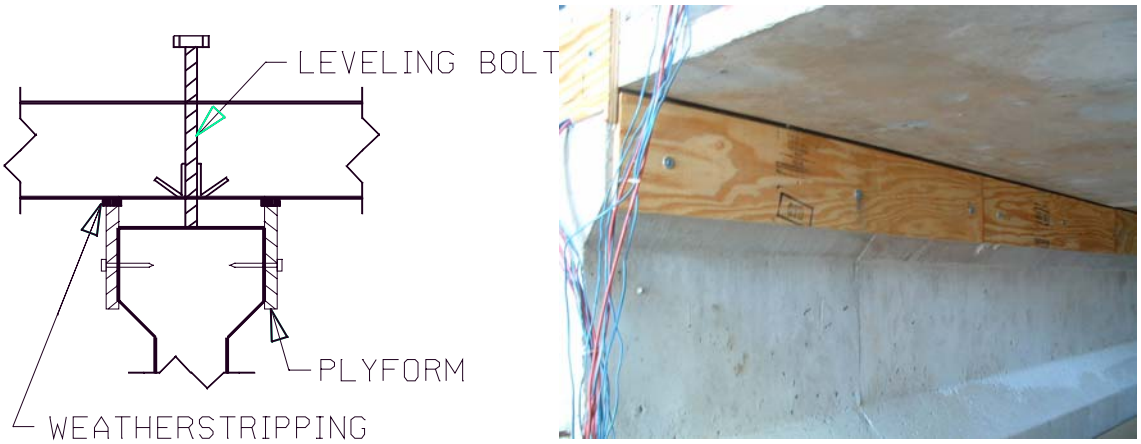

Figure 27. Formwork Detail for Haunch.

The haunch and shear pockets were poured on 4/13/06. The haunch and shear pockets for girder 2 were poured from 2:10 p.m. to 2:55 p.m. The haunch and shear pockets for girder 1 were poured from 3:10 p.m. to 3:40 p.m. Grout cubes were filled from the first few wheelbarrows for the girder 2 pour.

The grout was mixed in a gasoline powered mortar mixer placed outside the lab. The grout used was Five Star® Highway Patch, the same grout used for the female-female transverse joints. After mixing, each batch of grout was then placed in a wheelbarrow and transported to the bridge via a forklift. The forklift placed the wheelbarrow on the bridge deck and the grout was poured into a shear pocket directly from the wheelbarrow. Two wheelbarrows were used during the operation. The grout was vibrated into place. Eight members of the Virginia Tech research team were used to perform this operation. The crew consisted of three people mixing and transporting the grout, two people using wheelbarrows to place the grout into the shear pockets, one person vibrating the grout, and one person shoveling the grout into the shear pockets. One person was also responsible for the grout cubes and pictures.

Many of the early batches of grout were stiff and set rapidly. After mixing several batches of grout, the members of the research team responsible for mixing and transporting the grout were able to produce fairly consistent mixes that were not too stiff.

The formwork was removed on 4/14/06 from 4:30 p.m. to 6:10 p.m. This was done by one member of the Virginia Tech research team. Although the grout was vibrated at each shear pocket to help the grout flow through the haunch to the next shear pocket, a few locations were not completely filled with grout. The two most noticeable locations were at midspan of girder 1 and girder 2. There were gaps in the haunch in between the shear pockets that were almost the entire depth of the haunch. The length of the gaps was about 4 in. Since these gaps occurred at favorable locations where shear stresses are close to zero, the gaps were not filled with grout.

The leveling bolts were removed on 4/17/06. This process was performed by one member of the Virginia Tech research team. The process took one hour to complete. The bolts had to be removed by using an air powered gun. The process for removing a bolt leaves a void

in the haunch and a hole that runs from the top of the deck to the top of the girder. The holes were not filled with grout, however in a field application they would be.

Grouting the Post-Tensioning Ducts

A hand powered Kenrich grout pump was used to grout the post-tensioning ducts. Three members for the Virginia Tech research team were used for this operation. One person operated the hand pump and two people mixed the grout. Five Star® Special Grout 400 with Devoider® Automatic Cavity Preventer was used to fill the post-tensioning ducts. This is a special grout used primarily for this type of application.

Before grouting, the blockouts for the post-tensioning anchorage device were completely grouted at the live end. At the dead end, the gaps were sealed with an expansive foam. The blockouts for the post-tensioning anchorage device at the dead end could not be filled with grout because of the load cells that were in place. The mortar mixer was used to mix batches large enough to fill an entire duct. The grout was pumped in at the live of each duct until grout was flowing freely from the vent on the dead end. Then both vents were sealed.

During grouting, several small leaks occurred at the epoxied male-female joints as the grout was being pumped through. Note that this occurred prior to the additional epoxy injected into the transverse joints on 5/12/06. No leaks occurred at the grouted male-female joints as the grout was pumped into the post-tensioning ducts.

This completed the construction phase of the research program. Other operations performed in the field that were not performed on the lab mockup include but are not limited to:

1. Milling the surface of the deck,
2. Placing a barrier rail,
3. Placing a wearing surface.

Time-Dependent Behavior

Temperature and Strain Measurements During Fabrication

Figure 28 shows the strains in Girder 1 up until 24 minutes after the strands were cut and Figure 29 shows the temperature in Girder 1 up until 24 minutes after the strands were cut. Refer to Table 2 for the notation for each gage presented in the legend of the following figures. The strains in the girder increased fairly linearly up until about 0.35 day from the moment the concrete was cast. From this point until the strands were cut, the strains decreased as the temperature increased.

The temperature increased steadily initially and then began to drop around 0.79 day. This coincides with the time the formwork was removed. Temperature evolution, strength gain, elastic modulus gain, bond development, and other effects make it difficult to determine the stress in the concrete immediately prior to cutting the strands.

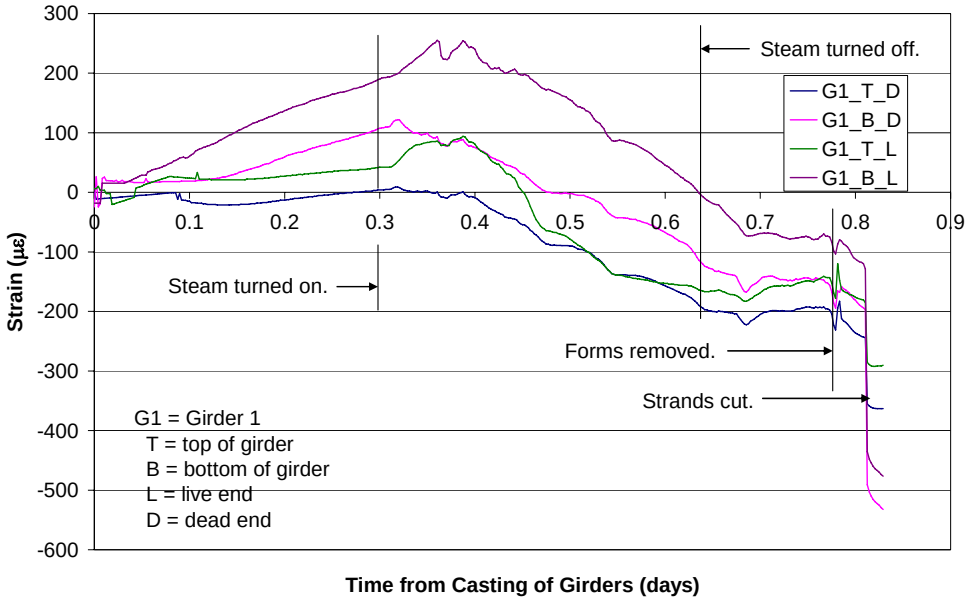

Figure 28. Variation of Strain with Time During Casting and Strand Release for Girder 1.

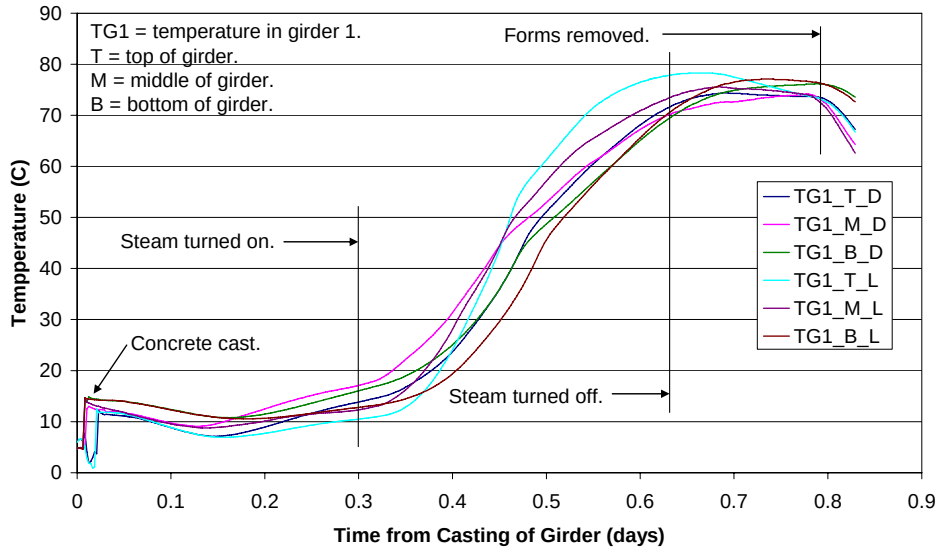

Figure 29. Variation of Temperature with Time During Casting and Strand Release for Girder 1.

At release of the prestressing strands, Figure 28 shows that the net increase in compressive strain is greater in the bottom of the girder than in the top of the girder, as expected. Similar behavior is observed for girder 2 during casting (see Sullivan Appendix H). The average elastic loss in girder 1 using the vibrating wire gage data was -8.56 ksi. The average elastic loss in girder 2 using the vibrating wire gage data was -9.31 ksi. The elastic shortening loss, calculated assuming an elastic modulus of 28,500 ksi, was -9.62 ksi.

Time-Dependent Behavior During Construction

After the panels and girders were shipped to the Virginia Tech Structures Lab, the Campbell system was reattached to the lab specimen. Data from the VWGs were gathered from the time the panels were placed on the girders until the end of the time-dependent study. Figure 30 presents the strains in girder 1, Figure 31 presents the strains in girder 2, and Figure 32

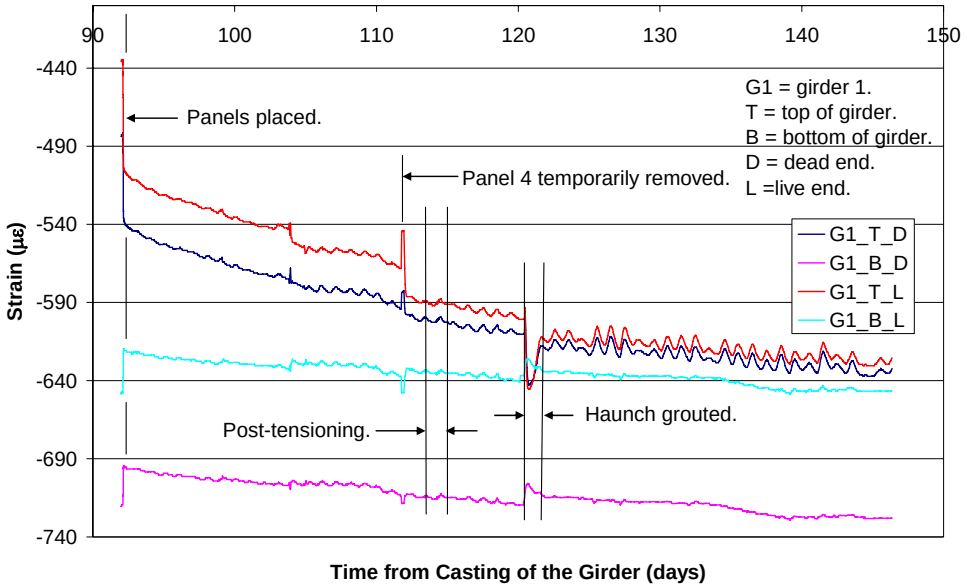

Figure 30. Variation of Strain with Time for Girder 1 in Lab.

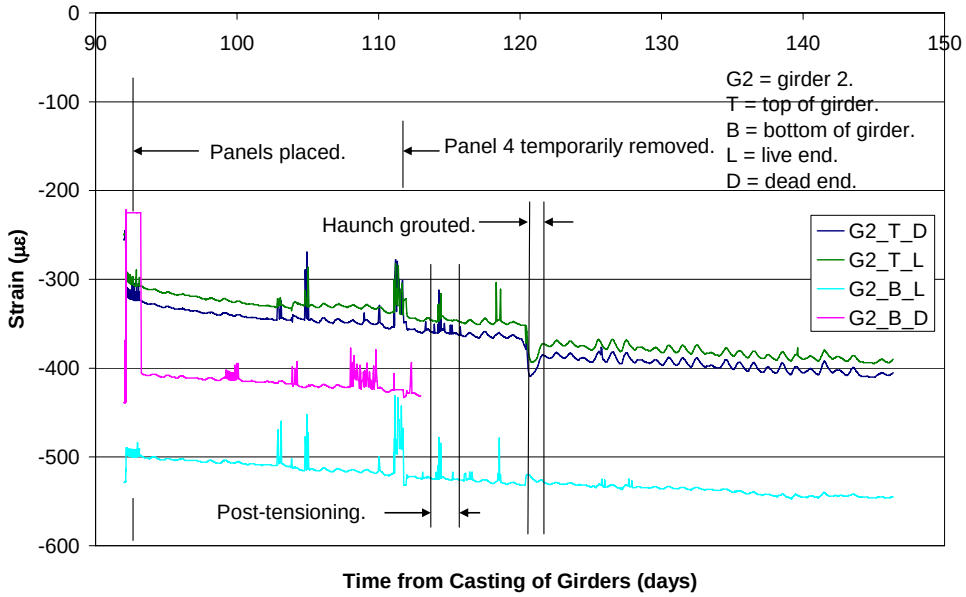

Figure 31. Variation of Strain with Time for Girder 2 in Lab.

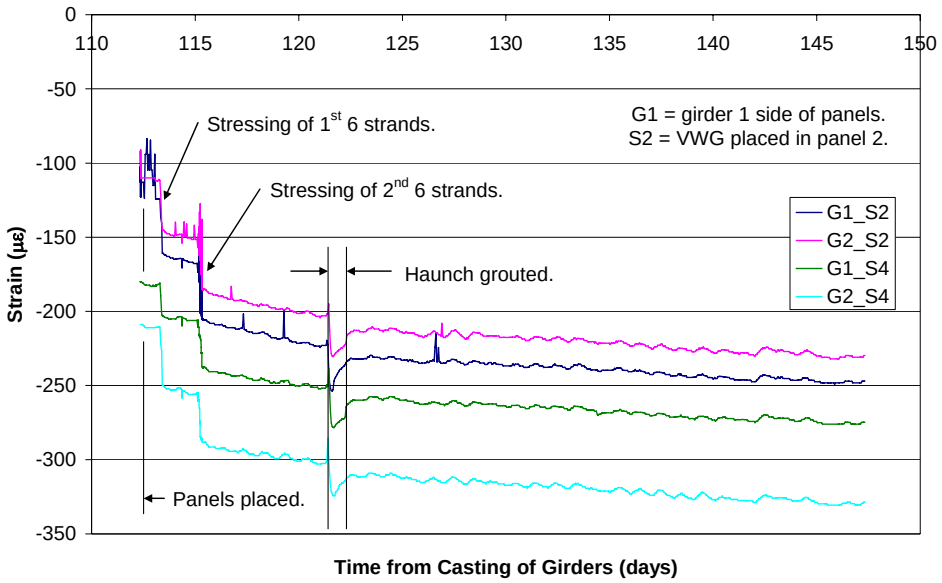

Figure 32. Variation of Strain with Time for Precast Panels in Lab.

presents the strains in the panels during the time intervals in the lab. Figure 33 displays the curvature in girder 1 during the time intervals in the lab. Notice that the start of the analysis in the lab is measured from the time the girders were cast. The general behavior of each member is discussed here along with the effects that key construction stages have on the system. The sign convention is positive (+) for tensile strains and tensile strain increments and negative (-) for compressive strains and compressive strain increments. The sign convention for curvature is positive (+) when the deck is in compression and the bottom of the girder is in tension and negative (-) when the deck is in tension and the bottom of the girder is in compression.

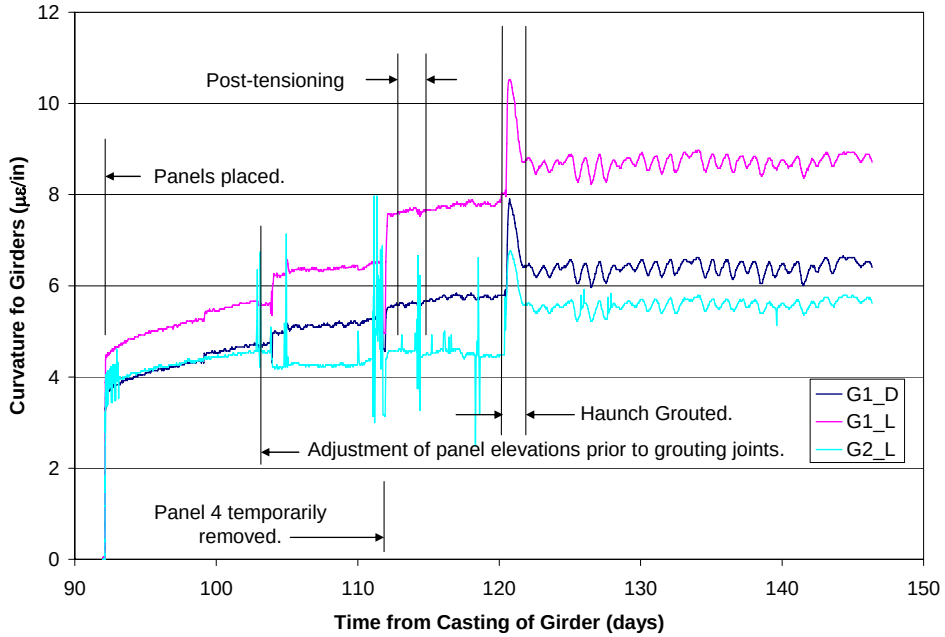

Figure 33. Variation of Curvature with Time for Girder 1 and Girder 2 in Lab.

During the 92nd day from the time the girders were cast, the panels were placed on the girders. The elastic strains associated with adding the panels are shown by an instantaneous gain or loss in strain in the plots. Table 5 compares the average VWG strains in the girders to the expected strains in the girders.

One of the first trends observed in the data in Figure 30 and Figure 31 is that the steel plate in the top flange in girder 2 apparently does act as compression reinforcement by reducing creep strains. The creep strains the girders experience were calculated from immediately after the panels were added to the end of the analysis. The total time increment is 54 days. The average creep strain associated with the two VWGs in the top flange on girder 1 was -107 με. The average creep strain associated with the two VWGs in the top flange of girder 2 was -88 με. This was a small, but noticeable difference in strain. Although there are five separate, discontinuous steel plates in girder 2, they still function as compressive reinforcement to some degree.

These creep strains are not only associated with the dead load of the panels, but also the dead load of the haunch, as well as from additional forces and moments introduced in the girder over time caused by differential creep and shrinkage in the composite system. Creep associated with the dead load of the composite system will cause the system to deflect downward. Creep associated with the prestressing in the girders will cause the system to deflect upward. Creep associated with the change in the post-tensioning force in the deck after composite action is present will cause the system to deflect downward. Differential shrinkage will cause the system to deflect downward since the panels were cast after the girders. These individual quantities are difficult to extract from the total creep and shrinkage measured by the VWGs.

During day 113 and day 115, the first six strands and last six strands were tensioned in the post-tensioning ducts of the panels. There was some concern prior to the operation that some of the post-tensioning force might be transferred to the girders via frictional forces developed at the interface between the leveling bolts and the top surface of the girders. However, there was no indication that any significant force was transferred to the girder, as shown in Figure 30 and Figure 31.

As can be seen in Figure 32, the average elastic strain in the four VWGs in the deck panels associated with the post-tensioning was -75 με. The expected elastic strain associated with the post-tensioning force was -66 με. The creep strains the panels experience were calculated from immediately after the completion of the post-tensioning operation to the end of the analysis. The total time increment was 34 days. The average creep strain associated with the four VWGs in the panels was -40 με.

Table 5. Comparison of Measured and Calculated Strains for Panel Placement on Girders

	VWG Measurement (με)		Calculated (με)	$\varepsilon_{VWG\_avg}/\varepsilon_{calc}$
VWG Location	**Girder 1**	**Girder 2**		
Top	**-62**	**-56**	**-72**	**0.82**
Bottom	**27**	**32**	**40**	**0.74**

During day 120, the haunch was cast. The system cambered upward during this process due to a temperature gradient introduced in the system from the heat of hydration. Figure 34 shows the variation in temperature in girder 1 during the casting process. The temperature change was greatest in the deck and smallest in the bottom of the girder.

Figures 30 to 34 can be used to examine the behavior of the system from the effects of the haunch being poured. Initially, the system cambered upward due to the temperature increase at the top of the girder. As the grout cooled, and began to shrink, the system deflected downward. However, the bridge did not return to its original position.

When comparing the strains in the girders and panels from day 120.25 to day 121.5, it is clear that residual strains and a residual curvature develop in the system. The changes in strain and curvature may be due to shrinkage of the haunch, the varying axial thermal strains and thermal strain gradients, and the change from a non-composite system to a composite system, as well as the dead load of the haunch. From a research standpoint, the effects from thermal strains and shrinkage strains arising from the casting of the haunch do influence the behavior of the system during the casting operation. However, the net effect they had was negligible and does not need to be considered in design.

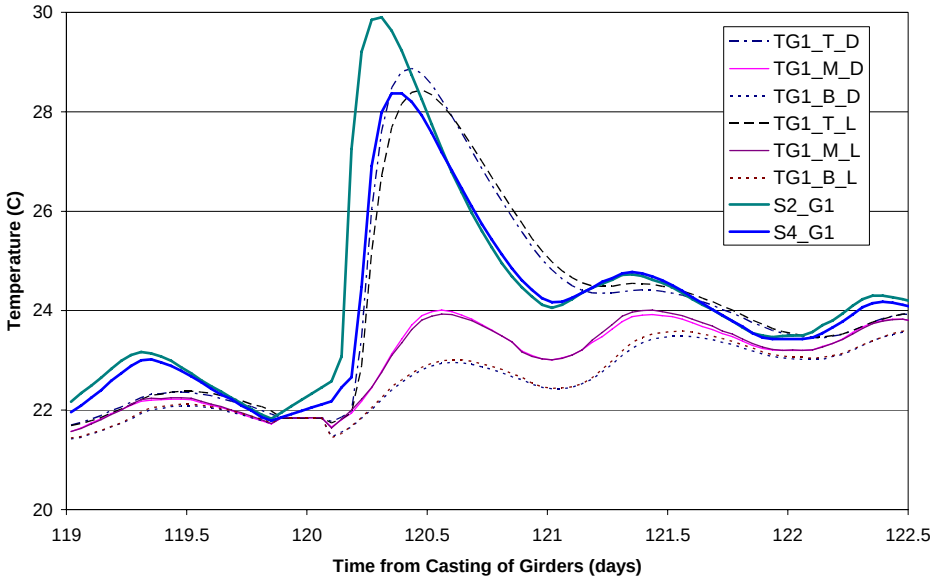

Figure 34. Variation of Temperature with Time in Girder 1 During Casting of Haunch.

Material Testing

Compression tests and split cylinder tests were performed to measure the compressive strength and tensile strength of the concrete in the panels and girders as well as the cube compressive strength of the grout in the haunch. The tests adhered to ASTM standards ASTM C 39: Standard Test Method for Compressive Strength Cylindrical Concrete Specimens,[13] ASTM C 496: Standard Test Method for Splitting Tensile Strength for Cylindrical Concrete Specimens,[14]

and ASTM C 109: Standard Test Method for Compressive Strength of Hydraulic Cement Mortars Using 2 in Cube Specimen (modified).[15] These tests were performed at key intervals during construction and testing. Figure 35 shows the results from the compression tests and Figure 36 shows the results from the split cylinder tests. Note that the compressive strength reported for grout in the haunch is the *cube* compressive strength.

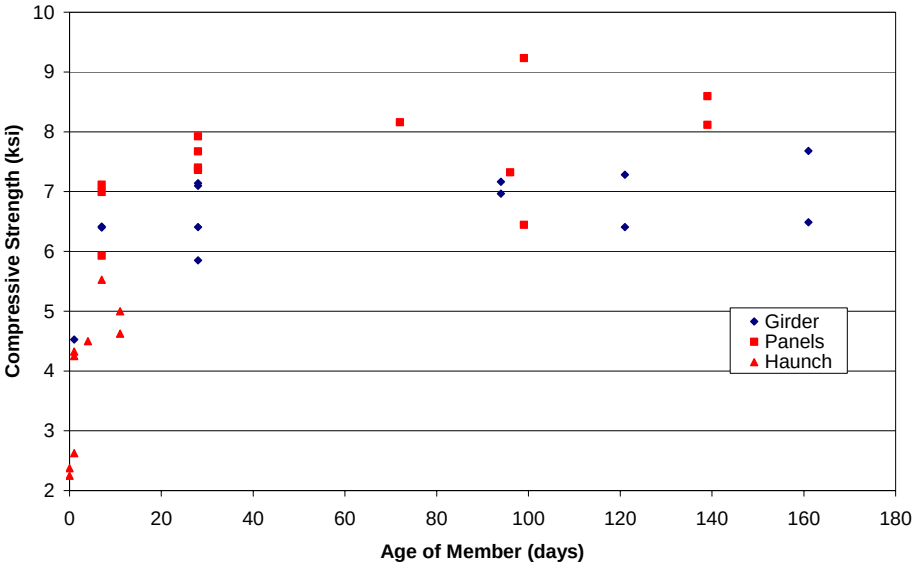

Figure 35. Compressive Strength of Materials Used for Lab Mockup.

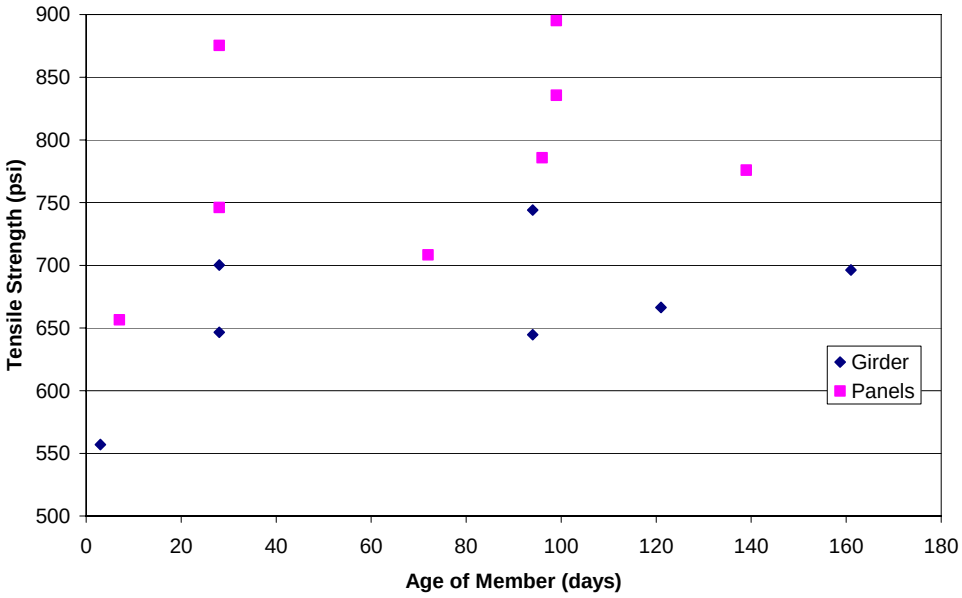

Figure 36. Tensile Strength of Materials Used for Lab Mockup.

The moduli of elasticity of the concrete used in the girders and panels were calculated using the VWG data at stages where elastic deformations took place. For the girders, the modulus of elasticity was calculated at the release of strands for the girders and at the time the panels were placed on the girders. For the panels, the modulus of elasticity was calculated at the time the strands were post-tensioned in the deck.

At the release of the strands in the girders, the average modulus of elasticity calculated using the VWGs was 4220 ksi for the girders. The average modulus of elasticity was calculated using the equation

$$E_{VWG} = \frac{1}{8}\sum_{i=1}^{8} \frac{1}{\varepsilon_{VWG}}\left(\frac{-P}{A_g} - \frac{Pe_g y_{VWG}}{I_g} + \frac{My_{VWG}}{I_g}\right) \quad [9]$$

Where: ε_{VWG} = strain in the top or bottom vibrating wire gage
P = prestressing force in the girder at the time the strands were released (kips)
A_g = cross sectional area of the girder (in^2)
I_g = second moment of area of the girder (in^4)
e_g = eccentricity of the strand group in the girder (in)
y_{VWG} = distance from the centroid of the girder to the location of the top or bottom VWG (in)
M_{g_DL} = dead load of the girder at the location of the VWG, 13 ft-4 in from the supports (k-in)

The eight VWGs produced eight moduli of elasticity, which were averaged. The value of the modulus of elasticity at the release of the strands in the girders was 3830 ksi when using the equation presented in Section 8.5.1 of ACI 318. The compressive strength used to calculate the modulus of elasticity was 4.52 ksi.

When the panels were placed on the girders, the average modulus of elasticity calculated using the VWGs was 6380 ksi for the girders. The average modulus of elasticity was calculated using the equation

$$E_{VWG} = \frac{1}{8}\sum_{i=1}^{8} \frac{M_{p\_DL} y_{VWG}}{I_g \varepsilon_{VWG}} \quad [10]$$

where, M_{p_DL} = dead load moment of the panels at the location of the vibrating wire gages (VWG), 13 ft 4 in from the supports (k-in). The value of the modulus of elasticity when the panels were placed on the girders was 4790 ksi using the ACI 318 equation. The compressive strength used to calculate the modulus of elasticity was 7.06 ksi.

At the time the strands were post-tensioned in the deck, the average modulus of elasticity calculated using the VWGs was 3580 ksi for the panels. The average modulus of elasticity was calculated using the equation

$$E_{VWG} = \frac{P_{average}}{A_{deck}\frac{1}{4}\sum_{i=1}^{4}\varepsilon_{VWG}} \quad [11]$$

Where: $P_{average}$ = the average post-tensioning force in the deck along the length of the lab mockup (kips)

A_{deck} = cross sectional area of the deck (in^2)

The four VWG in the panels were averaged to produce the average modulus of elasticity, as shown in Equation 11. The value of the modulus of elasticity at the time the strands were post-tensioned in the deck was 4880 ksi using the ACI 318 equation. The compressive strength used to calculate the modulus of elasticity was 7.32 ksi. Table 6 presents a summary of the comparisons for the elastic moduli calculations.

Table 6. Comparison of VWG Calculation and ACI 318 Calculations for Elastic Moduli

	f'c (ksi)	E_{VWG} (ksi)	E_{ACI318} (ksi)	E_{VWG}/E_{ACI318}
Strand Release for Girders	4.52	4220	3830	1.10
Panel Placement	7.06	6380	4790	1.33
Post-Tensioning of Deck	7.32	3580	4880	0.73

Live Load Testing on Dead End

Initial Static Test on Dead End

Figure 37 shows the deflections of the dead end of the lab mockup during the initial static test at the outside loading point and at the inside loading point (see Figure 11 for test setup). When the final load of 68.6 k/frame was reached, no cracking was observed in the girders or panels, the LVDTs showed no indication of relative slip, and the strains in the shear connectors were well below the nominal yield strain.

Cyclic Testing on Dead End

The lab mockup was subjected to 2 million cycles of load. Static tests were performed approximately every 100,000 cycles. Figure 38 shows the deflections at the dead end of the lab mockup at a load of 40 k/frame with respect to the number of cycles. There was an increase in the deflection of girder 2 after 1.7 million cycles. However, neither the LVDTs nor strain gages in the shear studs indicate girder 2 was experiencing a loss in composite action. Measurements of strain at the level of the prestressing strand indicate that the increase in tendon stress from 0 to 40 k/frame was less than 2 ksi, and that there was no significant change in that stress over the 2 million cycles. The strains in the shear connectors were also very small. The largest strain observed was 16 με, which was less than 1 percent of the nominal yield strain. This indicates the shear connectors were not engaged in resisting the horizontal shear stresses developed during the cyclic testing. There was no cracking at the transverse joints and no relative vertical movement between adjacent panels was measured by the wirepots. No cracking was observed in the girder or deck. The cyclic testing had minimal effects, if any, on the degree of composite action in the lab mockup

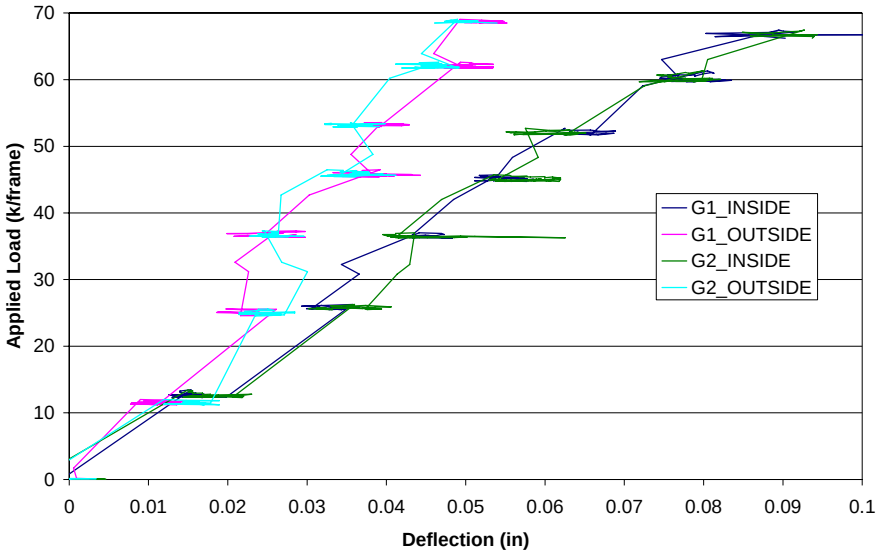

Figure 37. Deflection During Initial Static Test at Dead End.

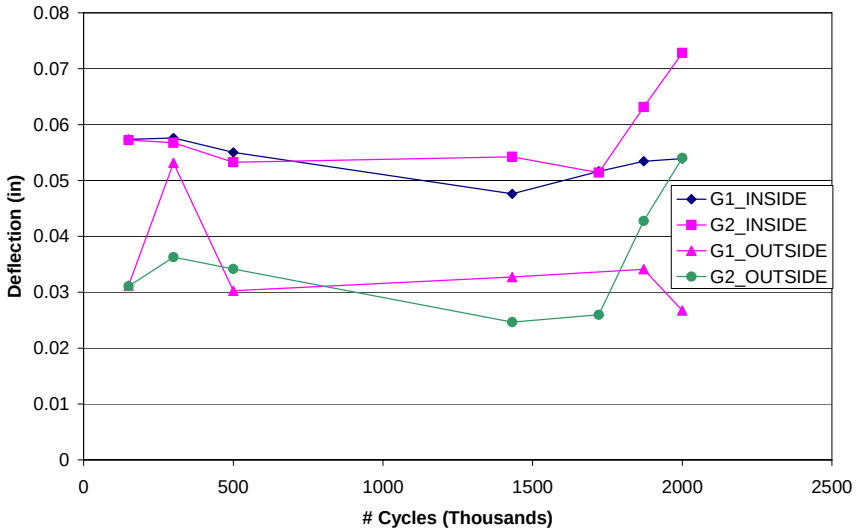

Figure 38. Variation of Deflections at 40 kips with Number of Cycles at Dead End.

Intermediate Static Test on Dead End

Figure 39 shows the deflections of the dead end of the lab mockup during the intermediate static test at the outside loading point and at the inside loading point. Signs of web shear cracking occurred around 65 to 70 k/frame. The first web shear crack was calculated to shear capacity (V_{n_punch}) of 126 k. The calculations for the punching shear capacity are shown in Sullivan.[7] The punching shear failure is shown in Figure 40. In order to continue with the testing, the locations of the wheel loads shown were changed from a transverse spacing of 4 ft to 8 ft. With the modified live load setup, the wheel loads were centered over the girder, preventing a punching shear from taking place.

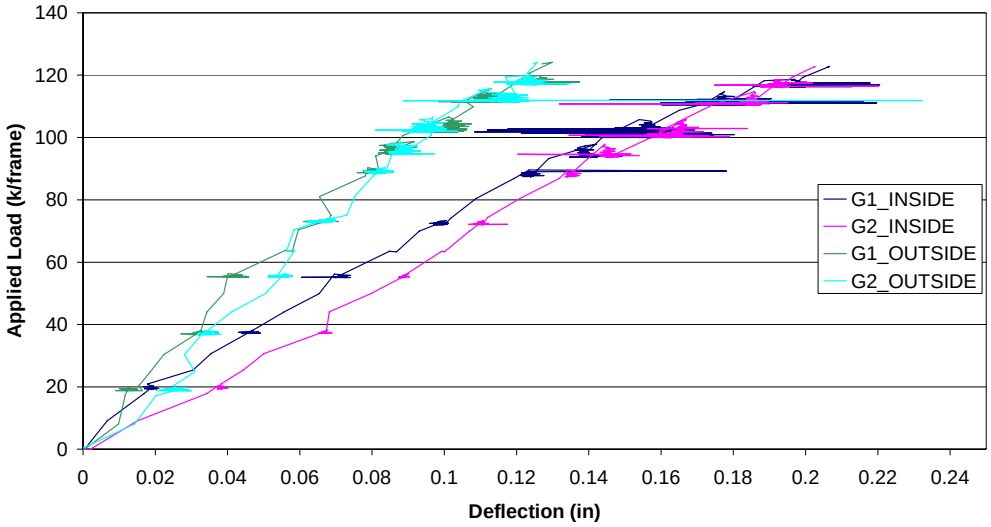

Figure 39. Deflections During Intermediate Static Test at Dead End.

(a) **(b)**

Figure 40. Punching Shear Failure at Dead End (a) Bottom Surface of Deck (b) Top Surface of Deck.

occur at 119 k/frame. This was based on an elastic analysis, comparing the principle stresses in the girder to the modulus of rupture. Web shear cracking was more pronounced at 96 k/frame. Flexural cracks occurred at the bottom of the girders, under the inside load point at 118 k/frame. The first flexural crack was calculated to occur at 126 k/frame. When the final load of 123 k/frame was reached, significant web cracking was observed. Measured crack widths varied from 0.005 in to 0.009 in. Crack lengths as long as 29 in were measured. The angles at which the cracks formed and propagated were estimated to be between 35° and 45°. The lab mockup was unloaded at 123 k/frame to prevent further damage that might have influenced the results for the live load testing at the live end. According to the data, no relative slip occurred at the transverse joints or at the horizontal interfaces at the haunch.

The strain levels in the shear connectors were less than 2 percent of the nominal yield strain. No relative slip occurred at the horizontal interfaces and no relative vertical movement

occurred between adjacent panels. The intermediate static test had minimal effects on the degree of composite action of the lab mockup.

Final Static Test on Dead End

During the final static test, the load was increased up to 249 k/frame. At this load, a punching shear failure occurred under the wheel load located adjacent to the outside female-female joint and adjacent to girder 1. The wheel load causing the punching shear failure was 125 k, compared to the design punching shear capacity (ϕV_{n_punch}) of 113 k and nominal punching.

Figure 41 shows the deflections of the dead end of the lab mockup during the final static test at the outside loading point and the inside loading point. At an applied load of 256 k/frame, there was a significant decrease in stiffness. One reason for the decrease in stiffness may be from the prestressing strands in the girders exceeding the nominal yield strain of the prestressing strands. The load at which the prestressing strands exceed the nominal yield strain was calculated to be 269 k/frame. When 272 k/frame was reached, the load was intentionally reduced to 237 k/frame. The load was then increased up to 287 k/frame.

Another contributor to the decrease in stiffness may be a loss of composite action. Cracking at the interface between the haunch and girder occurred at 209 k/frame for girder 1, and 183 k/frame for girder 2. As the load increased, the cracks continued to propagate. No cracking was observed at the interface between the haunch and deck panels for the entire range of loading. This was believed to be attributed to the large portion of the interface between the panels and haunch that passes through the shear pockets. This part of the interface consists of a monolithic pour of grout through the depth of the shear pocket. The entire interface between the girder and haunch consists of two dissimilar materials cast at different times.

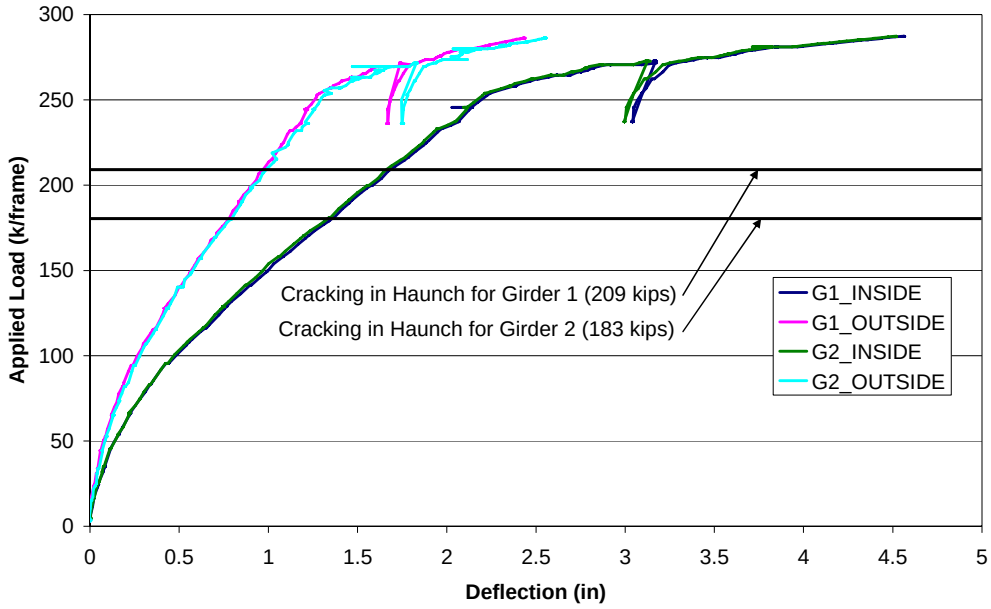

Figure 41. Deflections During Final Static Test at Dead End.

Figure 42 shows the strains in the shear connectors for the final static test. At an applied load of 256 k/frame, the rate at which the strains increased with respect to the load increased. This indicated that the shear connectors were engaged in resisting the horizontal shear stresses as the cracking at the interface between the haunch and girder continued to increase. The strains in the shear connectors were less than 50 percent of the nominal yield strain for the entire range of applied loads. The LVDTs indicated there was no relative slip even though there was cracking at the interface between the haunch and girder and the strain rate in the shear connectors increased.

Figures 43 and 44 show the cracking pattern at the dead end of girder 1 and girder 2. The cracking pattern for the two girders was very similar. As the load increased, the flexural cracks propagated through the depth of the girder and new flexural cracks continued to develop and propagated at locations away from the inside loading points. At 200 k/frame, some of the flexural cracks between the two loading points became flexural shear cracks as the direction of the crack propagation turned toward the inside loading points. Web shear cracks formed anywhere between 2 ft and 4 ft from the end of the girder at an approximate orientation of 35° to 45° and propagated in both directions. One end of a web shear crack propagated toward the support and the other end of the web shear crack propagated toward the outside load point. At 243 k/frame, flexural cracks formed in the deck panels. Flexural crack widths were as large at 1/8 in in the girders.

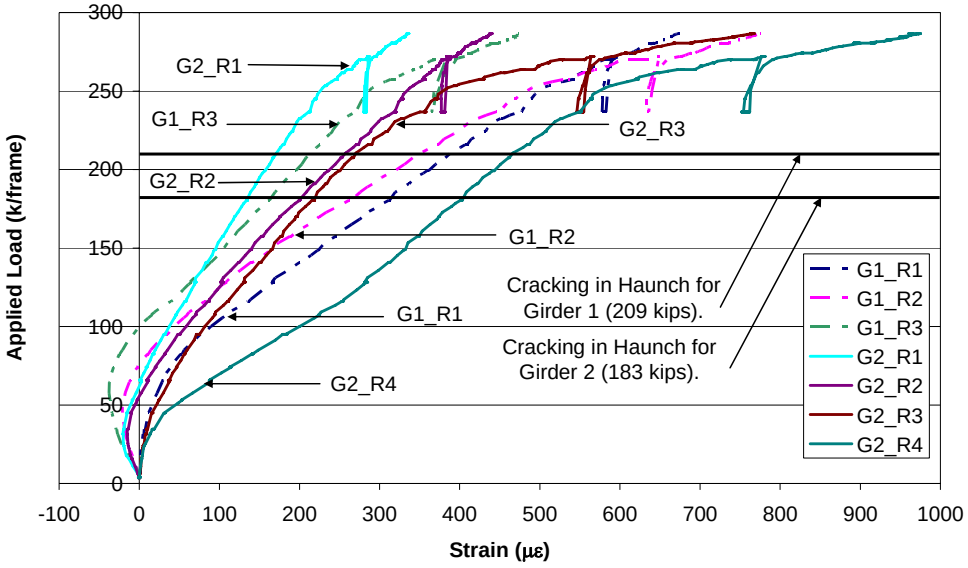

Figure 42. Connector Strains During Final Static Test at Dead End.

Figure 43. Cracking Pattern at Dead End for Girder 1 During Final Static Test.

Figure 44. Cracking Pattern at Dead End for Girder 2 During Final Static Test.

The cracking at the interface between the haunch and girder was more extensive in girder 2, compared to girder 1. Additionally, the cracking at the interface between the haunch and girder occurred at a smaller applied load for girder 2. Recall the interface between girder 2 and the haunch consisted of grout from the haunch and the steel plates that were cast with girder 2. The interface between girder 1 and the haunch consisted of grout from the haunch and concrete from girder 1, which has a higher cohesion value. The wirepots at the female-female transverse joints indicated there was no relative vertical movement at the joints.

After the final static test, the bottom surface of the deck between the two girder lines was examined and cracking at the inside and outside grouted female-female joints was observed. The cracking occurred at the interface between the grout for the joint and the concrete for the panels. Because cracking patterns were not monitored at this location during the test for safety reasons, the load at which the cracks occurred was unknown. However, after the conclusion of the first

final static test where the punching shear occurred, no cracking was observed at the grouted female-female joints. Therefore, the load at which the grouted female-female joints cracked was greater than 249 k/frame.

At 287 k/frame, crushing occurred on the top surface of the bridge deck, adjacent to the inside load points. The applied axial load of 287 k/frame results in an actual flexural capacity of 23,700 k-in, which was slightly less than the calculated flexural capacity of the lab mockup, which was 24,800 k-in. This calculation is shown in Appendix A of Sullivan.[7]

Both the shear studs and the hooked reinforcing bars performed exceptionally well as shear connectors for 4 ft pocket spacing. The strains in the shear connectors were less than 50 percent of the nominal yield strain. Additionally, the deflections at the inside load points and outside load points were the same for girder 1 and girder 2.

Live Load Testing on Live End

Initial Static Test on Live End

During this test the load was increased monotonically to a load of 70.2 k/frame. At this load, no cracking was observed in the girders or panels. There was no cracking at the transverse joints and no relative vertical movement between adjacent panels was measured by the wirepots. No cracking was observed at the horizontal interfaces at the haunch. The LVDTs also showed no indication of relative slip. The strains in the shear connectors were well below the nominal yield strains. The maximum deflection under the inside load point was approximately 0.11 in, which is slightly larger that observed on the dead end. The cracks that formed at the dead end during the intermediate static test may have more of an influence on the behavior of the live end than originally anticipated.

Cyclic Testing on Live End

The lab mockup was subjected to 2 million cycles of load. Static tests were performed approximately every 100,000 cycles. Figure 45 shows the deflections of the live end of the lab mockup at 40 k/frame with respect to the number of cycles that had been performed. The deflections changed very little over the course of cycling. Similar to the dead end tests, the increase in stresses in the prestressing strands were small (less than 2 ksi), and there was no variation over the course of cycling.

The strains in the shear connectors were less than 1 percent of the nominal yield strain. Similar to the cyclic test results for the 4 ft pocket spacing, the shear connectors were not engaged in resisting the horizontal shear stresses developed during the cyclic testing for 2 ft pocket spacing.

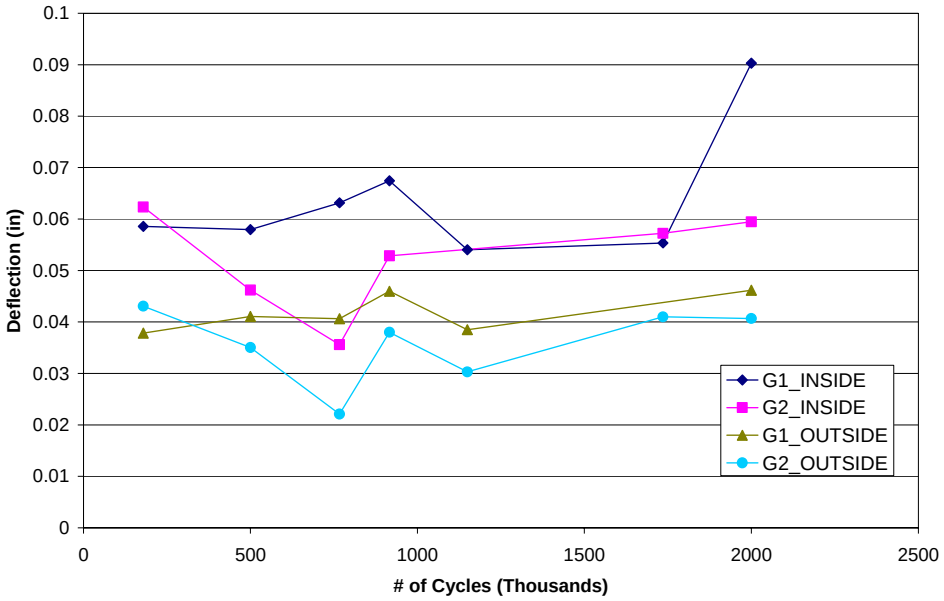

Figure 45. Variation of Deflections at 40 kips with Number of Cycles at Live End.

Intermediate Static Test on the Live End

Figure 46 shows the deflections of the live end of the lab mockup during the intermediate static test at the outside loading point and the inside loading point. The load was increased up to 159 k/frame for each load frame. This corresponds to 4.94 times the AASHTO wheel load of 16 k. There is evidence of nonlinear behavior in Figure 46 for applied loads greater than 130 – 140 k/frame. Web shear cracking occurred at 113 k/frame. The web shear cracking was more significant at 148 k/frame. The first web shear crack was calculated to occur at 119 k/frame. This was based on an elastic analysis, comparing the principle stresses in the girder to the modulus of rupture. The crack widths in the web ranged from 0.007 in to 0.016 in when the peak load of 159 k/frame was reached. The angles at which the cracks propagated ranged from 26° to 45°. Flexural cracks formed underneath the applied load points and between the applied load points. The flexural cracks initiated at an applied load of 122 k/frame and continued to propagate through the depth until the applied load reached 159 k/frame. The first flexural crack was calculated to occur at 126 k/frame. At this point, the test was stopped. The flexural crack widths varied from 0.008 in to 0.016 in when the peak load of 159 k/frame was reached.

At 139 k/frame, there were cracks in the haunch. This cracking in the haunch occurred over a length of 20 in. However, no relative slip occurred at this location. Although cracking in the girder had decreased the stiffness of the system, it was believed that the decrease in stiffness was not from a loss in composite action and that full composite action still was present. This was verified by examining the strain levels in the shear connectors. The maximum strain was 133 με, which was 8 percent of the nominal yield strain. This indicated there was not any relative slip to engage the shear studs and cause them to yield. The epoxied male-female joints also showed good performance. No visible cracking was noticed and there was no relative vertical movement at the epoxied male-female joints.

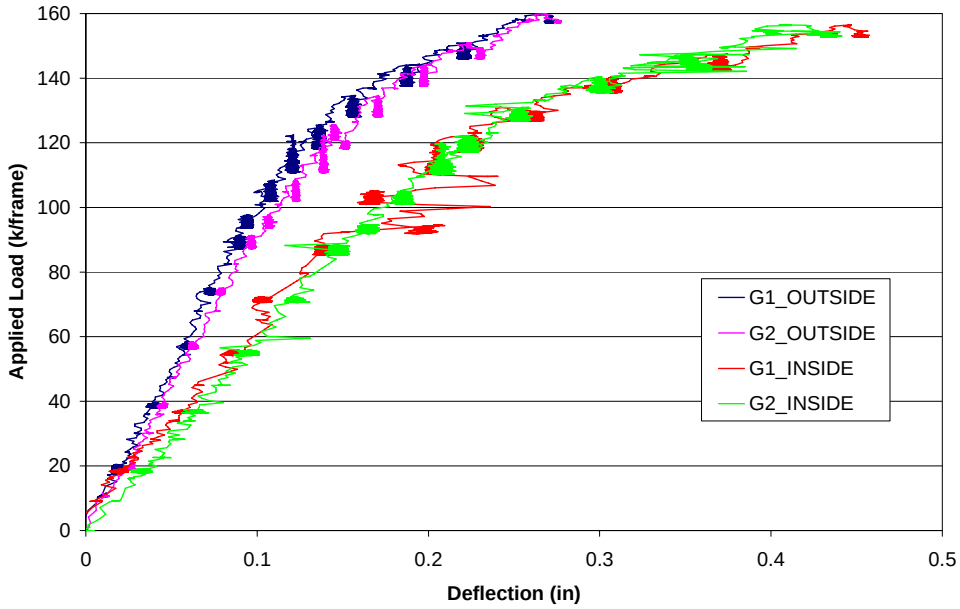

Figure 46. Deflection During Intermediate Static Test at Live End.

Final Static Test on Live End

Figure 47 shows the deflections of the live end of the lab mockup during the final static test at the outside loading point and the inside loading point. The initial stiffness of the lab mockup at the loading points was less than the initial stiffness at the loading points during the initial static test and intermediate static test on the live end. This was due to the many loading and unloading cycles the dead and live end underwent along with the cracking that occurred during the intermediate static test and final static test at the dead end and during the intermediate static test at the live end.

At an applied load of 296 k/frame, the lab mockup was completely unloaded. The stiffness of the lab mockup as it was unloaded was similar to the initial stiffness before the final static test. After the lab mockup was completely unloaded, the residual deflection was 0.96 in at the outside load point and 2.07 in at the inside load point. The residual deflections can be attributed to:

1. Cracks that remained open upon unloading.
2. Residual strains in the prestressing strands and mild reinforcing steel.
3. Residual slip at the interface between the haunch and girder from rough cracks.

Cracking occurred at the interface between the haunch and girder at applied loads of 260 k/frame and 196 k/frame for girder 1 and girder 2, respectively. The rate at which the strains in the shear connectors increased with respect to the applied load was greater than the strain rate increase prior to cracking in the haunch. Figure 48 shows the strains in the shear connectors for

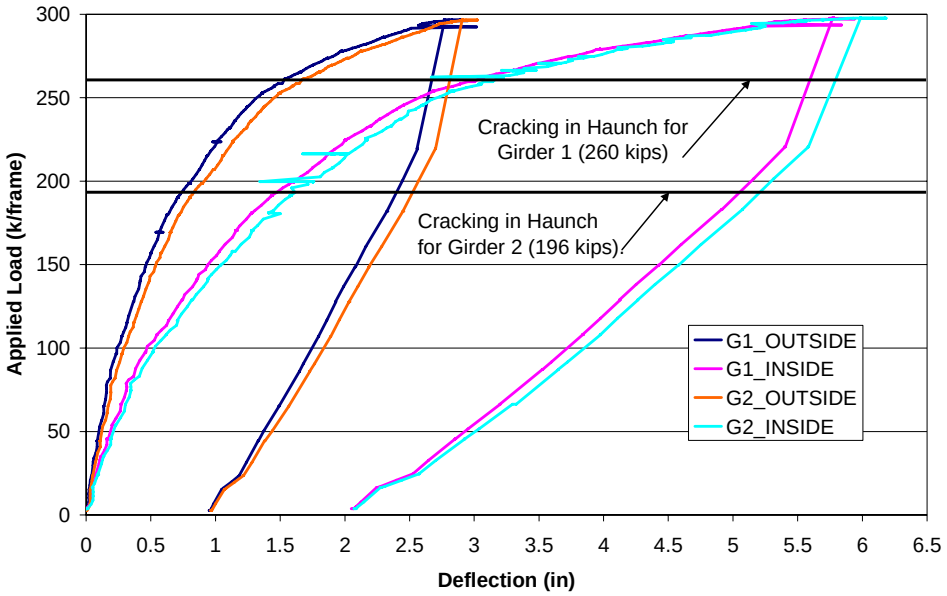

Figure 47. Deflections During Final Static Test at Live End.

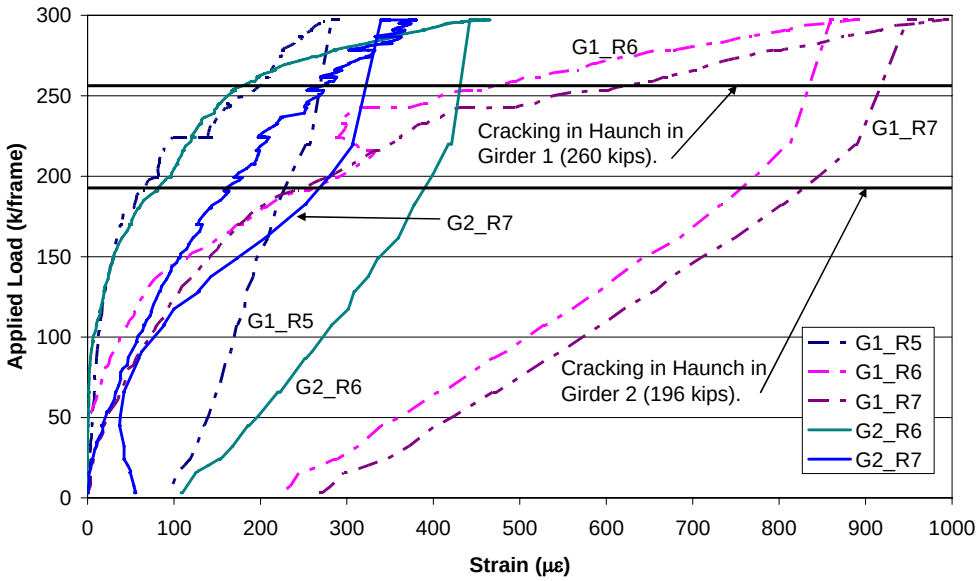

Figure 48. Connector Strains During Final Static Test at Live End.

the final static test at the live end. The increase in the strain rate with respect to the load indicates the shear connectors were engaged in resisting the horizontal shear stresses after cracking at the interface between the haunch and girder. After the lab mockup was unloaded, there were residual strains in many of the instrumented shear connectors. This was likely due to residual slip at the interface, which does not allow the shear connectors to return to their

undeformed configuration. The residual strains in the shear connectors did not result from nonlinear material behavior. The strains in the shear connectors are less than 50 percent of the nominal yield strain for the entire range of applied loads.

Figures 49 and 50 show the cracking pattern at the live end of girder 1 and girder 2. The cracking pattern for the two girders was very similar. However, the shear cracks in girder 1 were more dispersed when compared to the shear cracks in girder 2. Additionally, not as many shear cracks were noticed in girder 1. The cracking patterns and progression of the cracks for the final static test at the live end were very similar to those in the final static test at the dead end. The wirepots at the epoxied male-female joints indicate there was no relative vertical movement at the joints. Cracking was observed at the inside male-female joint an applied load of 260 k/frame.

At an applied load of 296 k/frame, crushing was observed on the top surface of the bridge deck. The applied load of 296 k/frame results in a flexural capacity of 24,500 k-in, which was 1.2 percent less than the calculated flexural capacity of 24,800 k-in.

The shear studs and hooked reinforcing bars performed well as shear connectors with 2 ft pocket spacing. The strains in the shear connectors were less than 50 percent of the nominal yield strains. The deflections at the inside load points and outside load points are the approximately the same for girder 1 and girder 2. Although, when the deflections are examined at a specific load level, girder 2 had slightly larger deflections than girder 1.

Figure 49. Cracking Pattern at Live End for Girder 1 During Final Static Test.

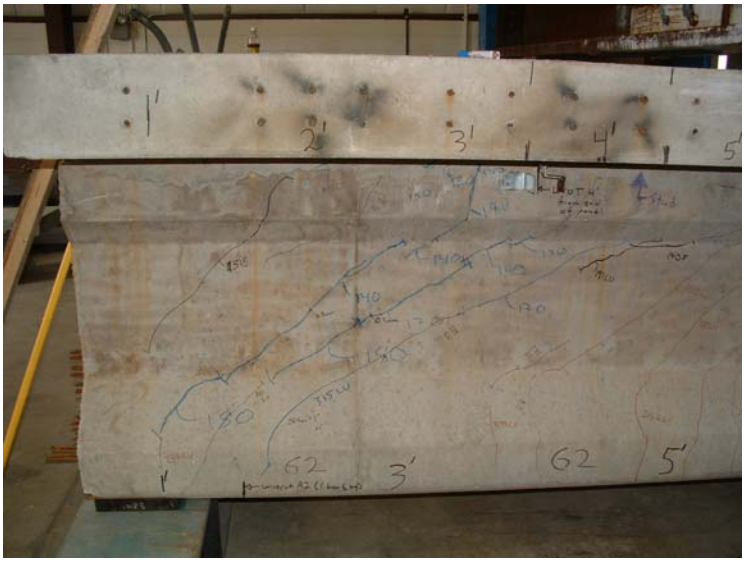

Figure 50. Cracking Pattern at Live End for Girder 2 During Final Static Test.

Comparison of Pocket Spacing and Connector Types

Stiffness

Examination of the load-deflection plots indicates that there was no significant difference in the initial stiffness between the ends of the bridge with 2 ft and 4 ft pocket spacing. There was also no discernable difference between the beams with hooked reinforcing compared to shear studs. The strain levels in the shear connectors are comparable for both ends of the lab mockup during the live load tests. During the final static tests, the peak strains in the shear connectors were less than 50 percent of the nominal yield strain and cracking was not observed at the interface between the haunch and girder until the final static tests at 183 k/frame. The difference in the initial stiffness at each end of the lab mockup was due to the influence of the existing cracks at the opposite end of the bridge. These results lead to the observation that neither the pocket spacing nor the connector type influences the stiffness of the lab mockup.

Fatigue

Both ends of both beams performed well during the cyclic testing. There were no significant increases in deflections or strand stresses. Neither the pocket spacing nor the connector type has an influence on the stiffness of the lab mockup or the fatigue performance of the bottom row of strands for the cyclic testing.

Strength

Both the live end and dead end of the lab mockup failed in flexure by crushing of the concrete on the top surface of the bridge deck. The maximum moment reached during the final static tests on the dead and live ends of the lab mockup were 23,700 k-in and 24,500 k-in, respectively. The pocket spacing had very little influence upon the flexural capacity of the lab mockup. The maximum shear reached during the final static tests on the dead and live ends of

the lab mockup are 206 k and 213 k, respectively. The lab mockup with either the 2 ft pocket spacing or 4 ft pocket spacing was capable of exceeding the required vertical shear strength.

Table 7 shows the ratio of the resulting horizontal shear force at each shear pocket from the final static tests to the nominal horizontal shear capacity at each shear pocket. Pocket 1 was closest to the live end of the bridge with the 2 ft pocket spacing and pocket 15 was closest to the dead end of the bridge with the 4 ft pocket spacing. The horizontal shear forces developed at the end pockets during the final static tests were 19 and 24 percent higher than the nominal horizontal shear capacity at the dead end and live end, respectively. This indicates the number of shear connectors could possibly be reduced and the lab mockup could still reach the required flexural strength, the required vertical shear strength, and the required horizontal shear strength.

The shear connector layout used for the lab mockup provided sufficient strength, which exceeds the nominal horizontal shear strength for the pockets in the outside panels (panel 1 and panel 5). Both the 2 ft pocket spacing and 4 ft pocket spacing are capable of providing the required strength. Additionally, the strain levels of less than 50 percent of the nominal yield strain at maximum loads in all of the connectors indicate both the hooked reinforcing bars and the shear studs perform well as shear connectors.

Table 7. Ratio of Applied Horizontal Shear to Horizontal Shear Capacity for Final Static Tests

pocket #	$V_{applied}/V_{prov}$ Dead End	$V_{applied}/V_{prov}$ Live End
1	0.47	1.24
2	0.47	1.24
3	0.47	1.24
4	0.47	1.24
5	0.47	0.37
6	0.47	0.37
7	0.47	0.37
8	0.52	0.41
9	0.56	0.58
10	0.56	0.58
11	0.64	0.67
12	0.49	0.67
13	0.52	0.70
14	1.19	0.49
15	1.19	0.49

Durability of Transverse Joints

The grouted female-female joints performed exceptionally well in all stages of the durability. No leaking occurred at the transverse joints during the ponding tests. However, a small leak was discovered at the inside male-female joint during the intermediate static test on the live end of the bridge. The leak was noticed around an applied load of 122 k/frame. After the intermediate live load test on the live end of the bridge was completed and the load was

completely removed, the leaking stopped. Water was ponded to complete stage 4 of the durability test, and no leaking was discovered.

It was concluded that water must have leaked into the transverse joint during stage 3 of the durability test. The water did not leak all the way through the joint to the bottom of the deck panels during this stage. During the intermediate static test on the live end, the epoxy cracked enough to allow water that was trapped during the 3rd stage of ponding to leak all the way through the joint. When the load was removed, the crack closed back up and did not allow water to leak all the way through the joint during stage 4. No leaking was observed when ponding was performed for stage 5 of the durability study of the transverse joints.

Finite Element Results

This section presents the finite element results of the time-dependent study, the push-off test models, the lab mockup models, and the parametric study.

Time-Dependent Analysis Results

Verification of Finite Element Models for Time-Dependent Behavior of Lab Mockup

A phased, time-dependent analysis was run in DIANA. The eight phases outlined in the "Methods" section were followed for this model. Preliminary analyses indicated the ACI 209 model[16] grossly over predicted the creep and shrinkage strains. The CEB-FIP Model Code 1990[9] creep and shrinkage model modeled the behavior of the mockup more accurately than the ACI 209 model. The CEB-FIP model code 1990 was used for all the finite element models. The creep and shrinkage functions used for the concrete in the girders and panels were also used for the grout in the haunch. The measured material properties were used for the panels, girders, and haunch.

Figure 51 shows the finite element strains in girder 1 compared to the experimental strains in girder 1. Figure 52 shows the finite element strains compared to the experimental strains in the panels. Because the experimental results revealed the creep and shrinkage behavior of girder 1 and girder 2 were very similar, only girder 1 was modeled in DIANA for the time-dependent study. The experimental results presented in Figure 51 and Figure 52 were adjusted such that the residual strains developed in the girders and panels during the casting operation were neglected. The effects from the heat of hydration were not included in the finite element models.

The FEA predicted higher (more compressive) strains in both the girders and the panels. However, the rate at which the compressive strains increased for the finite element results was very close to the rate at which the compressive strains increased for the experimental results. The magnitude of the strains from the elastic shortening during the post-tensioning operations matches the experimental data exceptionally well. This indicates that the parameters used to define the development of the elastic modulus with time were accurate.

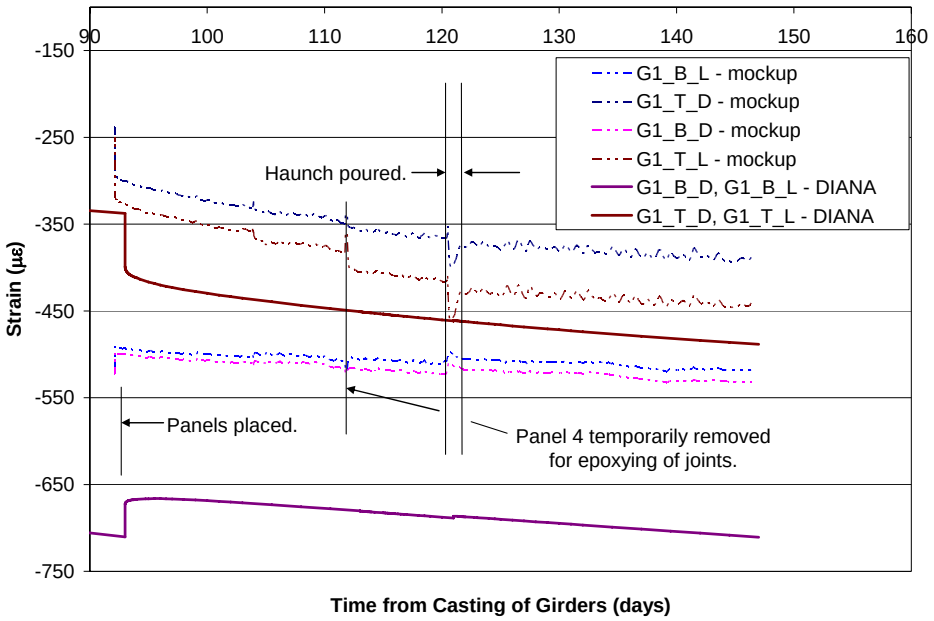

Figure 51. Comparison of Strains in Girder 1 from Finite Element Results to Strains in Lab Mockup.

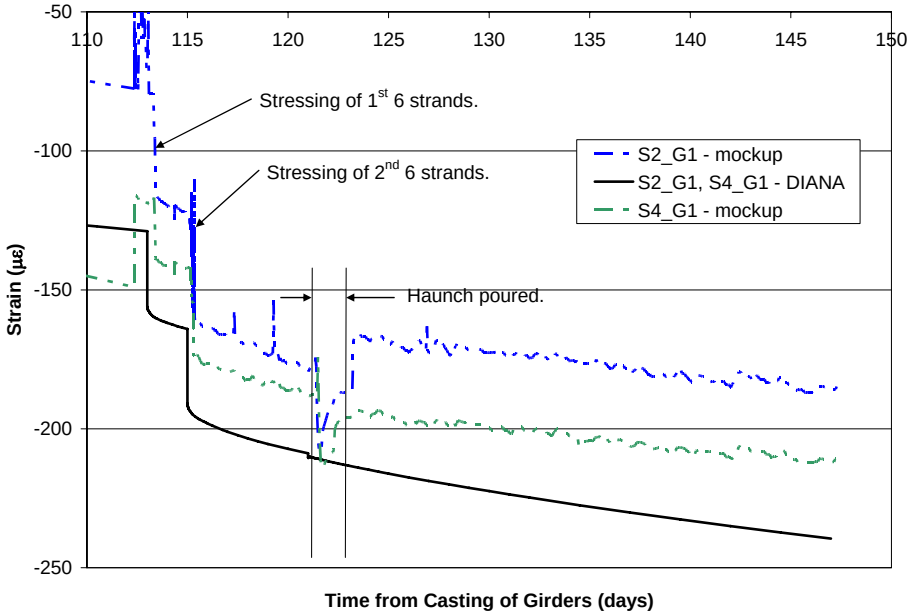

Figure 52. Comparison of Strains in Panels from Finite Element Results to Strains in Lab Mockup.

Further Look at the Time-Dependent Behavior of Lab Mockup

Figure 53 shows the finite element results for the strain profile through the depth of the lab mockup at selected time intervals after the system was made composite. The location of the strain profile is 13 ft-4 in from the support. The haunch was poured on day 121 making the system composite. During the early time intervals of the composite system, there was little

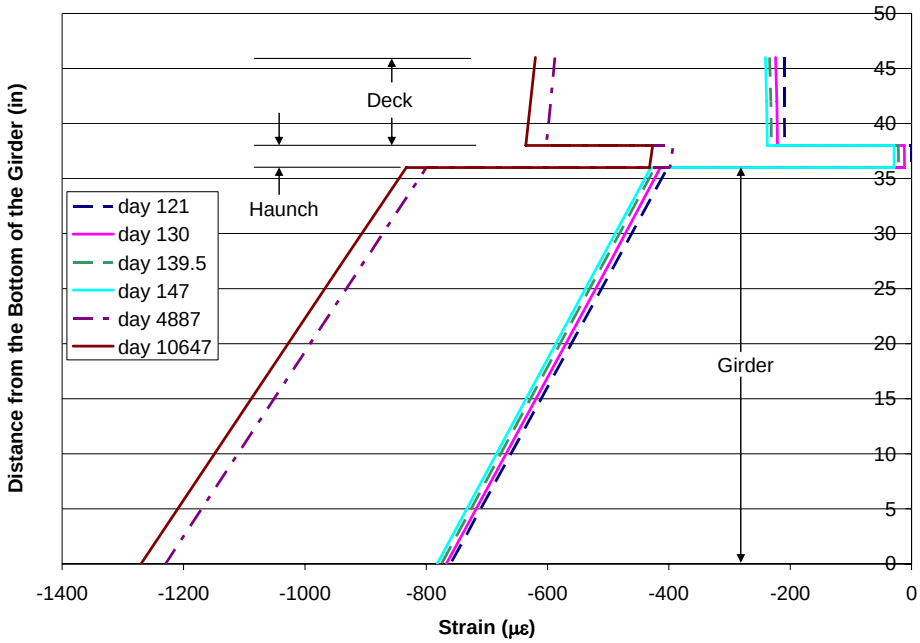

Figure 53. Strain Profiles in Composite Section for Different Times During Service Life.

change in strain in the girder, haunch, and deck. Additionally, the curvature remained fairly constant over the duration of the analysis.

Figure 54 shows the stress profile through the depth of the lab mockup at selected time intervals after the system was made composite. Similar to the strain profile behavior, the stress profile does not have any significant changes for the early time intervals. The compressive stress

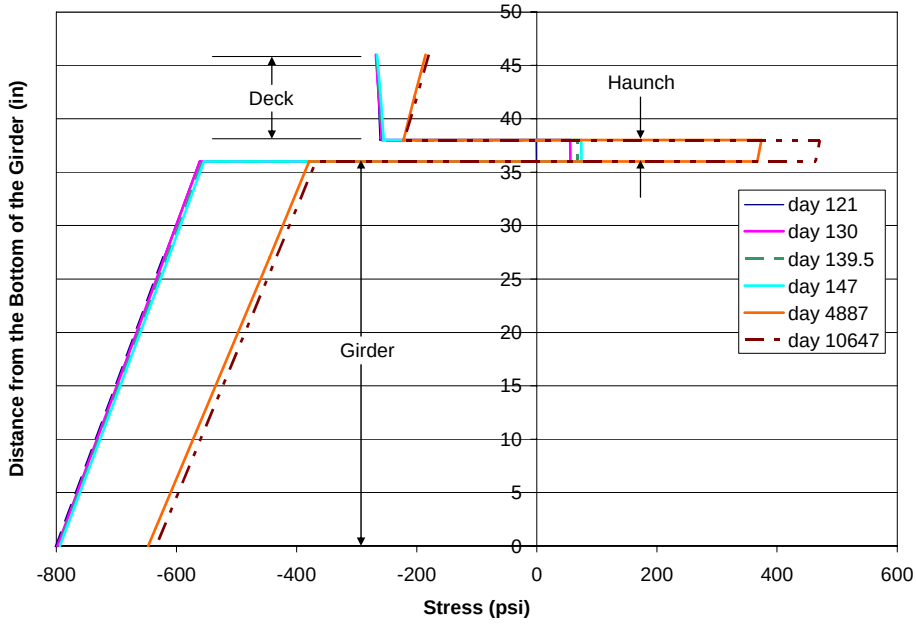

Figure 54. Stress Profiles in Composite Section for Different Times During Service Life.

in the girder undergoes a fairly uniform decrease over time. The largest change observed during the early time intervals was a 74 psi increase in stress in the haunch. At day 10,647, the average stress in the haunch was 468 psi, which was greater than the expected cracking stress of 380 psi. By the time the haunch was poured, the girders and panels have experienced most of their shrinkage. The grout in the haunch was restrained during the shrinkage process, creating tensile stresses.

Like the compressive stresses in the girder, the compressive stresses in the deck also decrease over time. However, the decrease in the compressive stress at the top of the deck was noticeably larger than the decrease in compressive stress at the bottom of the deck. The initial stress at the top of the deck was -298 psi and the stress at the top of the deck at day 10,647 was -180 psi. The compressive stress in the top of the deck decreased by -118 psi, which was a reduction in compressive stress of 39.6 percent.

The increase in compressive strains in the structure can be misleading. Although the deck, haunch, and girder were contracting with time, the viscoelastic behavior of concrete causes the stresses to decrease with time in this case. This relaxation effect is illustrated in Figure 53 and Figure 54, showing the compressive strains in the deck, haunch, and girder increased with time and the compressive stresses in the deck and girder decreased over time and the tensile stresses in the haunch increased over time.

Estimation of Prestress Losses and Recommended Initial Levels of Post-Tensioning

Issa[4] recommends an initial post-tensioning level of -200 psi for simply supported bridges to keep the joints in compression under live loads. A post-tensioning level of -100 psi was needed to secure the tightness of the joint under live loads and an additional -100 psi was included to account for creep and shrinkage effects. The results of the finite element study on the lab mockup showed the reduction in the compressive stress in the top of the deck was 118 psi and the reduction in the compressive stress in the bottom of the deck was 77 psi. This resulted in an average reduction in the compressive stress in the deck of 98 psi, which was surprisingly close to Issa's lump sum estimate of 100 psi for the losses due to creep and shrinkage, considering Issa's research is based on deck panel systems with steel girders. The initial average level of post-tensioning of -268 psi proved to be adequate, although a lower initial level of post-tensioning may have been satisfactory as well.

Push-Off Test Results

Verification of Finite Element Models for Push-Off Tests

The finite element results based on the smeared cracking approach were compared to Wallenfelsz's results for push-off specimen tests. The load vs. relative slip behavior was compared to evaluate the modeling methodologies proposed for the shear connectors and material interfaces. The comparisons are used to predict whether the results for the finite element models for the live loads on the lab mockup are conservative and reliable.

Figure 55 shows the finite element results for the push-off test compared to Wallenfelsz's hooked bar specimen results at small relative slip values. The finite element results match Wallenfelsz's results very well up until a relative slip of 0.02 in. At this point, the finite element solution diverged.

The finite element results indicated the peak strain in the shear connector occurs near the interface of the haunch and girder. There was a rapid decrease in strain in the shear connectors as the distance from the haunch was increased. This may partially explain why the Wallenfelsz's results indicated the strain levels were low. It was difficult to place the ER strain gage on the shear connector close to the interface between the haunch and girder. Additionally, the ER strain gage was wrapped in an aluminum sheet to protect it. The aluminum sheet may allow slip between the grout and the aluminum sheet itself, affecting the measured local strain and strain gradient along the length of the shear connector.

In most of the test results by Wallenfels,[10] there was a sudden drop in load and a large increase in the relative horizontal slip after the peak load was reached. The only way to pick this up in the finite element solution was to run a displacement controlled analysis. The finite element model had not captured the unloading portion of the load vs. relative slip curve because it was run under force control. Additionally, there were convergence problems associated with the localized cracking that occurs in the vicinity of the shear connector and interface when the smeared cracking model was used instead of the discrete cracking model.

In order to help stabilize the convergence behavior when attempting to capture the post-peak behavior of the load vs. displacement curve, the softened elastic modulus approach was adopted. The elastic modulus used to simulate the cracked region is 0.25 percent of the elastic modulus for concrete in the panel and girder. The size of the softened elastic zone was

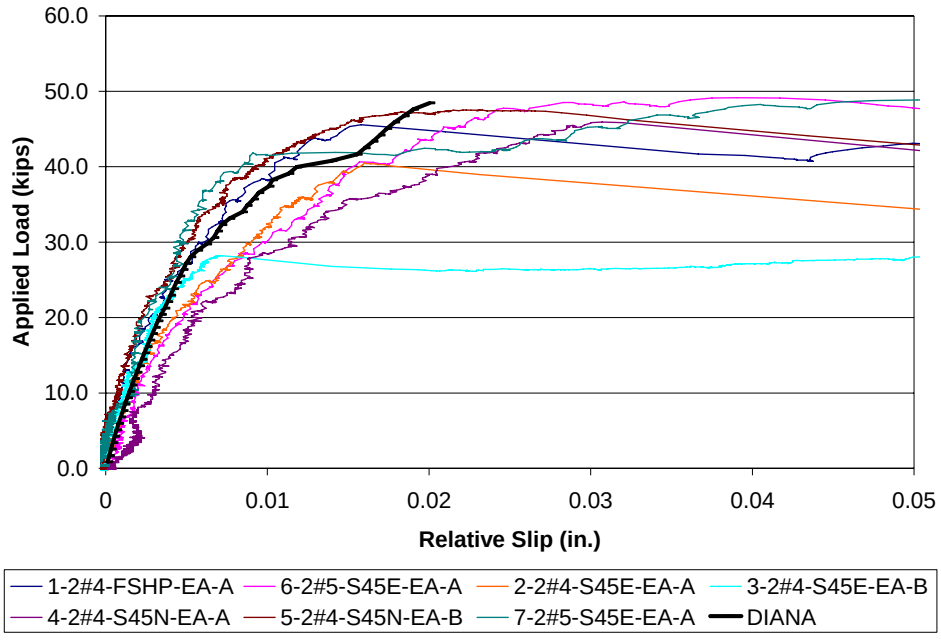

Figure 55. Comparison of Relative Slip of Push Off Specimen at Small Relative Slip Values Using Smeared Cracking Approach.

approximately 2 in by 2 in, as determined from the results of the analyses with a smeared cracking model activated.

Figure 56 shows the finite element results compared to Wallenfelsz's results with 2 No. 4 bars as the shear connectors. A similar plot of the finite element results compared to Wallenfelsz's results with 2 No. 5 bars as the shear connectors can be found in Sullivan.[7] The softened elastic modulus approach resulted in a more stable convergence behavior of the model. Both of the finite element models for hooked reinforcing bars as shear connectors underestimated the peak load reached by Wallenfelsz as well as the capacity predicted by Equation 1, the AASHTO LRFD shear friction equation.

The stiffness of the finite element models was slightly less than the stiffness from Wallenfelsz's results prior to the peak load being reached. This was expected when using the softened elastic modulus approach because a region was specified as being "cracked" by reducing the elastic stiffness when, in fact, the region had not cracked yet. For applied loads greater than 40 k, localized cracking in the vicinity of the shear connector and interface was significant enough that the softened elastic modulus approach accurately captured the slip values and corresponding loads. For applied loads less than 40 k, the localized cracking in the vicinity of the shear connectors and interface was not as significant. Therefore, the smeared cracking approach was more applicable for capturing the gradual progression in the number of cracks and the propagation of the cracks.

When the results for the smeared cracking approach and softened elastic modulus approach are compared for a model with two No. 5 bars, the smeared cracking approach results in a peak load that was approximately 6 percent higher than the model using the softened elastic modulus approach. However, both approaches accurately capture the load vs. displacement behavior of the push-off specimen. The smeared cracking approach was more accurate at

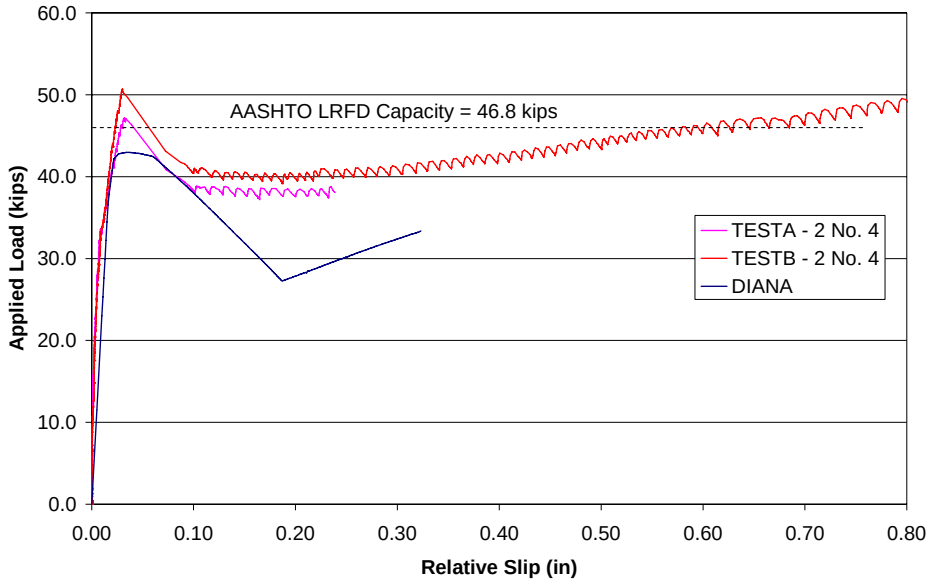

Figure 56. Comparison of Relative Slip of Push Off Specimen for 2 No. 4 bars with Softened Elastic Modulus Approach.

capturing the peak load and the softened elastic modulus approach was able to capture the post-peak behavior of the specimen for slip values up to approximately 0.2 in.

For slip values between 0.1 in and 0.2 in, the finite element model was not able to capture the behavior of the push-off specimen as accurately as it did for slip values between 0 in and 0.1 in. As stated earlier, the purpose of the finite element models for the push-off specimen is to propose a modeling methodology for modeling the shear connectors in the finite element models for the lab mockup. The experimental results for the mockup indicate that the slip values at the interfaces were much less than 0.2 in.

Based on these preliminary analyses, and observations from the lab mock-up tests, it was determined that the smeared cracking model was the best approach for the shear connectors in the full mock-up finite element analysis.

Live Load Analysis Results

Load vs. Deflection Response for the Lab Mockup

Figure 57 shows the displacement behavior for girder 1 at the live end of the lab mockup at the inside load point. The initial stiffness of the finite element model matched the initial stiffness of the experimental results until an applied load of 127 k/frame. At this point, nonlinear behavior was observed in the system due to the development of multiple flexural cracks under the load points as well as the beginning of shear cracks in the web of the girder. Because the peak load for the intermediate live load test was only 159 k/frame, the results from the final static test were compared to the finite element results for applied loads greater than 159 k/frame. The stiffness of the finite element model was greater than the stiffness of the final static test results

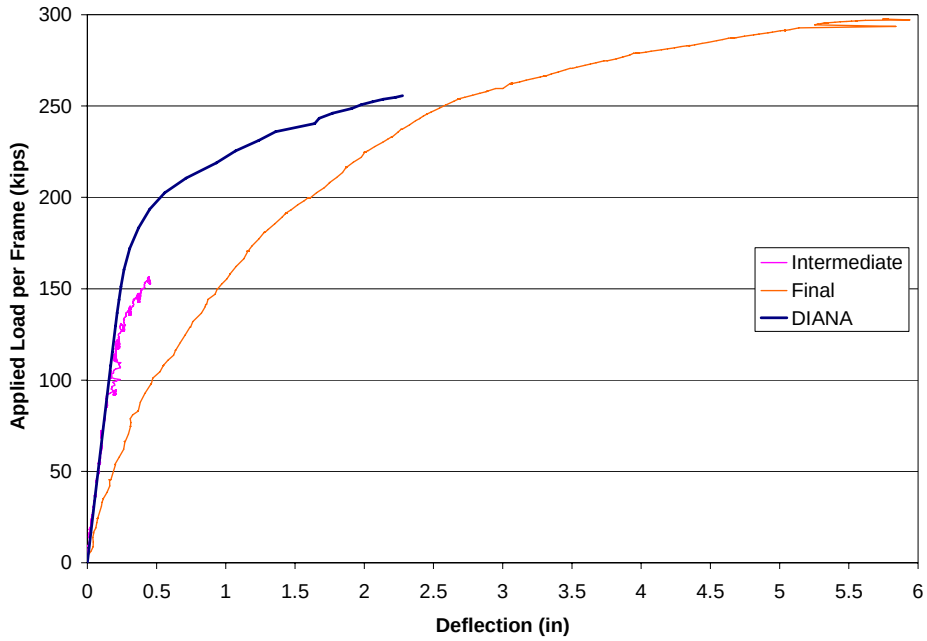

Figure 57. Deflections in Finite Element Model for Girder 1 at Live End Compared to Experimental Results.

for applied loads less than approximately 190 k/frame because of the unloading and reloading effect. The stiffness of the finite element model decreased at a faster rate than the experimental results from the final static test for applied loads greater than 190 k/frame. For applied loads approaching the capacity of the lab mockup and the capacity of the finite element model, the stiffness of the finite element model was very close to the stiffness of the lab mockup. The finite element results diverged at an applied load of 256 k/frame. Divergence does not necessarily indicate the structure modeled had "failed." With the multiple nonlinearities associated with this model, numerical difficulties were encountered at higher applied loads. This was especially true with the presence of extensive cracking, leading to a numerical collapse when there was no stiffness left at an integration point because of cracking.

Strains in the Shear Connectors in Lab Mockup

Table 8 presents a comparison of the axial strain in the shear connectors at the dead end of the bridge with the hooked reinforcing bar shear connectors. Recall that 4 ft pocket spacing was used at the dead end of the bridge. Similar tables for the other shear connector type and pocket spacings can be found in Sullivan.[7] The experimental strains listed in Table 8 are taken from the ER strain gages mounted on the shear connectors. The ER strain gages on the shear connectors were located approximately 1 in from the top face of the top flange of the girder. The finite element strains listed in Table 8 are the strains in the shear connectors 0.25 in from the top face of the top flange of the girder. This was done to capture the high strains that develop in the region for larger slip values. In general, the finite element strains were smaller than the experimental strains for a large portion of the applied load. This underestimation of the axial strain may be due to the clamping effect being ignored. Other possible discrepancies associated with local behavior of the connectors and slip at the interface are:

Table 8. Comparison of Axial Strain in the Shear Connectors Dead End with Hooked Reinforcing Bars

Pocket #	Applied Load per Frame (kips)	Experimental Strain (με)	DIANA Strain (με)
13	108	15	16
	151	105	28
	201	199	86
	218	231	148
	235	262	375
	252	291	742
14	108	60	13
	151	165	40
	201	325	108
	218	380	370
	235	433	765
	252	490	1300

1. Accuracy of localized cracking and crushing based on mesh refinement.
2. Connectors that had nodes at the same x, y coordinate but had different z coordinates were lumped together in the same plane for the sake of the plane stress analysis. This created a stiff spot in the model that may have lead to premature localized cracking and crushing.
3. A perfect bond between the reinforcement and shear connectors was assumed to exist.
4. Accuracy of the shear stress vs. relative slip relationship at the interface.

At higher levels of applied load, the finite elements strains were higher than the experimental strains. As mentioned previously, at higher loads a steep strain gradient developed through the depth of the connector with the maximum strain occurring at the interface between the girder and haunch. Therefore, the peak strain in the connectors for the finite element results may slightly overestimate the strain. This will lead to a shear connector, or series of shear connectors, yielding prematurely and leading to higher slip values and a lower corresponding degree of composite action. For the sake of the parametric study in evaluating the current shear connector design provisions in AASHTO LRFD, this is satisfactory.

Although the strains in the shear connectors from the finite element results were much larger than the corresponding experimental strains at higher applied loads, both sets of results do show that in many of the cases the shear connectors did not yield. This is contrary to the design equation, which bases strength calculation on f_y.

Strain Profiles for Lab Mockup

The strain profile through the depth of the lab mockup at a distance of 13 ft 4 in from the dead end of the bridge is shown in Figure 58. The section was taken through girder 1, which

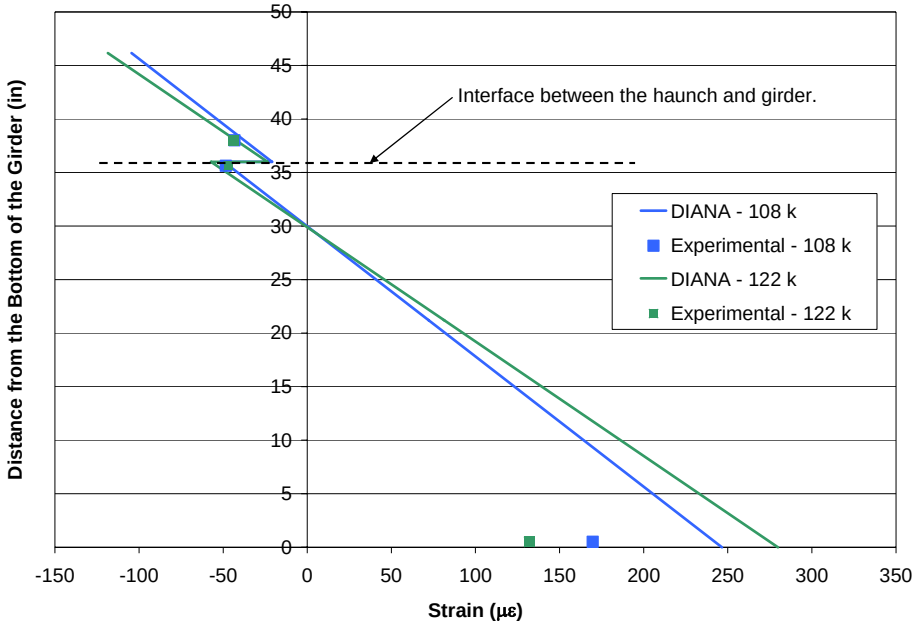

Figure 58. Strain Profile at Dead End for Hooked Reinforcing Bar Connectors.

contains hooked reinforcing bars for shear connectors. Two different applied load levels were examined, 108 k/frame and 122 k/frame. The experimental data that the finite element results were compared to for the strain profiles were taken from the intermediate static tests. The strain profile from the finite element model showed satisfactory correlation with the experimental data. The largest differences between the finite element results and experimental results existed at the bottom of the girders.

There were three possible causes for the differences in the strains toward the bottom of the girders.

1. Restraint provided by the bearing pads, which had a tendency to decrease the strains. The boundary conditions for the finite element model consisted of a pin and roller system. Therefore, the bottom flange was not restrained from expanding, resulting in larger finite element strains.
2. Effect of the level of composite action on the strain distribution. The method used for modeling the shear pockets resulted in reduced levels of composite action compared to Wallenfelsz's results. This caused the curvature to increase and resulted in larger finite element strains at the bottom of the girder.
3. Tension stiffening effect. When cracking occurred in the lab mockup, there was still uncracked concrete between the existing cracks with tensile strength. The level of tension in the concrete ranged from zero at the location of the cracks to a maximum tensile strain in the concrete between the cracks. Therefore, the level of strain in the strain gages was affected when cracks were located in the vicinity of the gages.

Figure 58 shows the finite element strains were similar to the experimental strains. The experimental strains are compared to the finite element strains in Table 9. The results showed a loss of composite action based on the discontinuities at the interface. Additionally, if full composite action was present and the strain in the top of the girder was a compressive strain, the strain in the bottom of the panel should have shown a higher compressive strain when subjected to positive curvature. Similar observations are made for girder 2 with the shear studs at the dead end of the bridge. The strain distribution for this combination can be found in Appendix I of Sullivan.[7]

Table 9. Comparison of Experimental Strains and Finite Element Strains for Lab Mockup Verification Study

	108 k/frame		122 k/frame	
ER Strain Gage Name	**Experimental (με)**	**DIANA (με)**	**Experimental (με)**	**DIANA (με)**
G1_D_U	-48.4	-46.5	-47.0	-53.6
PG1_D_L	-43.3	-37.4	-43.8	-42.2

Cracking Patterns for Lab Mockup

The cracking patterns and the loads at which they occur for finite element results matched the experimental results. The first flexural crack occurred in the lab mockup at 118 k/frame in girder 1. For the finite element results, the first flexural crack occurred at 126 k/frame. The cracking loads in the finite element models were the same for girder 1 and girder 2. Noticeable

shear cracking occurred in the lab mockup between 95 and 105 k/frame. For the finite element models, the first shear crack occurred at 119 k/frame. This was the same for both girders.

Further details on the comparison of FEA to experimental cracking can be found in Sullivan.[7] Overall, the FEA very closely matched the occurrence and progression of cracking in the lab mock-up. This included flexure and shear cracking, as well as cracking in the haunch near the shear connectors. This comparison served to strengthen the conclusion that the modeling methods were sound and could be used reliably in the parametric study.

Parametric Study for Live Load Tests

Load vs. Deflection Response for Different Shear Connector Models

Figures 59 through 62 show the load vs. deflection response curves for the different shear connector types and quantities examined in the parametric study. The location of these vertical deflections was at the inside loading points. The results for the load vs. deflection response at the outside loading points were very similar and can be found in Appendix I of Sullivan.

Recall that model MOCKUP had the exact number of shear connectors used for the lab mockup. Model 1_100 had close to the exact number of shear connectors required per pocket using Equation 1. Model 1_75 had approximately 75 percent of shear connectors required per pocket using Equation 1. Model 1_50 had approximately 50 percent of shear connectors required per pocket using Equation 1. Model 8_R had close to the number of shear connectors required using Equation 8. The shear connectors were distributed in an even manner among the pockets. The connectors were also distributed among the shear pockets so the dead end and live end of the bridge had approximately the same amount of shear connectors. Model 8_L had close to the number of shear connectors required using Equation 8. Unlike model 8_R, the shear connectors were distributed among the pockets such that more shear connectors were placed in locations with high shear stresses.

An applied load of 118 k/frame for either end of the test setup produces the design moment for service load levels. An applied load of 187 k/frame produces the required flexural strength. Models with larger vertical deflections indicate a larger loss in composite action than models with smaller vertical deflections. At service load levels, the difference in the performance of the different connector quantities was negligible compared to the difference in the performance of the different connector quantities at ultimate load levels. Because the design of the connectors was based on ultimate load levels, the discussion of the different shear connector types and quantities will be limited to ultimate load levels. The peak load for each model in Figures 59 to 62 does not indicate the actual capacity of the system for a given shear connector type and quantity. This was the last load step where the solution converged without numerical difficulties.

Based on the load-deflection plots, several observations can be made about the deck panel system. When comparing Figure 59 to Figure 60, 4 ft pocket spacing provided approximately the same degree of composite action as 2 ft pocket spacing when hooked reinforcing bars were used as shear connectors. The only two models for which this statement

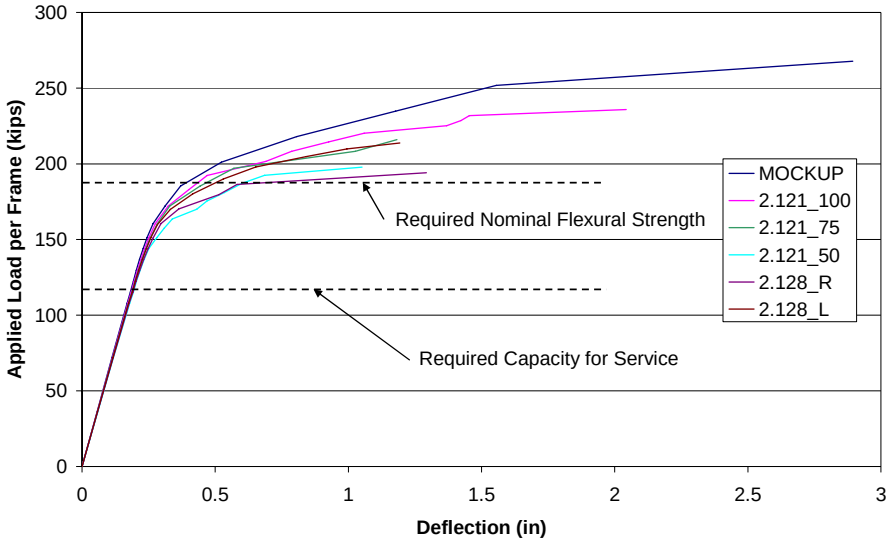

Figure 59. Comparison of Load vs. Deflection Response for Different Hooked Reinforcing Bar Quantities with 4 ft Pocket Spacing at Inside Load Point.

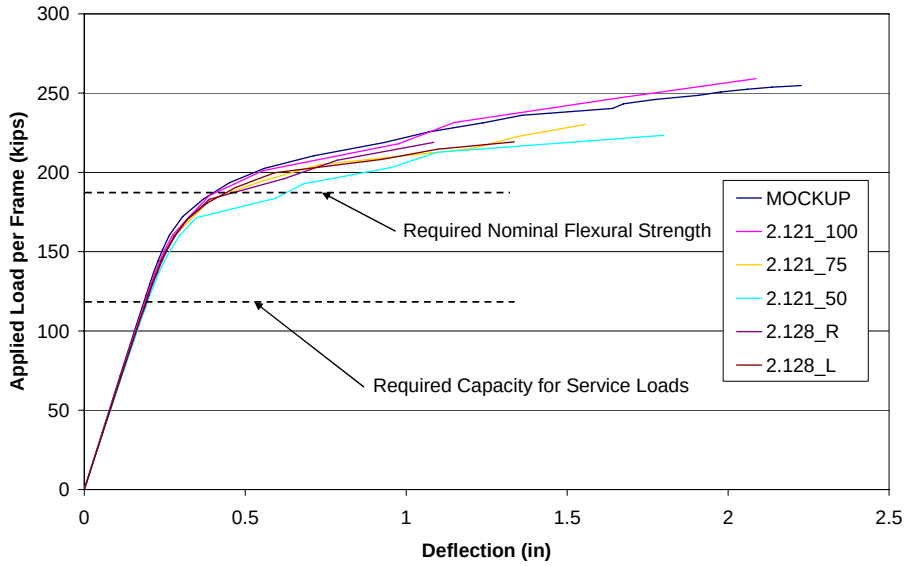

Figure 60. Comparison of Load vs. Deflection Response for Different Hooked Reinforcing Bar Quantities with 2 ft Pocket Spacing at Inside Load Point.

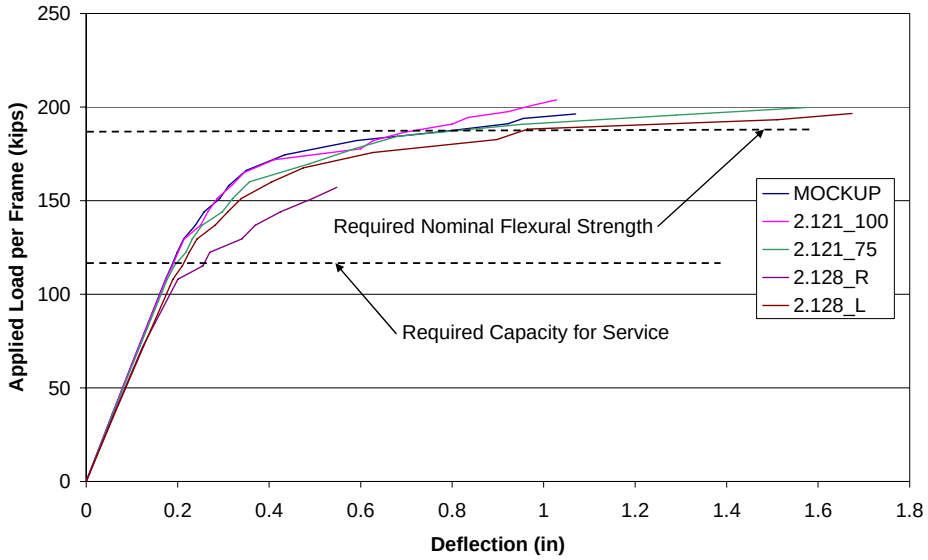

Figure 61. Comparison of Load vs. Deflection Response for Different Shear Stud Quantities with 4 ft Pocket Spacing at Inside Load Point.

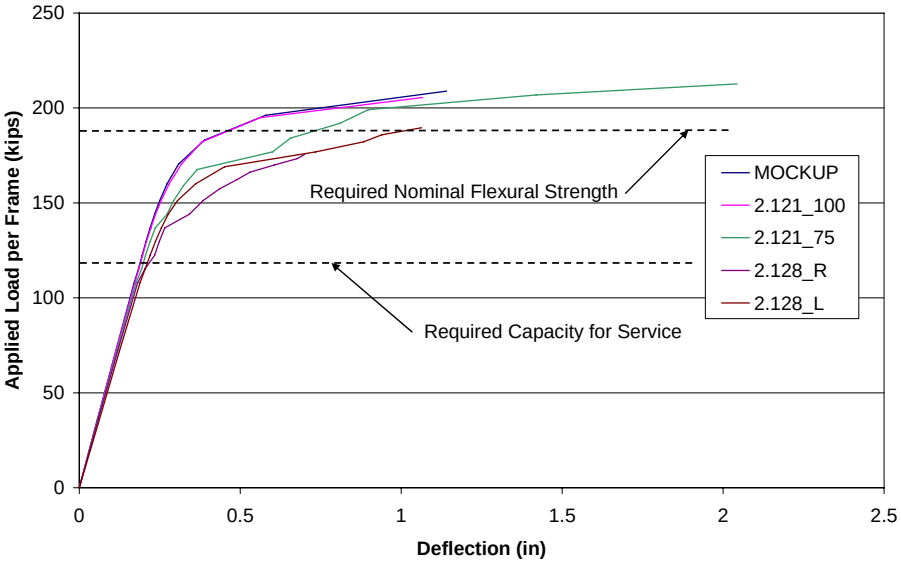

Figure 62. Comparison of Load vs. Deflection Response for Different Shear Stud Quantities with 2 ft Pocket Spacing at Inside Load Point.

did not hold true were models 8_R and 8_L. For these two models, the 2 ft pocket spacing provided a higher degree of composite action. When comparing Figure 61 to Figure 62, the 2 ft pocket spacing clearly provided a higher degree of composite action than the 4 ft pocket spacing when shear studs were used as shear connectors. Figure 60 and Figure 62 show that all of the models examined with 2 ft pocket spacing performed better with hooked reinforcing bars than with shear studs for shear connectors. However, the difference in the performance of the system with the two different types of shear connectors for models MOCKUP and 1_100 was very small. As the number of shear connectors was decreased for models with 2 ft pocket spacing, the models with the shear studs had a larger difference in the degree of composite action when compared to models with hooked reinforcing bars

It is advisable to use the quantity of connectors provided in models MOCKUP and 1_100 for either 2 ft pocket spacing or 4 ft pocket spacing with hooked reinforcing bars and for 2 ft pocket spacing with shear studs. The experimental data showed that shear stud connectors with 4 ft pocket spacing perform as well as any other combination of pocket spacing and connector type. Because the finite element results are conservative, 4 ft pocket spacing is acceptable to use with shear studs as shear connectors. The model 1_75 showed that reducing the required number of shear connectors did result in a small loss of composite action, but the stress levels in the connectors were still considered acceptable. This indicates the number of connectors required by AASHTO LRFD for the lab mockup is conservative and could have been reduced by as much as 25 percent.

The results indicate that there was a large loss in composite action when the connectors in the deck panel system were designed with Equation 8 and were redistributed in a uniform manner among the pockets, compared to when the connectors were designed with the same equation and were distributed to locations with high shear forces. However, when 2 ft pocket spacing was used with hooked reinforcing bars as shear connectors, the difference in the load vs. displacement behavior for models 8_R and 8_L was small compared to any other combination of shear connectors and pocket spacing. The connector stresses in the shear connectors for 8_R were still noticeably larger than the connector stresses for 8_L. When it is desirable to have the same number of connectors in each pocket in order to reduce the different shear pocket sizes and strand patterns in the panels, additional shear connectors should be provided at locations with small shear forces instead of distributing the total number of required connectors in a uniform manner among the pockets.

The finite element results show that both the 2 ft pocket spacing and 4 ft pocket spacing perform well for hooked reinforcing bars as shear connectors. The results for the hooked reinforcing bars as shear connectors indicate that the number of connectors required per pocket may be decreased. Two ft pocket spacing performs the best when shear studs are used as the shear connectors. However, when the minimum number of shear studs is provided from the AASHTO LRFD shear friction equation, 4 ft pocket spacing is an acceptable alternative to 2 ft pocket spacing.

CONCLUSIONS

Constructability Study

Transverse Strand Pattern in Deck Panels

Based on fabrication cost and the ease of fabrication, it is desirable to have one strand pattern. Because of the different pocket spacings used for the lab mockup, it was not possible to use one strand pattern. Using one strand pattern would have reduced the total number of feet of prestressing strands that had to be used for the transverse prestressing for the panels.

Transverse Joint Configuration

The grouted female-female joint performed well without any problems during construction or when water was ponded for the durability study. The grouted female-female joints were more forgiving when the edges of the panels were bowed. Additionally, the grouted female-female joints allowed the panels to be placed on the girders more rapidly when compared to panel placement with epoxied male-female joints. The grouted female-female joints allowed the panels to be placed on the girders without having to slide the panels together while avoiding conflicts with any shear connectors that were already in place.

The constructability study and durability study revealed that the epoxied male-female joints were susceptible to leaking if the edges of the panel formwork were bowed. If the epoxied male-female joints are used for future projects, tight tolerances must be used to assure that the two panels forming the epoxied male-female joint are in firm contact with one another along the length of the joint. An alternative is match casting.

Leveling Bolt System

The Dayton Richmond B-14 coil bolts and F-53 thin slab coil inserts worked well for the leveling bolt system. The weight of the deck panels was supported on three coil bolts without any strength related problems. There was some difficulty adjusting the elevation of some of the panels with the leveling bolt system. In some cases, the thin slab coil inserts were not at a 90° with the bottom of the panel surface. This problem was solved by using a jack hammer to widen the hole above the coil insert. This allowed the coil bolt to be installed at the same angle as the coil insert. In order to avoid this problem in the future, a wider blockout should be provided in case the coil bolt has to be inserted at an angle. This is shown in Figure 63.

Steel plates provided on top of the girders for the coil bolts to bear on prevented any of the post-tensioning force from being transferred to the girders during the tensioning operation. The steel plates are shown in Figure 23 and Figure 63. Dial gages were used to measure any change in the deflection of the girder to show none of the post-tensioning force was transferred to the girders.

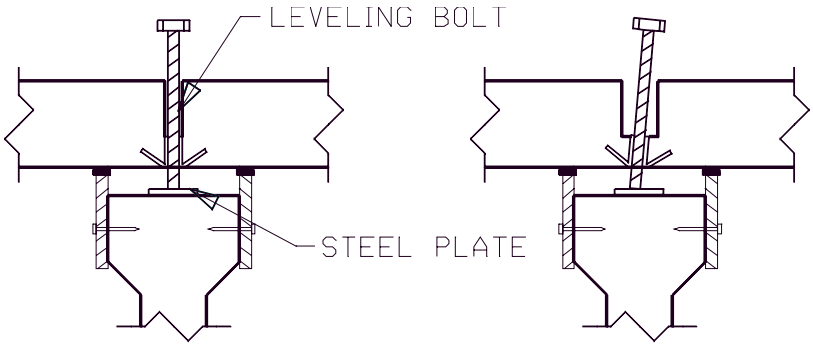

Figure 63. Leveling Bolt Blockouts (a) Old Configuration (b) New Configuration.

Formwork for Haunch and Transverse Joints

The methods used to form up the grouted female-female transverse joints and the haunch worked well and minimal leaking was reported during the grouting operations.

Grout Specifications

The Five Star® Highway Patch grout was used for the female-female transverse joints and haunch. This grout met the specifications recommended by Scholz.[11] The grout performed well in terms of providing the required compressive strength in the joints at the time the strands were post-tensioned in the deck. The grout also performed well during the live load testing program. No cracking was observed in the grout for the haunch, transverse joints, and shear pockets.

The finite element time-dependent study revealed that it is important to have a grout with very low shrinkage properties. Both the panels and girders restrain the shrinkage of the grout in the haunch, creating large tensile stresses.

Shear Connector Type and Pocket Sizes

Using shear studs as shear connectors allows for more rapid placement of the panels on the girders and eliminates a tripping hazard. The hooked reinforcing bar detail was easy to install at the precast plant, but was more troublesome during construction. The panels could not be moved very far relative to the beams after being set. This caused difficulties during the epoxying of the male-female joints.

Time-Dependent Behavior

Both the experimental and finite element results showed the level of post-tensioning in the lab mockup was sufficient to keep the transverse joints in compression through the service life of the bridge. The average initial level of post-tensioning in the deck for the lab mockup was 270 psi, after considering all instantaneous losses. The experimental results showed the change in strain in the deck from creep and shrinkage effects was only -40 με. The finite element results showed the average reduction in the compressive stress in the deck was 70 psi. This resulted in an average compressive stress in the deck of -200 psi at 10,647 days.

The finite element results showed that significant tensile stresses developed in the haunch. The age of the panels and girders relative to the age of the haunch restrained the shrinkage of the haunch. The tensile stresses could have been reduced if

1. The panels and girders were not as old at the time of the grouting operation,
2. The post-tensioning operation was performed closer to the time of the grouting operation, and
3. A very low shrinkage grout was used.

The AASHTO equations for prestress loss were developed for prestressed I-girders with a cast-in-place composite deck and are therefore not appropriate to calculate the loss of compression in the precast deck panel system. Issa's[4] recommendation of -200 psi for an initial level of post-tensioning for simply supported bridges can be used to provide an estimate for the required level of post-tensioning in the deck. This initial level of post-tensioning assumes that there will be a reduction in the compressive stress in the deck of 100 psi from creep and shrinkage effects. This loss in compression from creep and shrinkage effects was shown to be a good approximation based on the finite element time-dependent results of the lab mockup.

When a more accurate estimate of creep and shrinkage effects on a bridge is desired, there are two approaches. Both methods require that all critical construction stages be considered. One approach is the time stepping method that requires the use of finite element based commercial software such as DIANA. The other approach is the age adjusted effective modulus method where a single time step is used for each construction stage. The development of the forces over these large time steps is compensated for by the aging coefficient. A system of equations is formulated based on equilibrium equations, strain compatibility equations, and constitutive relationships. This method, along with recommendations for initial prestress levels in decks in a variety of structural systems can be found in Bowers.[17]

Live Load Testing Program

Transverse Joint Configuration

The performance of a transverse joint configuration was shown to be a constructability issue and not a strength or fatigue issue for a simply supported span configuration. Both the epoxied male-female joints and the grouted female-female joints performed well when subjected to the vertical loads adjacent to the joints as well as the moments developed from the live loads.

Strength and Fatigue Performance

The lab mockup failed in flexure at both the live end and dead end. The moment at which the failure occurred at both ends of the lab mockup was within 4.5 percent of the calculated flexural capacity. Although the lab mockup did not fail in vertical shear, considerable shear cracking was observed in the girders at both ends of the lab mockup. The peak shear forces in the lab mockup from the live loads were 9 percent less than the calculated vertical shear capacity.

The experimental results showed the horizontal shear forces developed at the shear pockets exceeded the calculated shear capacities by as much as 24 percent. The excess capacity of the pockets along with the low strain levels in the shear connectors and high cracking loads in the haunch indicated the number of shear connectors could be reduced in the shear pockets. The finite element results indicated that the number of shear connectors could be reduced by as much as 25 percent. The method used for modeling the shear connectors neglected the clamping effect, which produced conservative finite element results by underestimating the level of composite action present. The results showed the AASHTO LRFD shear friction equation was the best equation of the equations examined to use for horizontal shear design. The finite element results showed that the total number of shear connectors required should not be redistributed evenly among the pockets. The number of shear connectors should be selected for each pocket based on the shear demand at the pocket location.

The lab mockup performed well when subjected to the cyclic testing. The stress range in the strands and the vertical deflection measurements remained constant. The strain levels in the shear connectors were less than 1 percent of the nominal yield strain.

Pocket Spacing

Both the 2 ft pocket spacing and 4 ft pocket spacing performed well. The 2 ft pocket spacing and 4 ft pocket spacing produced levels of composite action that allowed the lab mockup to reach the required flexural strength and the required vertical shear strength.

Shear Connector Type

Both types of shear connectors worked well based on the live load test results. The hooked reinforcing bars and the new shear stud detail had axial strains less than 50 percent of the nominal yield strain.

RECOMMENDATIONS

VDOT's Structure & Bridge Division should consider the following design guidelines when using full-depth precast deck panels on prestressed I-girders.

Strand Pattern

1. *To enhance the ease of construction and reduce cost, designers should minimize the number of different strand patterns in the panels.* To facilitate this, the pocket spacing should be kept constant in all panels.

Transverse Joints

2. *For easy construction, designers should continue to detail a simple, female-female keyed joint infilled with grout for the panel-to-panel connection.*

Shear Connectors

3. *For easy construction, designers should consider using the embedded steel plate with post-installed shear studs to create the composite connection between the precast girder and the deck panels.* The embedded plate should be at least 1½ in narrower than the top flange of the girder. The Dayton Richmond B-14 coil bolts and F-53 thin slab coil inserts can be used as the leveling bolt system. The blockout for the coil bolt in the slab should be large enough to account for a coil insert that is not flush with the bottom surface of the panel. Either 2 ft or 4 ft can be used as the pocket spacing when AASHTO Type II girders are used.

Grout Specifications

4. *The grout specification developed by Scholz11 should be used for the grout in the haunches and pockets.*

Formwork

5. *The haunch and transverse joints can be formed with plyform and weather stripping.* Details shown in Figure 23 and Figure 27 performed well.

Level of Post-Tensioning

6. *An initial prestress of 270 psi should be used to keep the transverse joints in compression throughout the service life of the bridge.* This recommendation is for simply supported spans on prestressed I-beams. A smaller level of post-tensioning may be provided if a more detailed creep and shrinkage analysis is performed as presented in Bowers.[17] A larger level of prestress will be required for continuous systems and precast deck panels on steel girders.

Design of Shear Connectors

7. *The following procedure should be used to select the number of shear connectors in each shear pocket:*

    1. The factored vertical shear force at the shear pocket under consideration is calculated.
    2. Equation 3 is used to determine the shear force per inch.
    3. The tributary pocket spacing is calculated. The tributary pocket spacing is half the pocket spacing on each side of the pocket under consideration.
    4. The horizontal design shear force is calculated by multiplying the shear force per inch by the tributary pocket spacing.
    5. Equation 1 is used to select the required area of steel per pocket. The top flange width and the tributary pocket spacing are used to calculate the area of concrete engaged in resisting the shear force.

6. For the new shear stud detail shown in Figure 2, the design of the shear studs on the bottom surface of the steel plate is also done using Equation 1. The spacing of the shear studs is determined assuming 2 shear studs will be placed in each row.
7. For the new shear stud detail shown in Figure 2, Equation 4 and Equation 5 must be satisfied. These equations define the fatigue resistance for an individual shear stud and place limits on the spacing of the shear studs.

Detailing of Shear Connectors and Shear Pockets

8. *Shear pocket spacings can be detailed with spacings up to 4 ft, but no greater than:*

$$s_{pocket} \leq d_v \cot(\theta) \qquad [9]$$

where θ is the angle at which the shear cracks form, according to modified compression field theory. The calculation for obtaining θ is outlined in AASHTO LRFD.[1] The angle, θ, can be conservatively taken as 45°.

9. *The following are recommended detailing standards when hooked reinforcing bars are used as shear connectors:*

    1. The reinforcing bars should be properly developed on each side of the haunch.
    2. The longitudinal spacing of the hooked reinforcing bars in a pocket is 2 in.
    3. The minimum transverse spacing of the hooked reinforcing bars is controlled by the bend diameter and should be no less than 4 times the diameter of the reinforcing bar.
    4. The minimum longitudinal distance between the edge of the shear pocket and the center of the first hooked reinforcing bar is 3 in.
    5. The width of the shear pocket should be at least 1 in smaller than the width of the top flange to avoid leaking during the grouting of the haunch.

10. *The following are recommended detailing standards when the new shear stud detail is used as the shear connector system (also see Figure 64):*

    1. The shear stud length should be 2 in less than the sum of the minimum haunch height and the thickness of the deck. If the haunch height varies considerably, more than one shear stud length may have to be used.
    2. The minimum thickness of the steel plate should be ¼ in when used with ¾ in diameter shear studs.
    3. The width of the steel plate should be 1 in greater than the width of the shear pocket.
    4. The steel plate should be cut to smaller lengths to facilitate easy placement of the plates in the top flange of the girder during fabrication. The length of each plate should be no longer than 10 ft when a ¼ in thick steel plate is used. This maximum length was selected for handling purposes and ease of installation.
    5. The longitudinal spacing of the shear studs in a pocket is controlled by Equation 4 and Equation 5. These equations place limitations on the spacing based on the fatigue capacity of an individual shear connector.

6. The transverse spacing should not be less than four times the diameter of the shear stud.
7. None of the shear studs on the top surface of the plate should fall at the same transverse and longitudinal location as the shear studs on the bottom surface of the steel plate.
8. Any plate that falls in the same location as a lifting eye for the girder will require a slot to be cut through the plate. The shear stud layout should compensate for this.
9. The minimum longitudinal distance between the edge of the shear pocket and the center of the first shear stud is 2 in.
10. A minimum cover of 1½ in should be provided from the edge of the top flange and the steel plate.
11. The width of the bottom of the shear pocket should be at least 4 in less than the width of the top flange to satisfy requirements 3 and 10.
12. A minimum top flange width of 4d+8 in is recommended, where d = stud diameter. This is done to provide at least 2 in between the edge of the pocket and the shear stud.

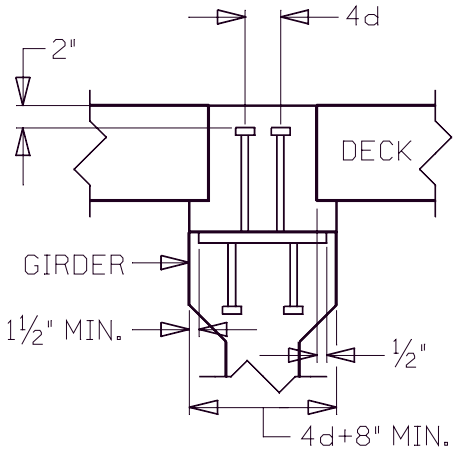

Figure 64. Requirements for New Shear Stud Detail.

COST AND BENEFITS ASSESSMENT

The initial construction cost of a bridge deck comprising precast deck panels may be higher than a cast-in-place deck, but tremendous benefit can be found in the greatly reduced construction time and greatly enhanced durability of the deck. Sources have quoted the initial cost of a bridge deck replacement with full-depth precast deck panels at between $50 and $70 per square foot, compared to cast-in-place (CIP) deck replacement costs between $28 and $40 per square foot.[19,20,21] However, the same sources have also noted the greatly reduced construction time for full-depth precast decks compared to CIP decks. Hayes, Seay, Mattern, and Mattern predicted 20 to 30 percent reductions in detour time with greater flexibility in staged construction options. This allows for closing lanes during low traffic times (nights and weekends), and reducing or eliminating lane closures during heavy traffic hours.

In conclusion, it is recognized that the initial costs for full-depth precast bridge decks are greater than for cast-in-place decks, but the reduced construction time and reduction in associated road user costs can easily offset the higher construction cost. A bridge replacement project in the Bristol District using full-depth precast deck panels has been proposed. The bridge

will be designed using the details recommended in this study. The bridge is scheduled for construction in March of 2010. An in-depth cost and benefit study will be conducted on this actual bridge construction project.

ACKNOWLEDGMENTS

This project was sponsored by the Federal Highway Administration and the Virginia Department of Transportation. The authors gratefully acknowledge the guidance provided by the engineers at the Virginia Transportation Research Council, including Michael Brown and Jose Gomez.

REFERENCES

1. American Association of State Highway and Transportation Officials,, *AASHTO Load and Resistance Factor Design Bridge Design Specifications*, 4th ed. Washington, DC, 2007.

2. Issa, M.A., Idriss, A., Kaspar, I.I., and Khayyat, S.K., Full Depth Precast and Precast, Prestressed Concrete Bridge Deck Panels, *PCI Journal*, January-February 1995, pp. 59-80.

3. Issa, M.A., Yousif, A.A., Issa, M.A., and Kaspar, I.I., Field Performance of Full Depth Precast Concrete Panels in Bridge Deck Reconstruction, *PCI Journal*, May-June 1995, pp. 82-108.

4. Issa., M.A., Yousif, A.A., Issa, M.A., and Kaspar, I.I., Analysis of Full Depth Precast Concrete Bridge Deck Panels, *PCI Journal*, January-February 1998, pp. 74-85.

5. Harrison, A., and LeBlanc, N.D., Design and Construction of a Full-Width, Full-Depth Precast Concrete Deck Slab on Steel Girder Bridge, *Journal of the Transportation Research Board, No. 1907*, Transportation Research Board, Washington, D.C., 2005.

6. TNO Building and Construction Research, *DIANA User's Manual*, Release 9, The Netherlands, 2005.

7. Sullivan, S., Construction and Behavior of Precast Bridge Deck Panel Systems, Doctoral Dissertation, Virginia Tech, Blacksburg, 2007.

8. Issa., M.A., Yousif, A.A., and Issa, M.A., Experimental Behavior of Full Depth Precast Concrete Panels for Bridge Reconstruction, *ACI Structural Journal*, May-June 2000, pp. 397-407.

9. Comite Euro-Internationale du Beton, CEB-FIP Model Code 1990. *Buletin D'Information No. 213/214*, Lausanne, Switzerland, 1990.

10. Wallenfelsz, J.A., Horizontal Shear Transfer for Full Depth Precast Concrete Bridge Deck Panels, Master's Thesis, Virginia Tech, Blacksburg, 2006.

11. Scholz, D.P., Performance Criteria Recommendations for Mortars Used in Full Depth Precast Concrete Bridge Deck Panels, Virginia Tech, Blacksburg, 2004.

12. MacGregor, J.G., *Reinforced Concrete Mechanics and Design,* 3rd ed., Prentice-Hall, Upper Saddle River, New Jersey, 1997, pp. 35-74.

13. ASTM International, ASTM C 39: Standard Test Method for Compressive Strength of Cylindrical Concrete Specimens, *Annual Book of ASTM Standards,* Vol. 04.02, West Conshohocken, Pa.,2003.

14. ASTM International, ASTM C 496: Standard Test Method for Splitting Tensile Strength of Cylindrical Concrete Specimens, *Annual Book of ASTM Standards*, Vol. 04.02, West Conshohocken, Pa., 2003.

15. ASTM International, ASTM C 109: Standard Test Method for Compressive Strength of Hydraulic Cement Mortars (Using 2 in. Cube Specimens), *Annual Book of ASTM Standards*, Vol. 04.01, West Conshohocken, Pa., 2003.

16. American Concrete Institute, *Manual of Concrete Practice, Prediction of Creep, Shrinkage, and Temperature Effects in Concrete Structures,* ACI 209R-92, Farmington Hills, Mich., 2002.

17. Bowers, S., Recommendations for Longitudinal Post-Tensioning in Full-Depth Precast Concrete Bridge Deck Panels, Master's Thesis, Virginia Tech, Blacksburg, 2007.

18. American Concrete Institute, *Building Code and Requirements for Structural Concrete (ACI 318-02) and Commentary*, Farmington Hills, Mich., 2002.

19. Hayes, Seay, Mattern, and Mattern, Bridge Deck Replacement Study, PowerPoint Presentation to the Virginia Department of Transportation, Structure & Bridge Division, Bristol District, Jan. 24, 2007.

20. Missouri Department of Transportation, *Deck Replacement with Precast Concrete Segments,* Research Investigation RI04-027, RDT 05-005, March 2005.

21. Balakrishna, S., Innovative Precast Concrete Deck Slabs, In *Proceedings of the 2006 Annual Conference of the Transportation Association of Canada,* Charlottetown, Prince Edward Island, Canada, 2006.

22. Rister, B.W., and Graves, C., *The Cost of Construction Delays and Traffic Control for Life-Cycle Cost Analysis of Pavements,* Research Report KTC-02-SPR 197-99 & SPR218-00-1F, Kentucky Transportation Center, Lexington, 2002.